Modelling the abundance and area use of wintering Red-throated Divers in the Outer Thames Estuary

Final

April 30, 2012

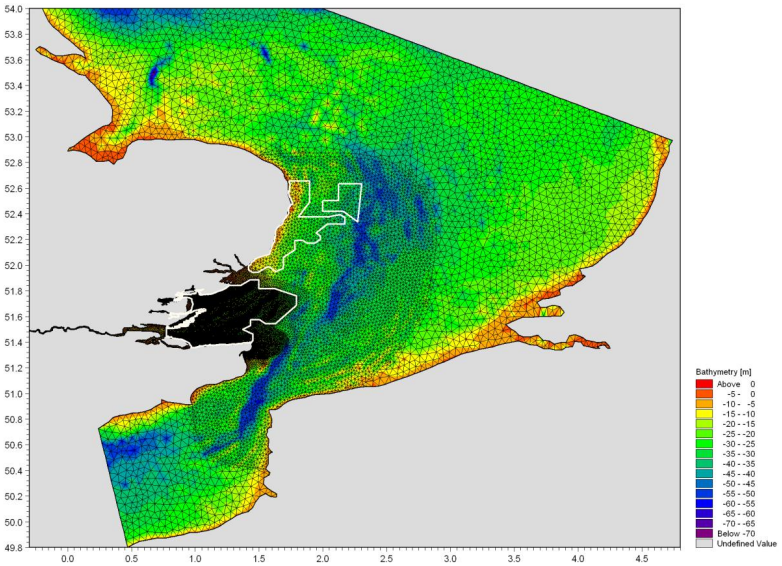

London Array Limited

Modelling the abundance and area use of wintering Red-throated Divers in the Outer Thames Estuary

Agern Allé 5
DK-2970 Hørsholm
Denmark

Tel: +45 4516 9200
Fax: +45 4516 9292
febi@dhigroup.com
www.dhigroup.com

Final

April 30, 2012

Client	Client's representative
London Array Limited	Toby Lee

Project	Project No
London Array Wind farm	11807584
Authors Henrik Skov Stefan Heinänen Sabine Lohier Chris Thaxter Ramunas Zydelis	Date 30 April 2012
	Approved by Jørgen Erik Larsen
	Final version

		Description			
RB	Classification ☐ Open	HSK	RZY	JLN	29 DEC 2010
R	Classification ☐ Open	HSK	RZY	JLN	30 SEP 2011
F	Classification ☐ Open	HSK	RZY	JLN	20 APR 2012
Revision		By	Checked	Aproval	Date

Key words

Red-throated Diver, London Array Wind farm, Distribution model, Outer Thames Estuary, Population effects

Distribution		No of copies
London Array Limited	TL, KJ	pdf
DHI, BTO	HSK, CT	pdf

CONTENTS

EXECUTIVE SUMMARY

DHI in collaboration with British Trust for Ornithology have been commissioned by London Array Limited to model the abundance and area use of Red-throated Divers *Gavia stellata* in the Outer Thames Estuary. London Array Limited has requested the work in support to the planning process for the second phase of the London Array Offshore Wind farm (LAOWF).

The main scope of the project has been to provide an independent and quantitative assessment of the density distribution of Red-throated Divers in the area with a focus on the situation at the LAOWF site. The regional population is defined here as the population wintering within the North Sea. The provision of this assessment covers the following milestones:
- Estimation of the relative importance of the LAOWF site as a habitat for wintering Red-throated Divers;
- Provision of unbiased estimates of the local population size of Red-throated Divers within the Outer Thames Estuary;
- Assessment of the thresholds for un-sustainable impact of habitat loss at the level of the North Sea wintering population of Red-throated Divers.

The milestones have been achieved through the application of state-of-the-art distribution models, which have enabled us to identify the most important habitats for wintering divers (mainly Red-throated Divers) in the Outer Thames Estuary based on analyses of the dynamics of diver distributions relative to the oceanographic dynamics of the Outer Thames Estuary. Survey data have been supplied from aerial and boat based surveys from the LAOWF, Kentish Flats, Gunfleet Sands, Greater Gabbard and Thanet survey and monitoring programmes.

Five models, one global model estimating mean abundance for the winters 2003/2004, 2004/2005, 2005/2006, 2009/2010 and 2010/2011, and four models estimating distribution patterns stratified by current scenarios (data from the same years, excluding 2009/2010), were established on the basis of the aerial visual and digital transect data using Generalised Additive Modelling (GAM). The aerial survey data were evaluated of sufficient quality and standardization to allow for integration of all data across the different monitoring programmes and platforms. Tests of the robustness of the diver distribution models relative to the amount of survey data showed that inclusion of more data is unlikely to have enhanced the performance of the models significantly.

Tests of the agreement between aerial visual and digital data on diver densities during the winter 2009/10 documented a high degree of correspondence. The spearman's correlation between the predicted presence of divers from the two platforms was 0.864 and between predicted densities 0.894. It can therefore be concluded, that the two types of data produce similar distribution patterns and order of the predictions although the digital data produce higher densities. The responses to the environmental data were very similar in the models based on both types of data.

Although the cumulative distance sample aerial surveys covered a large part of the region, uneven coverage between periods meant that densities estimated for the stratified distribution models had to be standardized into indices of habitat suitability averaged across years to allow for direct comparisons between current scenarios. Because of zero inflation the GAM models were fitted using a two-step (hurdle model) approach. The first step consisted of a presence-absence part, fitted with a binomial error distribution, and in the second step all zeros were excluded and the density of divers was fitted with a gamma error distribution.

The five diver distribution models were mainly created on the basis of the parameters from the hydrodynamic model. Overall, a high degree of consistency was seen with respect to the predicted distribution patterns from the five models. With respect to important variables, the highest degree of consistency was seen in the stratified models when comparing flow phases with strong currents with flow phases representing slack water.

The important parameters in the global model indicated a higher probability of presence of divers in offshore slope areas with low density of ships characterised by high current speeds, eddy activity and low water levels. The important parameters for densities of divers in the global models were (low) current velocity and (strong) current gradients. As the global model was established on all data across the tidal flow phases these parameters reflect a mixture of the key parameters determined by the stratified models. The two stratified distribution models for strong tidal flows both indicated a higher probability of presence of divers in the shallower areas with high vertical velocities, - a characteristic of most of the Outer Thames where divers were recorded. The two stratified distribution models for weak tidal flows both indicated a higher probability of presence of divers over the shallow slopes with moderate currents, - indicating more discrete patterns of distribution during low and high tide as displayed in the deployed models and by the well-defined small areas of fronts developed along the slopes during these flows (Appendix 2).

The parameters in the positive density parts of the stratified models described a large amount of the variability in the surveyed densities of divers, and the interaction term between X and Y coordinates was less important than in the presence parts.

The parameters in the positive density part of the stratified models stressed the importance of current gradients and shallow slopes to high densities of divers during the low velocity phases. Additionally, low current speed, eddy activity, high slopes and low ship density were also important parameters in the positive part during high tide. During ebb current low current speed and strong upwelling were important parameters to high densities, while during flood current high current speed and low density of ships were important. Accordingly, the key parameters for the positive part of the models representing strong flows further indicated the use of wider areas during these scenarios. As the parameter current gradient marks horizontal frontal activity the results of the stratified models suggest that divers in the Thames Estuary primarily use these supposedly high-productive sites during weak tidal flows.

The deployed diver models resolved areas of high densities (≥ 3 birds/km^2) extending across the eastern parts of the Outer Thames Estuary over Sunk Sand, Long Sand and Kentish Knock. Multiple fine-scale high-density patches were predicted along these sand bars with a spatial scale matching the estimated scale of aggregative response observed during single surveys. A large patch (approximately 12 * 12 km) of very high densities (≥ 5 birds/km^2) was estimated at the eastern end of Long Sand and Kentish Knock. A smaller patch of higher densities was depicted in the northern parts of the Outer Thames Estuary SPA. Areas in the North Sea deeper than 30 m, several inshore areas and the shipping lanes, were estimated as supporting virtually no divers. The parts between the high-density and low-density areas and the coastal areas of Suffolk and Norfolk representing the northern parts of the Outer Thames Estuary SPA, were indicated as having medium densities (< 3 birds/km^2) of divers in all studied winters.

In all current scenarios and winters the major part of the Outer Thames Estuary has been classified as either of low or medium habitat suitability. The habitat suitability models stratified by flow regime depicted striking patterns of suitable habitat, and consistent systematic changes in these patterns with the flow regime. During ebb current and low tide, areas in the south-western part of the estuary generally showed low habitat suitability, while during flood current and high tide prominent patches of very high habitat suitability were estimated in this part of the estuary. Superimposed on the east-west oscillation changes in the north-south location of the most suitable habitats was estimated around the sand bars. During the flow phases with slack water (low tide, high tide) divers were estimated to display a more concentrated distribution along the slopes of the sands than during the phases with stronger currents (ebb current, flood current). Finally, the patch off the Suffolk-Norfolk coast seemed most extensive during flood current and high tide.

Accordingly, depending on flow phase the LAOWF site experiences both medium, high and very high habitat suitability to divers, with the proportion of the site having very high suitability changing between 51 % and 79 %. The largest area of suitable habitat to divers in the LAOWF footprint was predicted during low and high tide, when high densities of divers coincide with the shallow, slope areas with strong current gradients found over Long Sand.

On the basis of the regional model for the five investigated survey winters total abundance of divers within the Outer Thames Estuary could be estimated for the whole area of 9,180 km^2. The mean abundance within the estuary was 7,100 (±1045) birds (mean density was 0.773). The confidence interval was calculated based on the standard errors. The mean density estimated within the Outer Thames SPA was 1.53/km^2 with an estimated mean abundance of 6,025 divers.

Although the Red-throated Diver is a widespread circumpolar species, only the population wintering in the North Sea, which consists of approximately 65,000 birds, has been considered for the assessment of the thresholds for un-sustainable impact of habitat loss on the wintering population of Red-throated Divers. An assumed coefficient of variation around this estimate was used to calculate the minimum population size, and in combination with published data on age of first breeding, adult survival, maximum population growth rate and a recovery factor a rough threshold for unsustainable biological removal of divers due to displacement from LAOWF could be estimated at 1,915 birds. This estimate refers to annual additive mortality the current population in the North Sea could sustain.

The validation of the Outer Thames Estuary hydrodynamic model showed that the predictive power of the model complex is strong, and that accurate hydrodynamic parameters have been supplied to the diver distribution models. Performances of the tide and surge predictions by 1-month comparisons between measured and predicted water levels at ten stations clearly indicated that the hydrodynamic predictions are accurate within the Outer Thames Estuary.

The validation of the modelled water levels and currents is especially important in relation to the diver distribution model, as water levels and several current parameters were used as potential habitat drivers. The comparisons between measured and predicted water levels at Dover, Felixstowe and Lowestoft showed that the water levels are reasonably well predicted in terms of phase and amplitude, with a RMSE in the order of 0.15 m - 0.25 m and a bias component of about 0.15 m. Similar tendencies were observed for water level predictions at Long Sand, Kentish Knock and Knock Deep which present a RMSE inferior to 0.3 m. The hydrodynamic complexity within the Outer Thames Estuary induced by the presence of sand bars and channels was also well represented.

The tests for spatial autocorrelation in the model residuals indicated that despite some spatial autocorrelation remained in the residuals most of the spatial structure could be explained by the environmental variables. Autocorrelations in both the presence/absence parts and positive parts were very low which indicates the spatial autocorrelation did not have an influential effect on the results.

The predictive accuracy of the diver models as tested on withdrawn data indicated that the models are capable of distinguishing presence from absence more than 75 % of the time which is acceptable given the high resolution of the model.

The Spearman's correlation coefficients of the combined models indicated that there is a clear agreement between predicted and observed values; the Spearman's correlation coefficient for the global model was 0.35. Given that the validation of accuracy was undertaken at a high spatial resolution (500 m) this result is satisfactory (many "suitable" samples will be unoccupied for example), and indicates that the predicted densities and habitat suitabilities are reliable. The deviance explained (variance explained) was higher in the positive part of all models, ranging between 31.3 % and 65.6 %. This indicates that the environmental variables are better at describing the distribution of densities than the simple probability of occurrence.

A moderate amount of error was associated with the predicted densities of wintering divers by the five models. The errors were generally below 30 %. For the global model, the errors were mostly well below 0.3 birds/km^2, and below 0.7 birds/km^2 in the high-density areas (density ≥ 3 birds/km^2).

1 INTRODUCTION

DHI in collaboration with British Trust for Ornithology (BTO) have been commissioned by London Array Limited (LAL) to model the abundance and area use of Red-throated Divers *Gavia stellata* in the Outer Thames Estuary. LAL has requested the work in support to the planning process for the second phase of the London Array Offshore Wind farm (LAOWF).

As part of the conditions for the construction of the second phase of this project, LAL is required to establish the impact of the construction of the extension to the LAOWF on wintering divers. The aim of the Red-throated Diver model is to allow for a detailed assessment of the risk to the regional wintering population of Red-throated Divers of the LAOWF development. This should be achieved through comprehensive modelling of the species' local habitat and estimation of the local population size which potentially could be affected by habitat exclusion from the wind farm upon finalisation of the construction of phase two of the project.

The rationale for focusing on the potential habitat displacement effect on divers at the site is the fact that the target area for the LAOWF development takes place in one of the key wintering areas to Red-throated Divers in Europe, as revealed through baseline monitoring from aircraft and ship. The larger part of the estuary has now become part of the Outer Thames Estuary SPA targeting the conservation of the species (Natural England 2009). Equally important, post-construction monitoring at established wind farms elsewhere, the Horns Rev 1, Nysted and Kentish Flats indicates that the species is sensitive to habitat displacement, and rarely enter the area of an established wind farm (Petersen et al. 2006, Gill et al. 2008). The species has a high protection status, is listed in the Annex 1 of the EC Birds Directive, and is red-listed in several countries.

This report covers the results of the detailed modelling scenarios of the fine-scale area use of divers, estimation of the dynamics of population sizes in the whole estuary and the wind farm footprint area. The report also contains estimations of thresholds for un-sustainable impact on the wintering population of the species in the North Sea.

The analysis applies state-of-the-art habitat models, which have enabled us to identify the most important habitats for wintering divers in the Outer Thames Estuary based on analyses of the dynamics of diver distributions relative to the oceanographic dynamics of the Outer Thames Estuary. Survey data have been supplied from aerial and boat based surveys from the LAOWF, Kentish Flats, Gunfleet Sands, Greater Gabbard and Thanet survey and monitoring programmes.

The provision of the model results covers the following milestones:

- Estimation of the relative importance of the LAOWF site as a habitat for wintering Red-throated Divers;

- Provision of unbiased estimates of the local population size of Red-throated Divers within the Outer Thames Estuary;

- Assessment of the thresholds for un-sustainable impact of habitat loss at the level of the North Sea wintering population of Red-throated Divers.

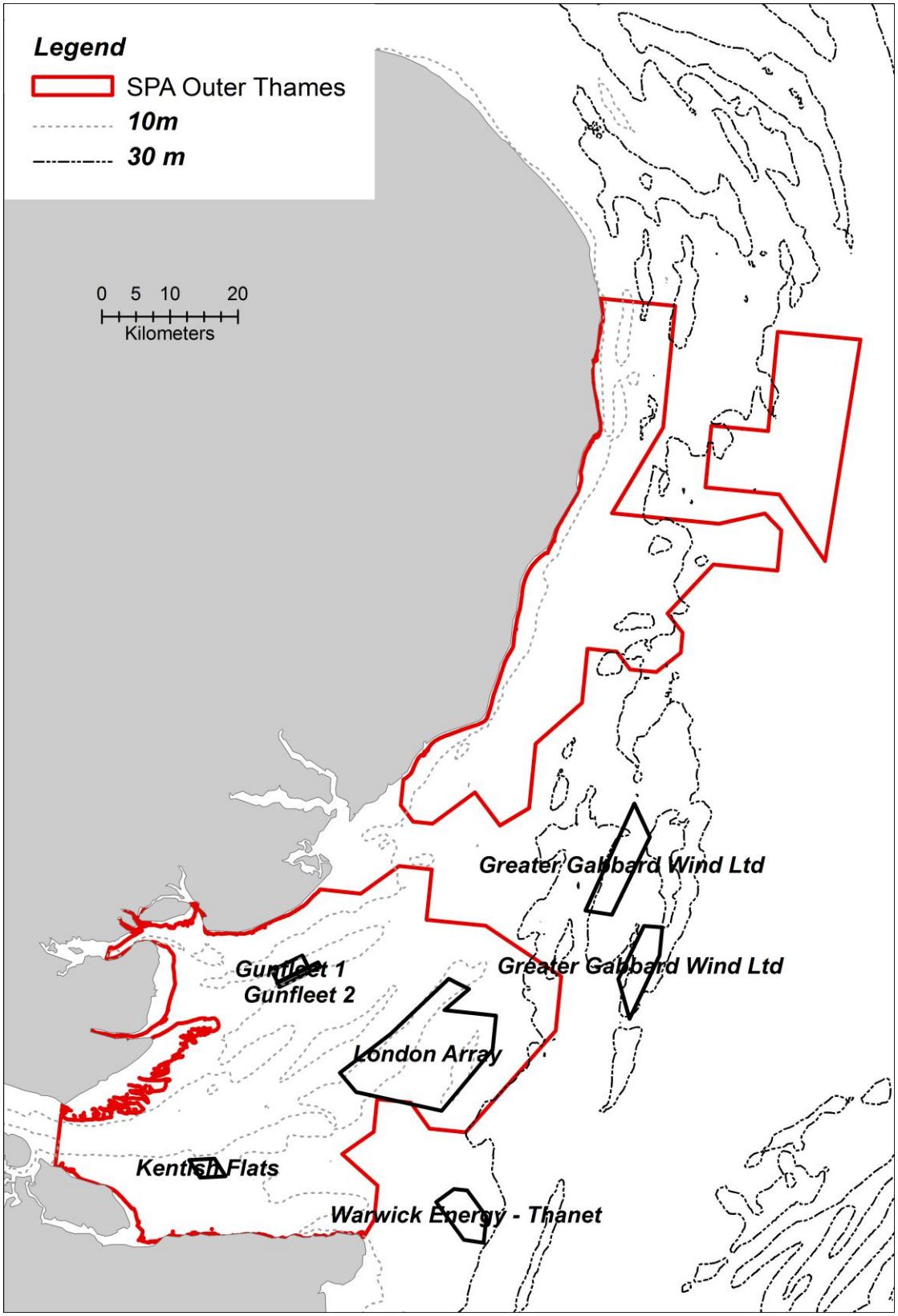

Figure 1. *The London Array Wind farm (LAOWF) site, and the boundary of the Outer Thames Estuary SPA. The location of other existing and planned offshore wind farms as well as the 20 m and 30 m depth contours is indicated.*

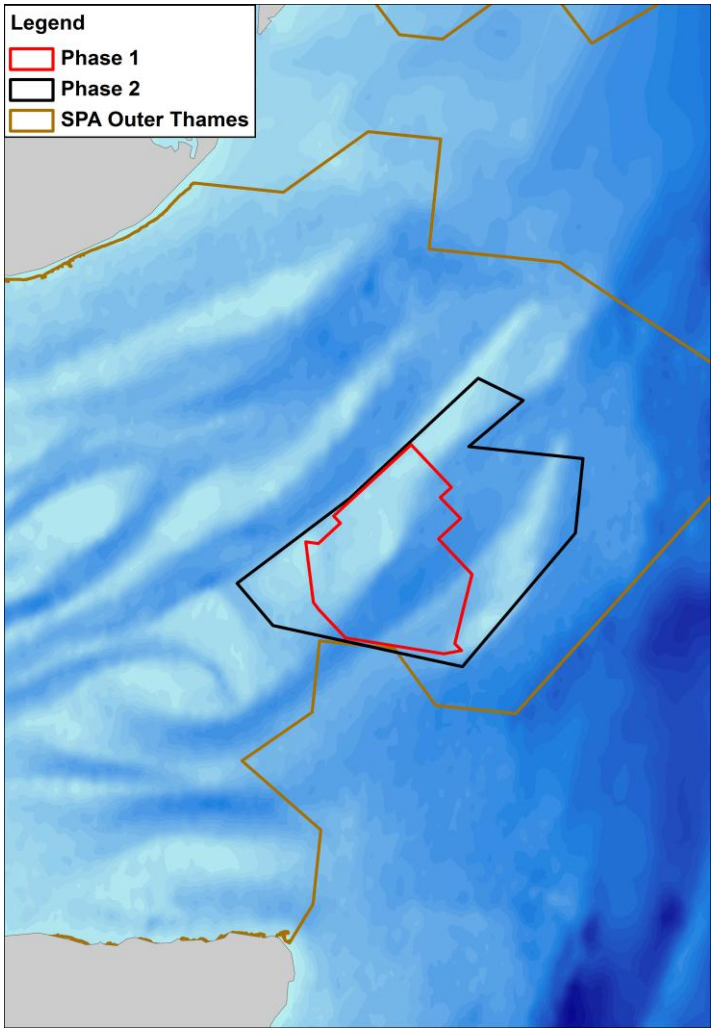

Figure 2. *The location of LAOWF Phase 1 and 2 turbines. The bathymetry of the Outer Thames Estuary is shown as a back-drop.*

2 METHODS

2.1 Available survey data

2.1.1 Visual survey data

Both aerial and boat survey data were available from several previous Baseline EIA wind farm surveys in previous years: London Array wind farm, Thanet offshore wind farm, Kentish Flats offshore wind farm, Greater Gabbard offshore wind farm, and Gunfleet Sands offshore wind farm (EMU 2002; PMSS 2005; RPS 2005; Royal Haskoning 2005; Banks *et al*. 2005, 2006; Jensen 2006). Individual surveys were often conducted over a period of two days to achieve the desired coverage. An overview of all available aerial survey data is given in Table 1.

The "Thanet" dataset was the most comprehensive, wide ranging, and high quality dataset that fed into the study, and covered the entire Outer Thames region, encompassing numerous previous wind farm surveys for EIAs such as Thanet, Gunfleet, Kentish Flats, and Greater Gabbard. Thus when referring to this dataset, reference is made to the collection of wind farm data rather than to the Thanet wind farm itself.

Standard protocols dictate that planes and boats must survey transects whereby birds are recorded into pre-defined distance bands away from the boat or aircraft (see Camphuysen *et al*. 2004 for details of survey methodologies). This allows for correction of a decrease in detectability away from the plane or boat. Thus, most surveys contained information on numbers of birds of several species per distance band and transect, plus information on whether birds were in flight or on the sea surface, and additional information such as ages, and sexes of birds, and flight heights.

Coupled with the observational data, standard GPS tracks were also available for some surveys, thus giving detailed information on the route the plane or boat took (hereafter defined as GPSU "track files"). These track files were necessary for the processing of data in this project (see below). GPS positions were recorded every *ca.* 4-5 s for aerial surveys and every *ca.* 60 s for boat surveys.

Figure 3 gives an overview of the coverage obtained by aerial surveys for the four current scenarios used for modelling the distribution of divers. Data from the period November to March were selected as representing the winter season. Although considerable coverage has been achieved by the aerial surveys it is clear that the coverage has been very uneven during the periods characterised by different environmental conditions.

2.1.2 Digital survey data

New digital methods using high definition imagery cameras have now come to fruition for offshore wind farms (for more information see Thaxter & Burton 2009). These require different survey protocols to traditional visual methods, because they do not employ transect counting of birds away from an aircraft, but instead one or more cameras survey a strip immediately below the aircraft. For these methods, all birds are assumed to be encountered, hence no distance correction is needed.

The digital data used in this study are from APEM that use still images that are taken as planes cross predefined equally-spaced GPS reference points. Thus a grid of images across the survey area was obtained for each month of survey. Automatic software recognition detected targets in the images, thereafter birds were manually identified to group level and if possible to species level. For further details of the methods for digital surveys employed by APEM see APEM (2010).

In the UK, digital methods including both video and still image methods are now being used throughout all Round 3 wind farm surveys, and can give advantages in that the planes fly at much greater altitude and thus have less chance of disturbing birds than visual methods. Therefore, to test for potential difference in habitat-association relationships between aerial and visual methods, comparisons between the two methods was conducted (see Chapter 3.4).

High definition digital data were available for four months during the winter of 2009-2010 and four months over the winter of 2010/11 (Table 1). Data processing for digital methods is described below in section 2.3.

Table 1. Time periods for aerial digital and visual datasets.

	Visual	Visual	Visual	Visual	Digital	
Month	**2003/04**	**2004/05**	**2005/06**	**2009/10**	**2009/10**	**2010/11**
November	12/11/2003	01/11/2004	08/11/2005			23/11/2010
	27/11/2003	02/11/2004	10/11/2005			24/11/2010
		10/11/2004	13/11/2005			25/11/2010
		12/11/2004	16/11/2005			
		18/11/2004	16/11/2005			
		19/11/2004	17/11/2005			
		24/11/2004	22/11/2005			
		25/11/2004				
		27/11/2004				
		28/11/2004				
December	17/12/2003	02/12/2004	02/12/2005	21/12/2009	21/12/2009	08/12/2010
		03/12/2004	06/12/2005	23/12/2009	23/12/2009	09/12/2010
		04/12/2004	07/12/2005			
		05/12/2004	08/12/2005			
			09/12/2005			
January		13/01/2005	11/01/2006	24/01/2010	24/01/2010	10/01/2011
		13/01/2005	13/01/2006	25/01/2010	25/01/2010	11/01/2011
		14/01/2005	14/01/2006		26/01/2010	17/01/2011
		15/01/2005	17/01/2006		27/01/2010	18/01/2011
		16/01/2005	18/01/2006			
		22/01/2005				
		23/01/2005				
		26/01/2005				
		27/01/2005				
February	10/02/2004	03/02/2005	01/02/2006		09/02/2010	14/02/2011
	15/02/2004	15/02/2005	02/02/2006		12/02/2010	15/02/2011
	16/02/2004	16/02/2005	03/02/2006			16/02/2011
	26/02/2004	28/02/2005	10/02/2006			
	27/02/2004		14/02/2006			
			18/02/2006			
			20/02/2006			
March	10/03/2004	02/03/2005	02/03/2006	04/03/2010		
	11/03/2004	04/03/2005	03/03/2006	05/03/2010		
		05/03/2005	06/03/2006			
		06/03/2005	07/03/2006			
		07/03/2005				
		08/03/2005				
		13/03/2005				
April				06/04/2010	06/04/2010	
				07/04/2010	07/04/2010	
				08/04/2010	08/04/2010	
				09/04/2010	09/04/2010	

2.2 Quality check of available survey data

Quality control was undertaken to disseminate coverage of high quality data, and avoid duplications. Primary focus was directed to the data from the winters of 2003/04, 2004/05, 2005/06, 2009/10 and 2010/11 when the most comprehensive coverage by aircraft was achieved.

The approach adopted for data processing required high quality information on the distribution and density of birds across the survey regions at the highest resolution possible (see below). However, this also relied on data being available for both bird observations and survey tracks. Data were available in a variety of formats, quality, and consistency, thus the match-up between tracks and observations was not possible in many circumstances.

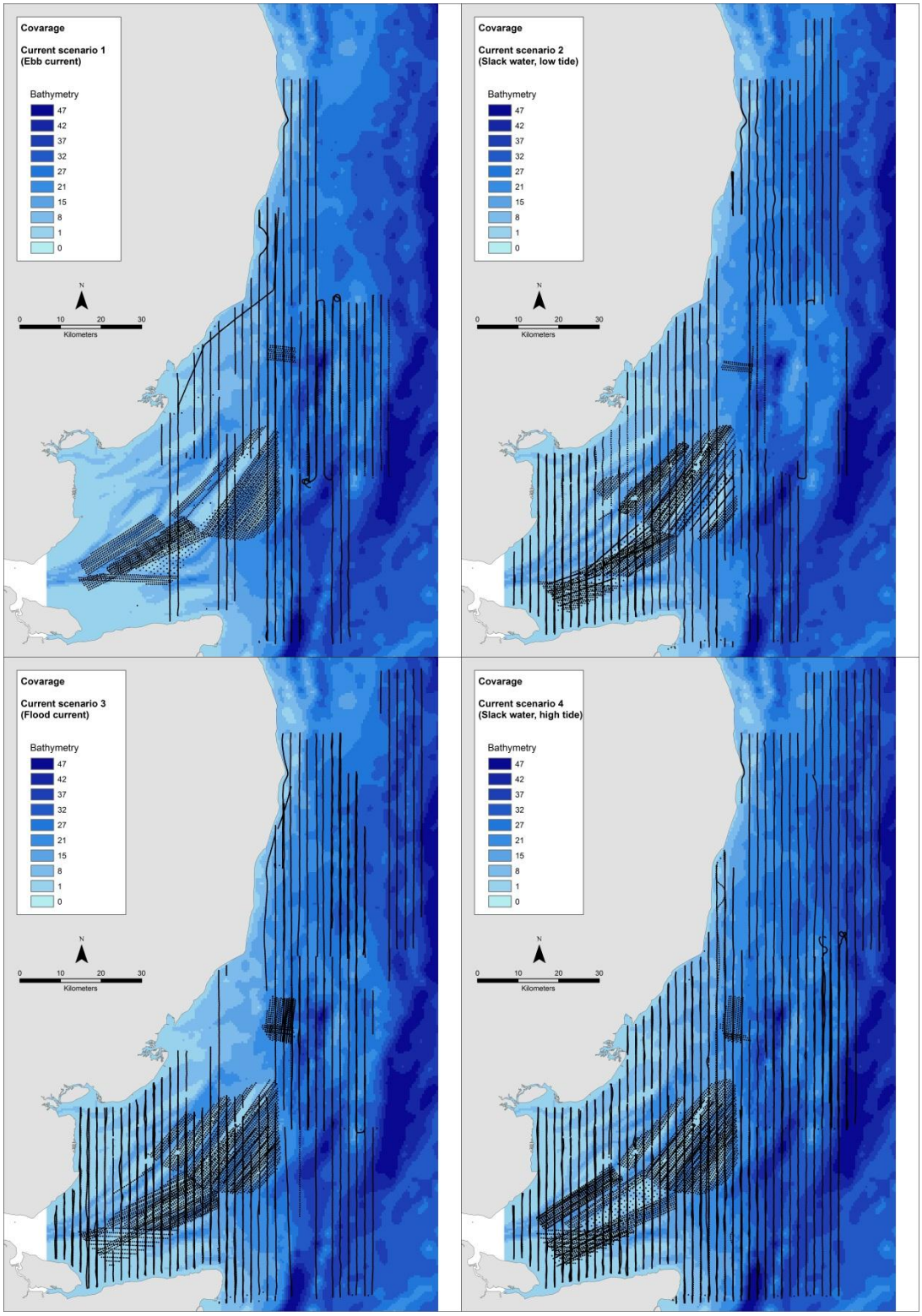

Figure 3. *Overview of the coverage of aerial surveys (visual and digital combined) stratified by the 4 current scenarios used for modelling the distribution of divers (see chapter 2.11.1).*

2.3 Processing of survey data

Visual data

Standard resolution for estimation of population abundance based on aerial and boat-based methods is at the transect level. However, input data for spatial habitat modelling required the highest resolution possible. All observational data of birds recorded had timestamps noted. Therefore it was possible to split transects from the observational data into smaller segments, which still contained the original information on the numbers of birds in distance bands. This was achieved simply by binning the time stamps of observations, between timestamps in the track file, i.e. between one GPS fix of the plane / boat and the next.

All surveys in this study were conducted using two observers counting birds from both sides of the planes or boats. However, on occasions, sections of transects were not fully covered on both sides between the start and end points of the transect (i.e. between the waypoints). Care was therefore taken to filter out such data and retain only those sections of transects that were covered on both sides, thus avoiding bias in Distance sampling corrections.

Final processed files therefore contained information on survey platform and date, the start time and end time of the "segment", the length of the segment, the transect ID from which the segment was derived, the area of the segment [aerial: length x (1000 m x 2), boat: length x (300 m x 2)], the easting and northing mid-point of the segment, and individual columns for counts of diver species, Red-throated Divers, and Black-throated Divers for each distance band. These counts were subsequently converted to densities by dividing by the segment area. Densities were then corrected for detectability by adjustment with the final detection function obtained through analyses in Distance (see below). Typically, individual segments were 300 m length for both aerial and boat surveys.

All processing of spatial data was carried out in ArcMap 9.3 (ESRI, Redlands, California), and processing of transects into segments was carried out in SAS 9.1 (SAS Institute, Inc.) and R 2.11 (The R Core Development Team, 2010).

Digital data

Digital data were initially processed by APEM, and supplied to BTO for further processing. Data on the date of image capture, time stamp, and birds encountered were processed summing the number of divers in each. Additional information on the mid-point position of each image was also supplied and then matched up with bird-images using a filename of common reference.

Given that few divers were identified to the species level from digital methods, all divers were grouped in this analysis, the predominance of which were likely red-throated divers. This also matched the same decision taken for all visual datasets in this project.

2.3.1 Snapshot counts and treatment of flying and sitting birds

For boat surveys, it is recommended that snapshot counts should be undertaken for birds in flight and should be instantaneous counts at fixed intervals along the transect (Camphuysen *et al*. 2004), adjusted in timing in relation to the speed of the boat (Maclean *et al*. 2009). This method aims to avoid issues relating to double counting of birds.

For Thanet and London Array aerial surveys, birds were recorded into distance bands perpendicularly to the transect line regardless of whether they were swimming or flying. Likewise, for boat data, records were present for both flying and sitting birds throughout transects. Snapshot counts for flying birds were made for Thanet every 2 mins (Jensen 2006, Maclean *et al*. 2009), but in the observation files this final information was not present.

For London Array, it was not possible to identify whether snapshot counts were conducted. The exact times of any sightings of flying birds at London Array were recorded in the same way as swimming birds, with the flight heights recorded as accurately as possible to assess the proportion that were flying at proposed turbine blade heights (MacLean *et al*. 2009). During surveys of the Greater Gabbard, snapshot counts were conducted at two-minute intervals but counts lasted for 5-10 seconds rather than being instantaneous (MacLean *et al*. 2009), but were present in the original data.

The separation of birds on the sea and in the air from boat surveys was necessary to avoid over-estimation of abundance (Camphuysen *et al*. 2004). Therefore, for boat surveys, separate files were produced for birds in flight and on the sea surface. However, due to difficulties outlined above in assessing snapshot counts for most surveys, it was assumed that all flying birds from boat surveys were representative of divers in each transect and thus were binned in the same way into transect segments using the GPS track data from the boat. These were then added to the birds on the seas surface. For aerial visual data, all birds whether flying or sitting were binned together into respective transect segments in line with the recommendations in Camphuysen *et al*. 2004.

2.4 Correction of distance bias

Because the detectability of a species decreases with increasing distance from the observer (Buckland *et al*. 1993), a distance correction function was applied to observed densities. This was conducted using program Distance v 6.0 (Thomas et al. 2010). Initially, it was investigated that the general functions for all data used in this study, namely "Thanet" aerial, Thanet boat, Gabbard boat, and London Array aerial visual datasets.

For aerial surveys, birds were recorded into four distance bands of: 44-163 m, 163-282 m, 282-426 m and 426-1000 m. For boat surveys, observations were recorded into five bands: 0-50 m, 50-100 m, 100-200 m, 200-300 m, and 300+ m. For aerial visual data, the first 44 m from either side of transect was removed, in which no observations could be seen (i.e. beneath the plane). For boat data, as stated above, distance correction was only applied to birds recorded on the sea surface, and also records were removed from the outer distance band for boat data prior to analysis (Camphuysen *et al*. 2004).

Distance corrections were tested on all diver species together ("Diver species", Red-throated Diver, and Black-throated Diver), and also for Red-throated Divers alone. The majority of divers identified to species in the Thames Estuary were Red-throated, however in the following all "diver species" groups are termed divers. Observations in the outer Distance bands can be few therefore truncating the analysis without this band may result in more precise estimations of density and detectability. Therefore, analyses were conducted with and without this final distance band included.

For both the aerial and boat data, the coefficient of variation was investigated of the p (probability of detection) values for London Array and Thanet aerial surveys,

and Gabbard and Thanet boat surveys, and found similar coefficients of variation (CVs) between each set, therefore these were merged to give one detection function for boat and aerial visual data.

Wave data

Sea state can have a large influence on detectability, higher waves reduce the likelihood of detection. Whilst survey guidelines describe that surveys may not be conducted in sea states above five for boat surveys and sea states above 3 for aerial surveys (Camphuysen *et al*. 2004), variation between conditions within these ranges could nonetheless influence detection of divers. Therefore, this data on wave height was also included to stratify the model.

Wave data were available for four locations in the region (see Figure 4): Long Sands (LS): Site depth: 1.5 m; Off seabed: 0.5 m; temporal range Feb-Jun 2004; Kentish Knock (KK): Site depth: 20 m; Off seabed: 0.5 m; temporal range: Feb-Jun 2004; Knock Deep (KD): Site Depth 20 m; Off seabed: 0.5 m; temporal range: Feb-Sep 2004, Jan-Mar 2005; and Drill Stone (DS): Site depth 35m; Deployed on sea surface; temporal range: Feb-Dec 2004.

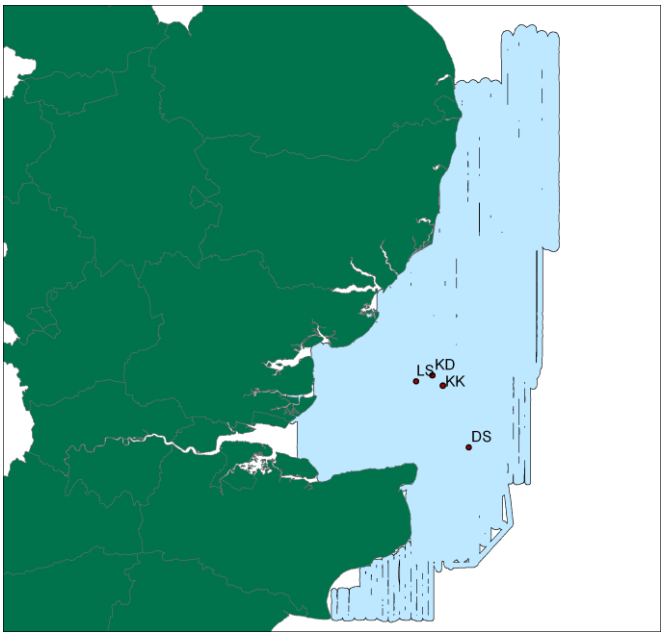

Figure 4. *Location of wave buoy data used in the study: Long Sands (LS), Kentish Knock (KK), Knock Deep (KD) and Drill Stone (DS), overlain with the total area under investigation in the study; wave data from Knock Deep were used for stratification.*

Initially it was assessed that the differences in detection functions between observations from two classes of wave heights. Measurements from Knock Deep were used that spanned the greatest survey period, and selected all survey data that fell between the temporal range stated above. Then selected an arbitrary cut-off point between lower and higher maximum wave heights at a value of 1.2 m after inspecting the distribution of maximum wave height measurements (Figure 5). For final assessment and application of the detection function, the parameter of interest was "p", here defined as the probability of detection.

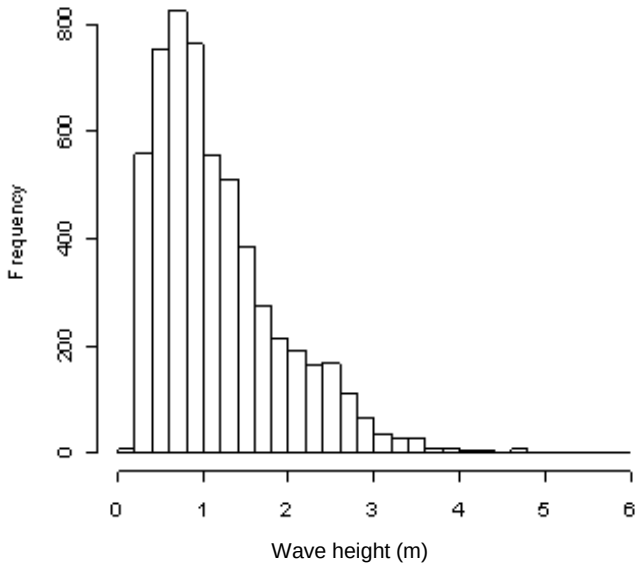

***Figure 5**. Distribution of wave height data from Knoll Deep.*

2.5 Geo-statistical analysis

A necessary first step when analysing transect survey data is the identification of the scale-dependent structures as well as the environmental parameters that are correlated to these structures. Such identification is formally carried out by geo-statistical analysis, which provides an understanding of how and at which scale, extrinsic and intrinsic processes influence the spatial distribution of the surveyed species.

The spatial structure of the diver data was analysed by means of geo-statistical analysis and variography, which determined the scale and structure of autocorrelations in the sampled transect data. The geo-statistical analyses were undertaken on the sampled data from each of the aerial and ship-based surveys, and aimed at defining the aggregative response using the range of any small-scale structures apparent in the variograms. The aggregative response is an essential parameter when developing species distributions models with the aim to determine distributions as accurately as possible (see chapter 5.4).

Although seabird distribution can be described along a continuum of spatial scales, seabird distribution data display a hierarchy of organisation from feeding aggregations, across feeding habitats to communities and ecosystems (Fauchald et al. 2000). The aggregative response is typically identified by spatial structures reflecting the scale of feeding habitats (Schneider & Duffy 1985).

2.6 Model framework

Modelling scenarios were designed in order to resolve the major oscillations in the distribution of divers in the Outer Thames Estuary in response to the dynamics of oceanographic conditions. The conditions in the estuary are strongly controlled by the tidal currents, while residual flows play a much smaller role (see later). Initial analyses of hydrodynamics showed that currents and location of frontal zones changed over short distances. A model framework was set-up which would enable us to resolve conditions at the LAOWF site at the highest possible resolution.

This was achieved by using DHI's integrated hydrodynamic and environmental model suite MIKE. A local fine-scale hydrodynamic model was set up and run with boundary conditions from DHI's regional model. The model covered all diver survey periods. The computed hydrodynamic and hydrographic parameters were then transformed into habitat describing variables. The survey data and potential dynamic habitat variables were then stratified into scenarios displaying different spatial patterns of diver distribution reflected by different oceanographic conditions in the estuary. The average density of divers was then modelled for each scenario using spatial modelling. By combining the output from the spatial models with oceanographic scenarios the dynamics in the density of divers in the footprint and the whole estuary could be estimated.

2.7 The Outer Thames Hydrodynamic Model Complex

The dedicated hydrodynamic model complex was established in order to provide detailed hydrographic parameters of the Outer Thames Estuary SPA. The Outer Thames hydrodynamic model complex has been set up using the DHI modelling system, MIKE 21/3 HD Flexible Mesh and has been run over the periods going from January 2002 to March 2006, November 2009 to March 2010 and November 2010 to February 2011, to overlap the timing of bird surveys, constituting approximately four years of continuous hind-cast and 2 additional winter periods (2009-2010 and 2010-2011).

The model system is composed of two components:

- A 2D hydrodynamic regional model of the North Atlantic and North West European Shelf.
- A 3D baroclinic hydrodynamic local model characterised by a fine resolution at the Special Protection Area and forced mainly by boundary conditions extracted from the 2D regional model.

2.8 Available measurements

2.8.1 Bathymetry

Several detailed bathymetry data sets have been used to generate the regional and local bathymetries. They are listed below and their coverage is indicated in Figures 6 and 7:

- Surveys over the London Array Offshore Wind farm area carried out by Osiris Projects commissioned by Shell U.K. Limited from April to August 2004. The bathymetry has been measured along NW–SE directed survey lines spaced every 500m, with 200m spaced cross lines;
- Data provided by the Port of London: in total 17 sets of data recorded between 1994 and 2010 covering part of the Thames Estuary located immediately west of the London Array Offshore Wind farm Array with a resolution varying between 2m and 80m;
- Measurements carried out from May to June 2007 by Osiris Projects under instructions of DONG Energy at the Gunfleet Sands Offshore Wind farm development area. Data consist of a grid composed of 300m spaced lines and 400m spaced cross lines. The maximum resolution is about 50m;
- Soundings conducted between December 2004 and March 2005 by EGS (International) Ltd. contracted by Thanet Offshore Wind Ltd. The data cover the Thanet Offshore Wind farm project area;

- Measurements made from February to March 2002 by EMU Ltd. for GREP within the area defined by the wind farm development at Kentish Flats. The survey grid system is approximately 50m to 100m spaced lines with 250m spaced cross lines.

A key challenge when generating model bathymetry from a wide range of data sets overlapping and recorded at different periods in time, is that some inconsistencies can appear during the interpolation process leading to unrealistic bed features. In order to avoid this, the following technique was applied.

This method operates on two data sets at a time, by fully integrating the information from more recent data record and adding to it the older set from which overlapping data and a narrow transition zone have been omitted. The transition zone is then filled by linear interpolation between the two sets. This procedure is iterated in the chronological order of the data recordings and leads to one smooth bathymetry set integrating the newest data.

These data have been supplemented to deep water by the following digital maps:

- Digital sea-chart (C-map data) along the European North West shelf and Faroe Islands' continental shelf until a water depth of 200m;
- The GEBCO (General Bathymetric Chart of the Oceans) One Minute Grid for depth larger than 200m;
- Data from the Danish Maritime Safety Administration in the Northern Kattegat and in the North Sea which have a resolution of 50m and 100m respectively.

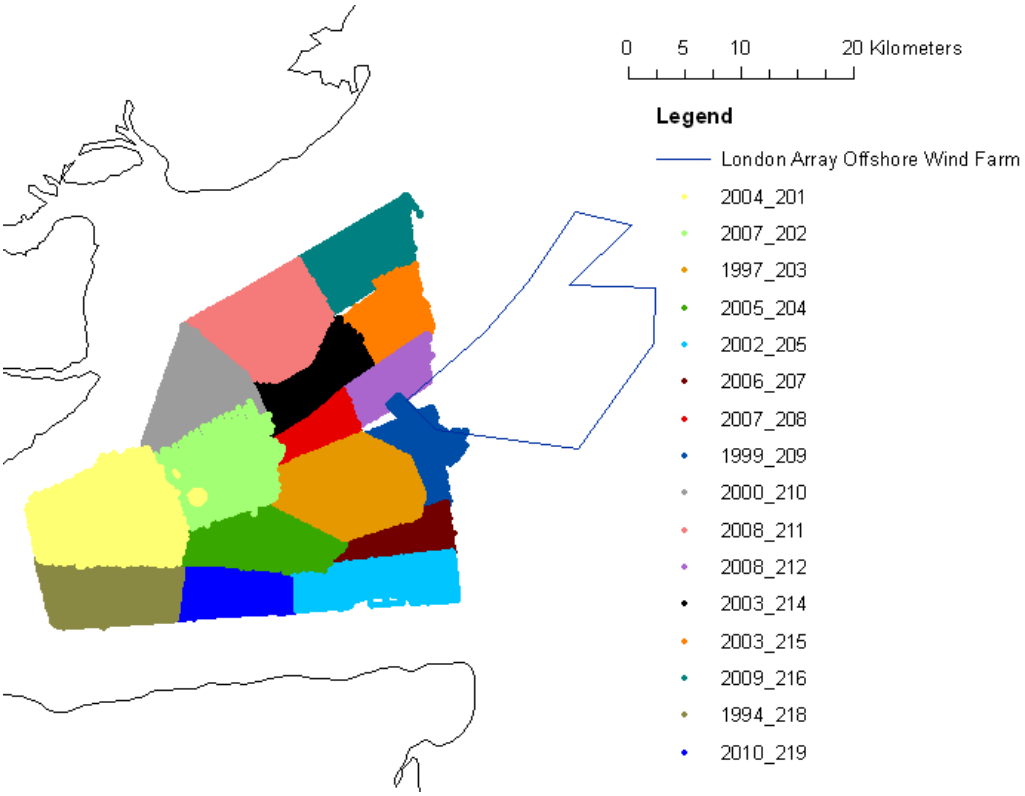

Figure 6. *Coverage of bathymetry data provided by the Port of London. In total 17 bathymetric surveys have been conducted between 1994 and 2010.*

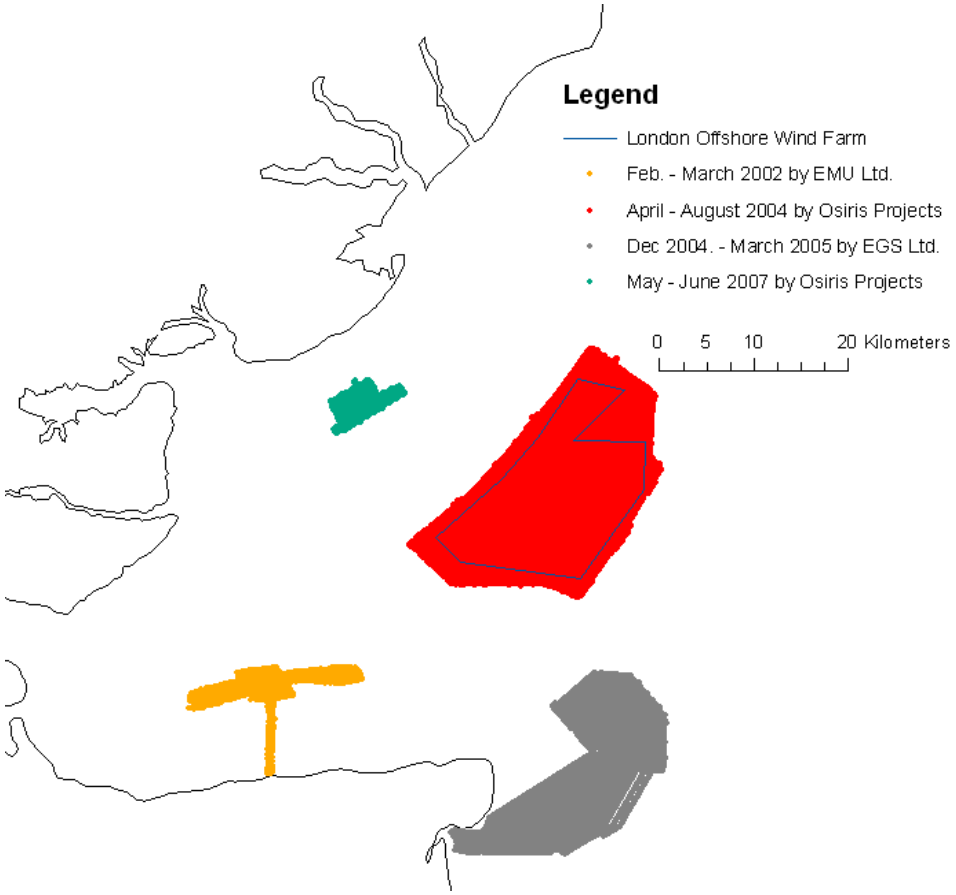

Figure 7. *Coverage of available local bathymetric data measured from 2002 to 2007.*

2.8.2 *Meteorological Data*

The meteorological data from 2002 to 2006 have been provided from Vejr2's meteorological ETA model and for the winters 2009-2010 and 2010-2011 from the regional WRF model run routinely by StormGeo for DHI which is based on the global weather model run by European Centre for Medium Weather Forecasting (ECMWF).

The data consist of atmospheric pressure, wind speed and direction at an elevation of 10 m and air temperature with a time resolution of three hours for 2002 and one hour from 2003. The spatial resolution of the ETA and WRF models is 0.15x0.15 and 0.1x0.1degrees respectively. Net precipitation, air relative humidity and cloudiness were available with the same spatial and time resolution from 2005.

2.8.3 *Hydrography*

Tide gauge measurements used during either the data assimilation or the validation process of the hydrodynamic modelling system are listed in

2 and indicated in Figure 8. Water levels recorded every 15 min at stations along the southern and western coasts of UK have been supplied by BODC. Along the northern coast of France, hourly data have been provided by SHOM. Data from both sources extend from 2002 to 2006, and 2009-2011.

In addition, measurements of water level have been carried out from 11 February 2004 to 2 June 2004 by EMU Ltd. within the London Array project area at Long Sand, Knock Deep and Kentish Knock (Figure 9). Current speed and direction have also been provided for the same period at the three locations (Table 3).

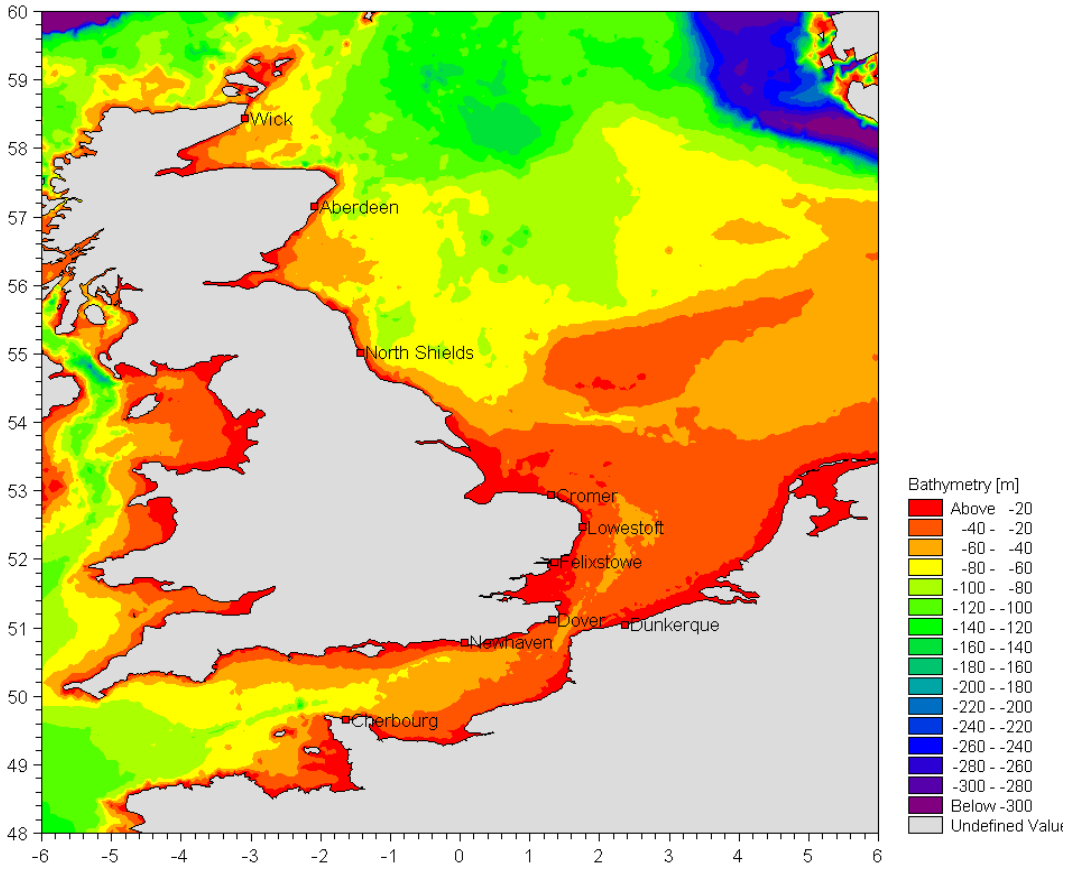

Figure 8. *Location of tide gauge stations along the North Sea and the English Channel used during the data assimilation / validation process of the hydrodynamic modelling system.*

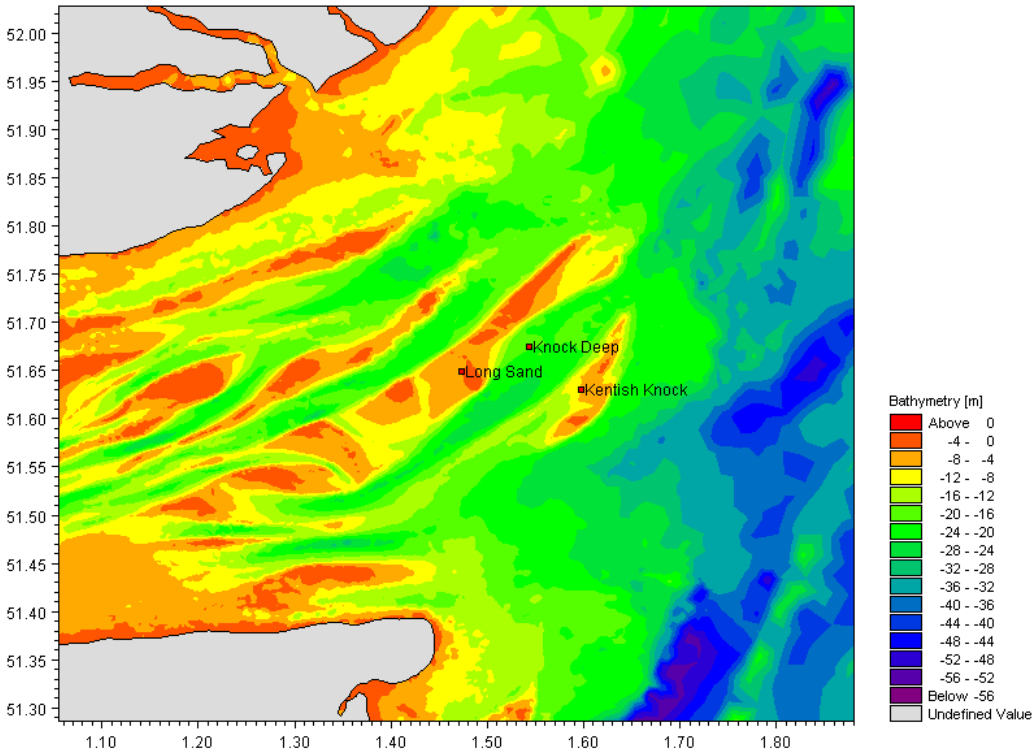

Figure 9. *Location of current and water level measurements carried out by EMU Ltd. at the Thames Estuary.*

Table 2. *Tide gauge stations used during the data assimilation / validation process of the hydrodynamic modelling system.*

Station	Longitude (deg E)	Latitude (deg N)	Country	Period of Measurements	Source
Aberdeen	-2.0833	57.15	UK	2002-2006	BODC
Cromer	1.30164	52.93419	UK	2002-2006, 01-11-2009->31-03-2010 01-11-2010->28-02-2011	BODC
Cherbourg	-1.63563	49.6513	France	2002-2006, 01-11-2009->31-03-2010 01-11-2010->28-02-2011	SHOM
Dover	1.3167	51.117	UK	2002-2006, 01-11-2009->31-03-2010 01-11-2010->28-02-2011	BODC
Dunkerque	2.36664	51.0481	France	2002-2006, 01-11-2009->31-03-2010 01-11-2010->28-02-2011	SHOM
Felixstowe	1.34655	51.95769	UK	2002-2006	BODC
Lowestoft	1.75	52.467	UK	2002-2006	BODC
Newhaven	0.05703	50.78178	UK	2002-2006, 01-11-2009->31-03-2010 01-11-2010->28-02-2011	BODC
North Shields	-1.433	55.017	UK	2002-2006, 01-11-2009->31-03-2010 01-11-2010->28-02-2011	BODC
Wick	-3.0833	58.433	UK	2002-2006, 01-11-2009->31-03-2010 01-11-2010->28-02-2011	BODC
Long Sand	1.47312	51.6485	UK	11-02-2004->20-03-2004 11-04-2004->02-06-2004	EMU Ltd.
Knock Deep	1.54363	51.6749	UK	11-02-2004->21-02-2004 29-03-2004->04-09-2004	EMU Ltd.
Kentish Knock	1.596817	51.62982	UK	11-02-2004->17-03-2004 29-03-2004->02-06-2004	EMU Ltd.

Table 3. *Current measurements carried out by EMU Ltd. within the London Array Offshore Wind farm area.*

Station	Longitude (deg)	Latitude (deg)	Period of measure-ments
Long Sand	1.47312	51.6485	11-02-2004->19-02-2004 15-04-2004->02-06-2004
Knock Deep	1.54363	51.6749	11-02-2004->21-02-2004 29-03-2004->04-09-2004 07-01-2005->19-03-2005
Kentish Knock	1.596817	51.62982	11-02-2004->17-03-2004 30-03-2004->02-06-2004

2.8.4 *Temperature and Salinity*

3D temperature and salinity grids of ¼ degree resolution in the horizontal plane and 10 m discretisation vertically have been extracted from the Generalized Digital Environmental Model (GDEM, Teague et al. 1990). GDEM data constitute a climatology which represents the long-term monthly average based on over 70 years of data; therefore deviations of this average are not taken into account.

2.8.5 *River Flow*

Surrounding rivers discharge freshwater to the Thames Estuary among which the River Thames provides the largest contribution. In-situ river discharge data have

been collected through the Environment Agency of UK and the National River Flow Archive (Table 4).

Table 4. *River discharge data included in the Outer Thames Estuary model.*

Location	Catchment area (km^2)	Mean flow (m^3/s)	Country	Source
Beam	49.7	0.33	UK	NRFA
Beverley Brook	43.5	0.54	UK	NRFA
Blackwater	337	1.38	UK	Environment Agency - UK
Blyth	92.9	0.43	UK	NRFA
Colne	238.2	1.06	UK	NRFA
Darent	191.4	0.64	UK	NRFA
Deben	163.1	0.77	UK	NRFA
Gipping	298	1.19	UK	Environment Agency - UK
Great Stour	345	3.18	UK	NRFA
Ingrebourne	47.9	0.32	UK	NRFA
Lee	1243	5.49	UK	NRFA
Mar Dyke	90.7	0.48	UK	NRFA
Medway	1256.1	10.9	UK	NRFA
Ore	54.9	0.31	UK	NRFA
Quaggy	33.5	0.15	UK	NRFA
Roding	303.3	1.81	UK	NRFA
Stour	844.3	3.1	UK	Environment Agency - UK
Thames	9948	65.63	UK	NRFA
Wandle	176.1	1.83	UK	NRFA

2.9 The 2D Regional Model

The regional hydrodynamic model has been set up with MIKE 21 Flexible Mesh HD with the purpose of providing accurate boundary conditions to the 3D local fine-meshed hydrodynamic model. The latter is forced by tide and wind and integrates data assimilation.

MIKE 21 FM HD computes on a flexible mesh the depth-integrated currents, driven by a combined forcing, which may comprise forces induced by tide, wind and waves. This model solves the depth-averaged shallow water equations of continuity and momentum and can reproduce temporal and spatial variations of water levels and currents. The applied driving forces can consist of wave forces (radiation stresses), water level differences or fluxes at the boundaries (tidal and river flow), wind and atmospheric pressure forces and Coriolis force.

The prediction capabilities of the hydrodynamic model including tide and surge and data assimilation scheme are strongly dependant on the pure tide wave propagation which needs to constitute a good background to the full model. Therefore prior to the validation of the tide and surge model integrating tide gauge assimilation, an analysis assessing the performance of the tide model has been conducted.

2.9.1 Mesh and Bathymetry

The regional model domain (Figure 10) covers the north western part of the Atlantic Ocean and the European North West Shelf, and extends from the Faroe Islands to Morocco.

A flexible mesh (Figures 11, 12) composed of approximately 63,000 triangles and 117,000 nodes has been created. Its resolution varies from ¼ degree at the western open boundaries and increases gradually to 1/10 degree at the European North West Shelf and Faroe Islands' continental shelf. The Outer Thames Estuary as well as the Strait of Dover are characterised by a mesh resolution of approximately 1/16 degree increasing to 1/30 degree at the adjacent coastlines.

The bathymetry has then been generated by interpolating the bathymetry data into the mesh described above. Figure 13 represents a close-up of the area of interest.

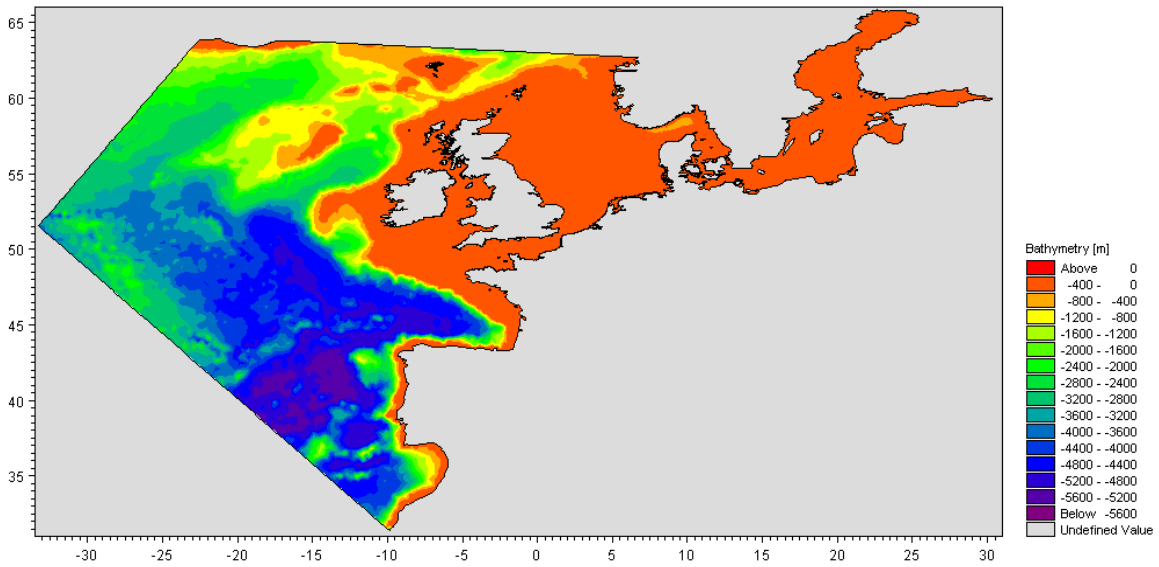

Figure 10. *Domain and bathymetry of the 2D regional model.*

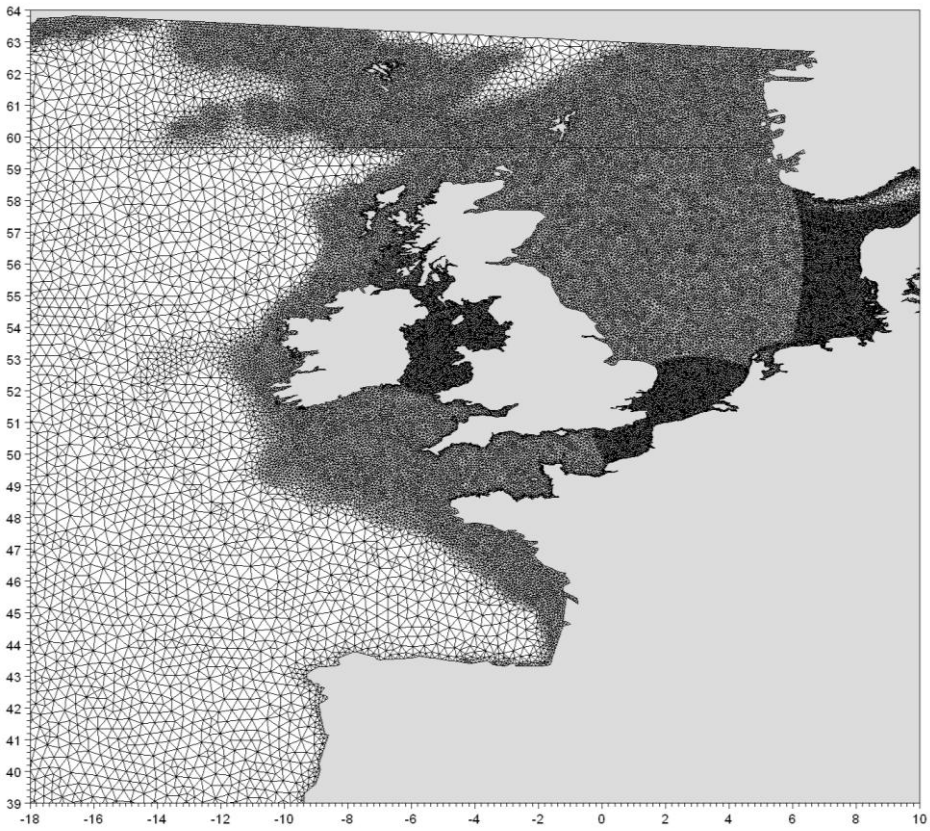

Figure 11. *Close up of the mesh of the regional model at the North West European shelf.*

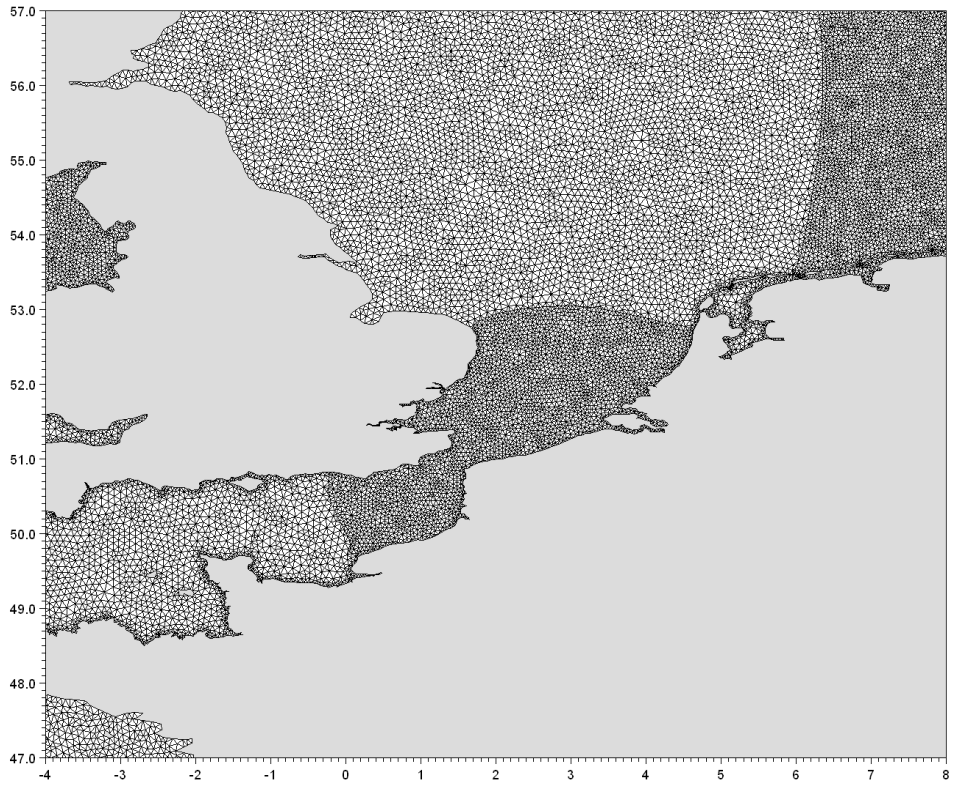

Figure 12. *Close up of the mesh of the regional model at the North Sea and English Channel.*

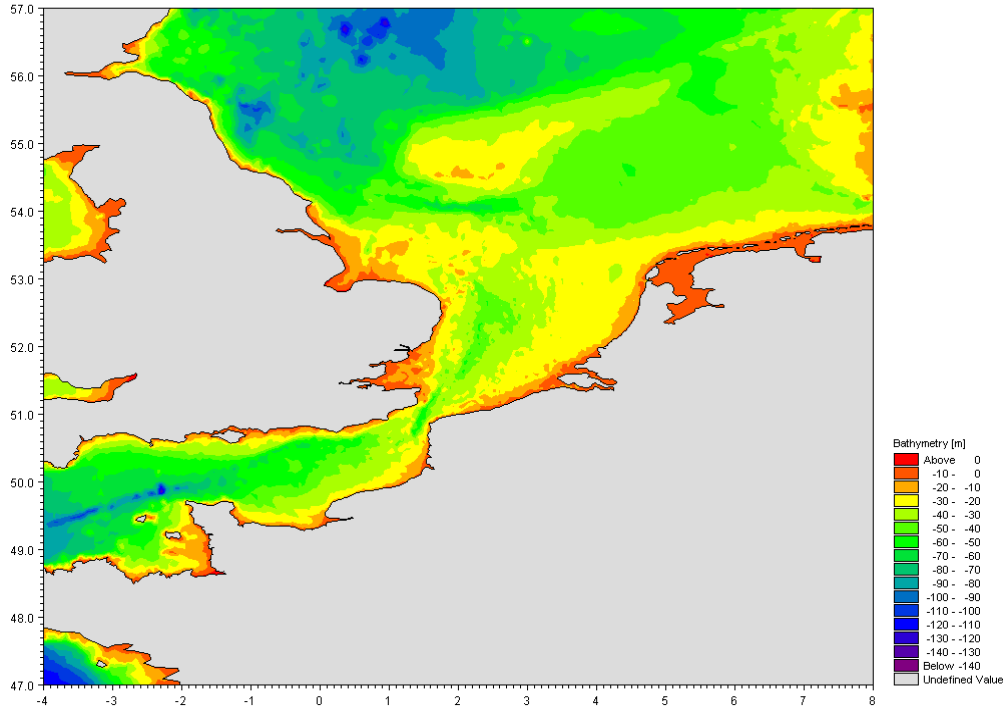

Figure 13. *Close up of the bathymetry of the regional model at the North Sea and English Channel.*

2.9.2 Set-up and Specifications

The 2D regional model has been set to simulate approximately four years of hindcast from 1 January 2002 to 31 March 2006. Calculations of the hydrodynamic of the system have also been performed for two additional periods extending from the 1 November 2009 to 31 March 2010 and 1 November 2010 to 28 February 2011. The imposed forcing is composed of the tidal, meteorological (wind and atmospheric pressure) and Coriolis forcings.

Tidal potential

The tidal potential forcing is implemented as a so-called equilibrium tide. It enters the momentum equations as an additional term representing the gradient of the equilibrium tidal elevations such that the elevation can be seen as the sum of the actual elevation and the equilibrium potential tide.

Wind forcing

The wind stress $\tau_s is$ defined by $\vec{\tau_s} = \rho_a c_f |U| \vec{U}$, where ρ_a is the density of the air, c_f represents the drag coefficient of the air and $\vec{U} = (U, V)$ are the wind components specified by Vejr2 data (cf Section2.8.2). The drag coefficient c_f has been set up as follows:

$$c_f = \begin{cases} c_a & w_{10} < w_a \\ c_a + \dfrac{c_b - c_a}{w_b - w_a}\left(w_{10} - w_a\right) & w_a \le w_{10} < w_b \\ c_b & w_{10} \ge w_b \end{cases}$$

Where the empirical factor c_a and c_b have been set to 0.001255 and 0.002425, w_a and w_b are equal to 7m/s and 25m/s.

Bed resistance
The bed roughness is specified through a Chezy formulation with a spatially constant Manning number equal to 40$m^{1/3}$/s.

Turbulence model
For horizontal turbulence modelling, the Smagorinsky formulation with a constant Smagorinsky coefficient of 0.28 has been used.

Boundary conditions
The three open boundaries are forced by pure tidal water levels generated from the Global Ocean Tide Model (Andersen et al. 2006, http://www.space.dtu.dk/English/Research/Scientificdata and models/Global_Ocean_Tide_Model.aspx) which includes the 12 major tidal constituents and has a spatial resolution of 0.25 degree.

Data assimilation
The data assimilation scheme considered for this project is the Steady Kalman Filter approach based on the Ensemble Kalman Filter. The Steady Kalman Filter assumes a long-term averaged Kalman gain matrix which has the advantage of reducing significantly the computational cost, while preserving good assimilation skills (Sørensen et al. 2004).

Among the tide gauge stations listed in 3 Wick, North Shields, Cromer, Cherbourg, Dunkerque and Newhaven have been assimilated, while the remaining ones Aberdeen, Lowestoft, Felixstowe and Dover have been used for validation purposes. Water levels around the project area rely primarily on the interplay between tidal waves propagating along the English Channel and the North Sea. Thus, the regional model has been constrained increasingly from upstream (by assimilating measurements from Cherbourg and Wick) to the Outer Thames Estuary to ensure accurate predictions.

2.10 The 3D Local Model

The interaction between steep bathymetry gradients due to the presence of sand banks delimited by channels and large tidal range varying across the area leads to very complex 3-dimensional hydrodynamics in the Outer Thames Estuary area. Moreover, freshwater discharged to the estuary by the River Thames and contiguous rivers results in the presence of hydrographic fronts which move back and forth with the tide propagation. These features are important to understand in order to facilitate potential habitat features to the divers in the Outer Thames Estuary. Thus, a local 3D baroclinic fine-scaled hydrodynamic model has been set up with MIKE 3 FM HD with the purpose of producing four years of detailed hindcast of the hydrodynamics of the Outer Thames Estuary.

MIKE 3 FM is DHI's general 3D simulation engine, describing elevations, current profiles and turbulence statistics (Rasmussen 1991). The model includes temperature and salinity such that baroclinic effects on the flow can be described. The model uses an unstructured mesh, based on tetrahedals or/and quadrilaterals, enabling a high spatial resolution in focal areas. The vertical discretisation can be based on a combined sigma-z grid. The model solves the 3D shallow water equations and can incorporate density effects through a UNESCO equation of state, linked to two transport equations for salinity and heat respectively. The numerical solution uses a finite-volume method, with a second order spatial representation, both in vertical and horizontal directions. The time marching is explicit, thus there is a strict Courant number criterion for stability. The relatively short time step enforced is balanced by a very efficient solution and ensures an accurate numerical solution.

The 3D local hydrodynamic model does not include data assimilation as the water levels within the area are governed by the boundary data from the encompassing 2D regional model. Including data assimilation in the 3D local model would therefore have a lesser impact than for the 2D regional model.

2.10.1 Mesh and Bathymetry

The extent of the 3D local model is represented in Figure 14. The modelled domain is delimited to the north between Humberside County at the British coast and north Holland at the Dutch coast and extends to the south until the eastern part of the English Channel.

The discretisation of the local model has been designed as a reasonable compromise between a high-resolution mesh resolving steep gradients in bathymetry and computational cost. The horizontal mesh of the area is presented in Figure 15, its resolution varies from 1/20 degree at the boundaries to a mean resolution of 400 m in the vicinity of the LAOWF site.

In this area, sand banks are resolved by triangles with a characteristic length of 200 m, while the channels in between present a resolution of 600 m. At the northern part of the Special Protected Area, the mesh is characterised by 1/40 degree elements. The vertical is discretised by 10 equidistant sigma layers, which is sufficiently accurate as the project area is well mixed by the effect of the strong tidal currents. This approach presents the advantage to adapt to the sea surface and the seabed which in the present study enables to describe accurately the seabed in shallow waters and large gradients of the bathymetry in the vicinity of the LAOWF.

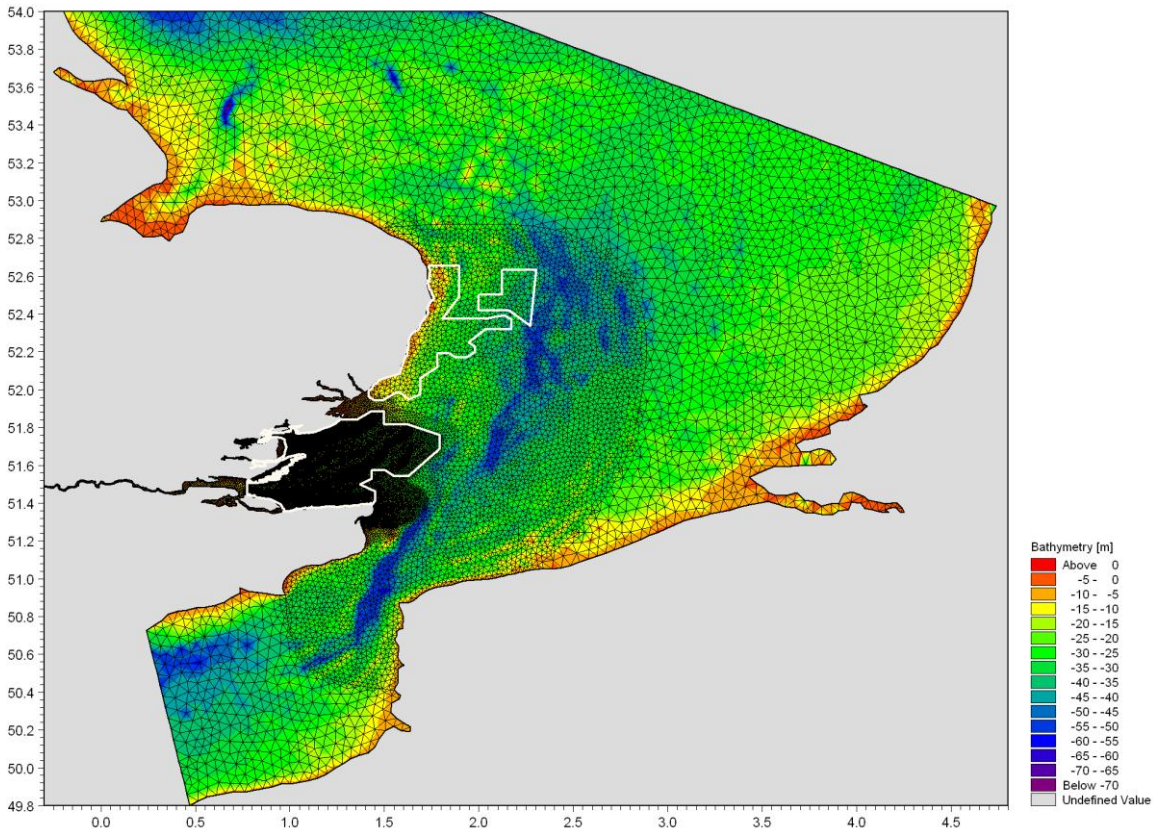

Figure 14. *Domain and horizontal mesh of the 3D local model. The Outer Thames Estuary SPA is indicated by white boundary.*

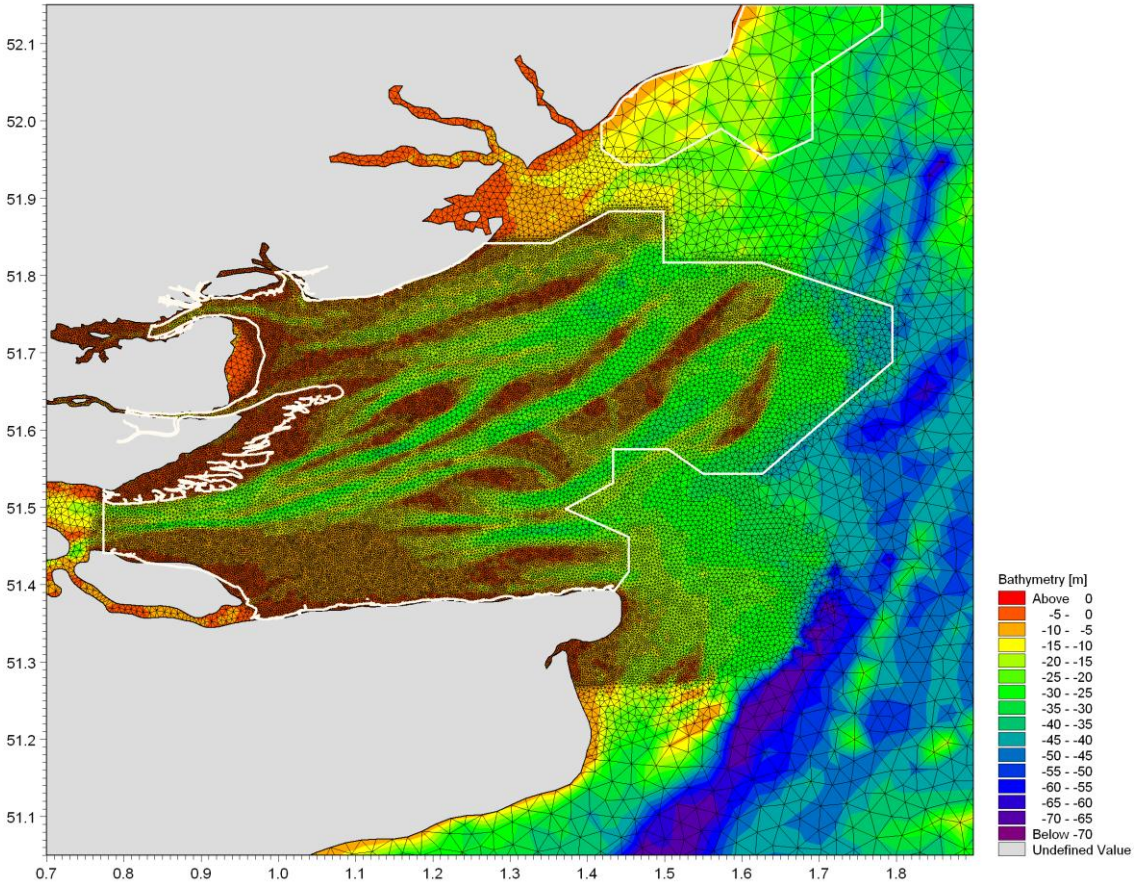

Figure 15. *Close up of the horizontal mesh of the local model at the southern part of the Outer Thames Estuary SPA delimited in white.*

2.10.2 Set-up and Specifications

The 3D local baroclinic model has been set up to simulate the hydrodynamics of the Outer Thames Estuary SPA for the period from 1 January 2002 to 31 March 2006. Two additional periods going from the 1 November 2009 to 31 March 2010 and 1 November 2010 to 28 February 2011 have been simulated as well.

The forcings which have been imposed are composed primarily of the tidal, meteorological and Coriolis forcings which have already been defined. In addition to the latter, discharges from the rivers listed in Table 3 have been input to system as sources.

Bed roughness

The bed roughness which affects the flow mainly in shallow areas has been defined as 10 cm at the sand banks at the Outer Thames Estuary SPA forcing the water to move through the channels where the roughness height has been set to 5 mm.

Turbulence model

The horizontal eddy viscosity has been included through a Smagorinsky formulation as for the 2D regional model, while the vertical eddy viscosity has been defined using a k-ε formulation.

Boundary conditions
At the open boundaries, barotropic flather conditions which constrain the surface elevation as well as the normal velocities along the boundaries have been imposed. The latter have been extracted from the 2D regional model (cf Section 2.9). It has to be noticed that the baroclinic current component has been omitted by assuming that the water column is poorly stratified at the boundaries defining the local model.

Temperature and salinity module
In order to include baroclinic effects, the salinity and temperature variables have been modelled considering 3D initial temperature and salinity fields as well as 2D vertical boundary conditions of temperature and salinity supplied through climatological data from GDEM). Heat exchange with the atmosphere has been included for the calculation of the transport equation for salt and temperature through the latent heat flux (the heat exchange due to vaporisation), the sensible heat flux (the heat flux due to convection), net infrared radiation from the sea and the insulation flux (the flux of solar energy into the sea). The total heat exchange depends primarily on a number of additional inputs; among them, the cloudiness, air temperature, atmospheric humidity and wind speed have been input to the model, as described earlier. The horizontal and vertical diffusion of salt and temperature have been implemented by scaling the eddy viscosity formulation using a scaling factor of 0.02. It has been imposed that the rivers supply freshwater to the estuary with no temperature difference.

2.11 Post-processing of hydrodynamic variables

The environmental variables used in the diver distribution models were either taken directly from the Outer Thames Estuary 3D hydrodynamic model, the available topographic, landscape and pressure data layers, or developed through post-processing of combinations of model simulation results.

Having established the time-varying fields of the above mentioned parameters, different kinds of temporal mean values were calculated such as seasonal means and means for different flow scenarios. A detailed description of the hydrodynamics and the variables extracted from the Outer Thames Estuary hydrodynamic model is found in chapter 2.12 and Annex 2.

2.11.1 Selection of model scenarios

The hydrodynamic model results stressed the influence of tidal currents on the conditions in the entire estuary, and documented significant changes in the current speeds and directions as well as in the location of frontal zones through the tidal excursions. In order to summarise these dynamics in a plausible way which would allow a sufficient sample size of diver observations for the diver distribution models a simple classification of the currents in the estuary was undertaken. The classification scheme enabled the current pattern over the entire area at every time step to be represented by a specific flag along a continuum from 1 to 4. Current scenarios were subsequently established by aggregating hydrodynamic data and diver observations into four stages (Figure 16):

1. Developed ebb-current driven by a strong gradient in water level from Lowestoft to Dover. During this phase the current within the area direction is SW-NE;
2. Flow reversing over the area (low tide) characterised by flow crossing perpendicularly the bars with a NW-SE direction;

3. Developed flood current driven by a strong gradient in water level from Lowestoft to Dover. During this phase the current within the area direction is NE-SW;
4. Flow reversing over the area (high tide) characterised by flow crossing perpendicularly the bars with a SE-NW direction.

The four flow phases comprised approximately equal proportions of time during the five modelled winter seasons; phase 1 mean proportion 25.9 %, phase 2 26.5 %, phase 3 20.3 % and phase 4 26.3 %. Although current patterns are systematic for the entire hindcast period spatial variation in the current direction exist, especially for scenarios 2 and 4. As the length of these different phases change with time depending on the variation of the gradient in water level between Lowestoft and Dover and a slight effect of the wind, the classification was based on a procedure which defined the current scenario by reading the current direction and speed at 3 locations, in the northern and southern part of the estuary as well as at the mouth of the River Thames.

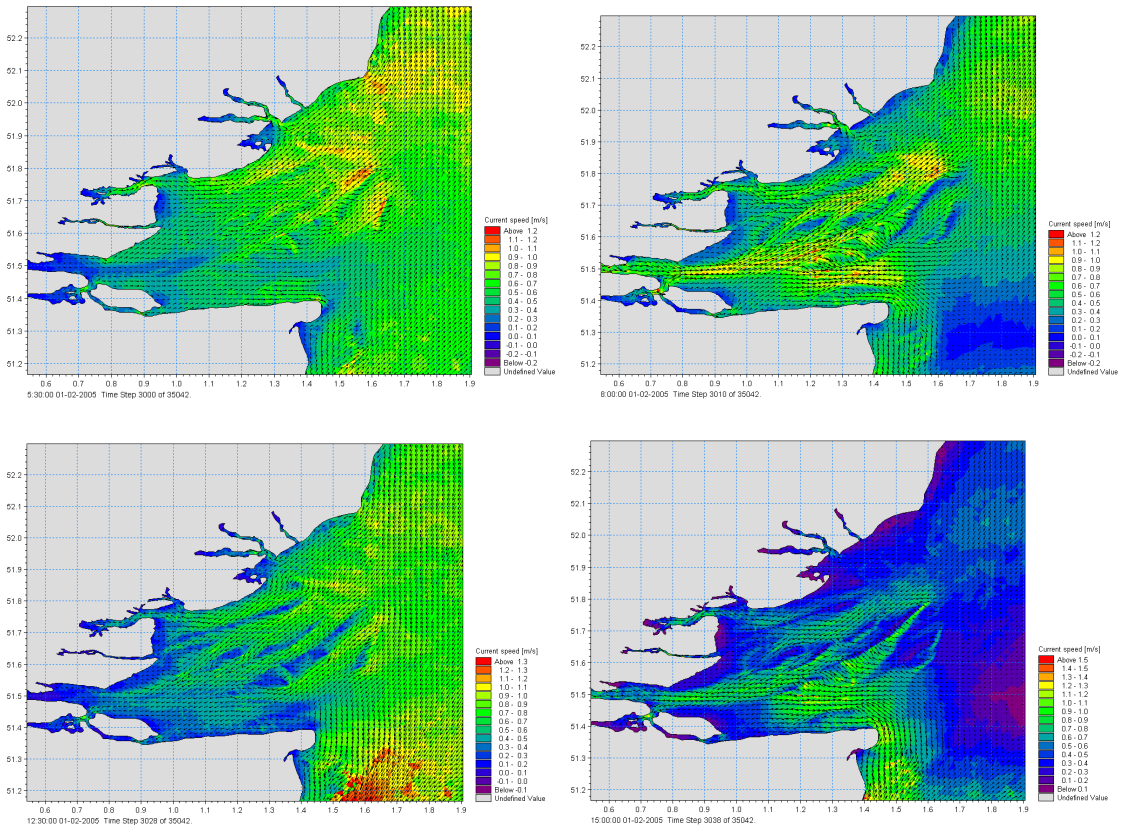

Figure 16. *Overview of four current scenarios showing changes in mean current speed and directions for each flow phase. Flow phase 1: ebb-current - current direction SW-NE. Flow phase 2: Flow reversing (low tide) – flow crossing sand bars NW-SE. Flow phase 3: Flood-current. Current direction NE-SW. Flow phase 4: Flow reversed (high tide) – flow crossing the sand bars SE-NW.*

2.12 Diver distribution models

By using species distribution models (SDMs, Elith & Leathwich 2009, Franklin 2009) it is possible to relate observed species distribution to a set of predictor variables (Tremblay et al. 2009, Sonntag et al. 2009, Zipkin et al. 2010). This approach is

used to overcome uneven sampling and to be able to predict the distribution in areas that are not surveyed, e.g. the areas in between the aerial transect coverage in the Outer Thames Estuary. As documented by the geo-statistical analyses (see below) diver distribution in the Outer Thames Estuary is characterised by a high degree of patchiness with aggregations being observed over areas of limited spatial extent. In addition, divers seem to change distribution in response to changing current conditions. To that end SDMs coupled to dynamic habitat variables deliver the solution by being capable of describing the spatial distribution and densities of divers at the finest spatial and temporal resolution possible.

The processes shaping the distribution of birds, including divers, are highly complex. As the relationships between the observed species and the measured environmental predictors are typically non-linear, it was chosen to use the non-linear modelling algorithm of generalized additive models (GAM, Hastie & Tibshirani 1990). GAMs are widely used (e.g. Guisan et al. 2002), and have been shown to perform well in comparisons with other methods (e.g. Moisen & Frescino 2002, Elith et al. 2006). In GAMs predictor variables can be modelled non-parametrically while it is also possible to include linear or polynomial terms, as well as interactions (Guisan et al. 2002). GAM can be said to be semi-parametric as the probability distribution has to be defined (Guisan et al. 2002). Formulation of the GAM can be written as (Franklin 2009):

$$g\big(E(Y)\big) = LP = \hat{\beta}_0 + \sum_{j=1}^{p} X_j \, f_j + \varepsilon,$$

where the expected value of Y, E(Y), is linked to the linear predictor, LP, with a link function, g(). The predictor variables, X, each with a smooth function f are combined to produce the linear predictor (LP), $\hat{\beta}_0$ is the coefficient and ε the error term. The method has previously been successfully applied for estimation of waterbird densities from transect survey data (Petersen et al. 2006). GAMs are completely data driven, and can be fitted using different error family distributions as for example Gaussian, binomial, Poisson, gamma, Tweedie, etc.. An overview of the model building process is shown in Figure 17.

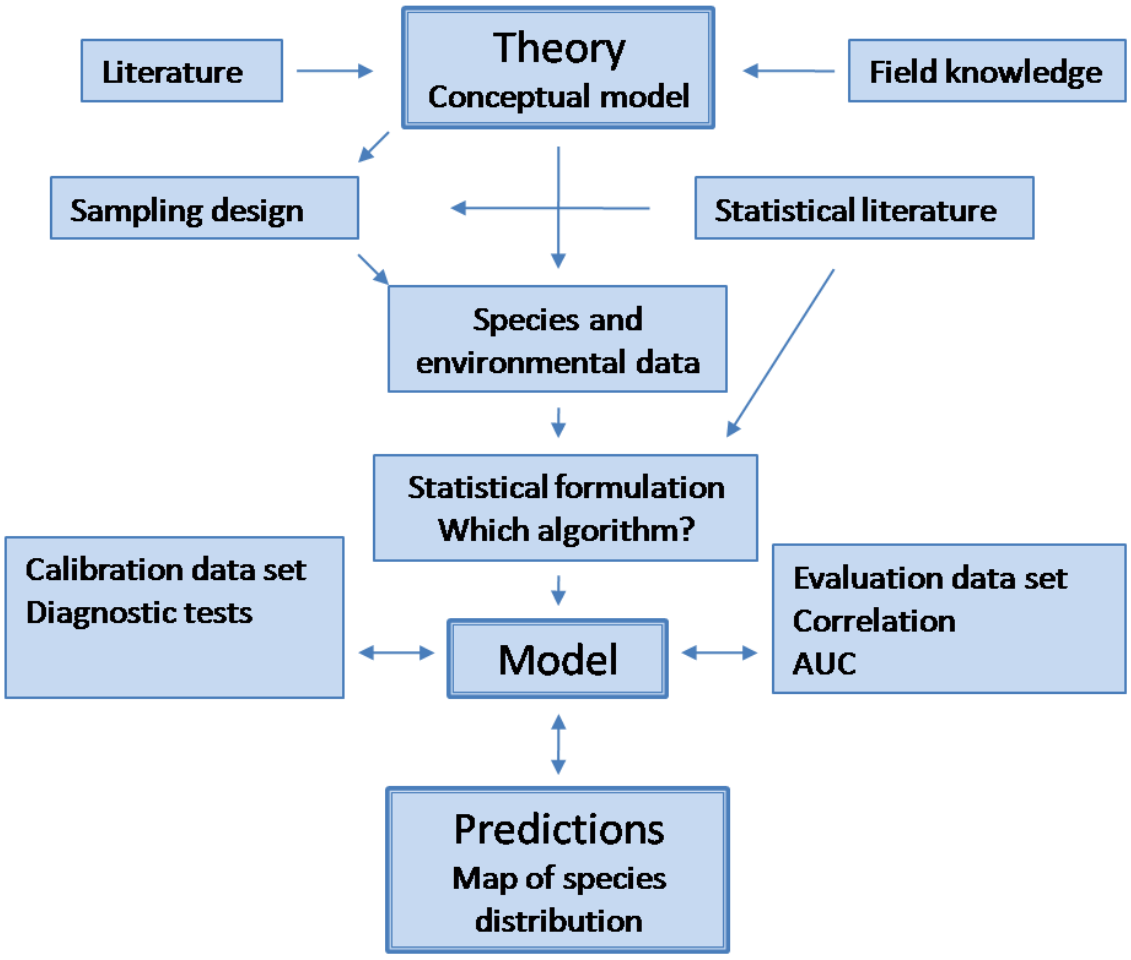

Figure 17. *Overview of the model building process, from theory to a final species distribution map. Modified from Guisan & Zimmerman 2000 and Franklin 2009.*

2.12.1 Selection of predictor variables

Spatial predictions of diver distribution at a fine resolution require environmental predictors that are able to describe the prevailing dynamic conditions in the region. A prerequisite for the dynamic predictors to be useful in predictive modelling is their availability as GIS data layers covering the entire Outer Thames Estuary during the whole survey period (see chapter on post-processing of hydrodynamic variables above). The selection of predictors is based on experience from modelling diver distributions at a fine resolution in the German Bight, Kattegat and the Baltic Sea (Skov et al. 2008, Skov et al. 2009, Skov et al. 2011).

Information on fine- scale prey distribution suitable for divers is not available for the entire Outer Thames Estuary. Even if data on prey densities were available it is unlikely that these data would increase the predictive or explanatory power of the models.

Model results from the German Bight and Kattegat have pointed at the importance of frontal features rather than parameters reflecting structures and processes at large scale like water masses and currents. This is in line with the findings of ubiquitous concentrations of other piscivorous species of seabirds at shallow sea fronts (Schneider 1982, Kinder et al. 1983), plume fronts (Skov & Prins 2001), bank fronts (Camphuysen et al. 2006) and shelf break fronts (Schneider & Hunt 1982, Follestad 1990). The general interpretation of these affinities has been the en-

hancement of the probability of prey encounter, which greatly maximize predators' foraging success (Schneider & Duffy 1985, Fauchald et al. 2010). Steep gradients in abundance of prey and predators have been documented at these structures. In the oceanographic context of the Outer Thames Estuary, these structures may be grouped as follows:

1. Horizontal low-frequency fronts;
2. Semi-permanent up-/down-welling cells;
3. Semi-permanent eddies.

The processes responsible for the increased predictability and probability of prey to marine predators at certain hydrographic fronts in the horizontal as well as vertical planes have been explained by their persistent occurrence. For this project variables have been selected which reflect conditionally stable processes and structures in the Outer Thames region. These variables essentially comprise the horizontal fronts and eddies. Similarly, regular upwelling and downwelling events are known to result in markedly enhanced biological productivity (Andrews & Hutchings 1980, Armstrong et al. 1987), and the variables reflecting these structures were also given high priority. Due to the high intensity of tidal mixing in the region the vertical water column structure, which potentially has a pronounced influence on the distribution of diving seabirds, was not considered.

Therefore the following dynamic variables were chosen: U velocity (eastern current composant), V velocity (northern current composant), Vertical velocity (W), current speed, current gradient, vorticity and water level. The parameter 'current gradient' or frontal strength was developed by calculating the local gradient (|dU/dx|+|dV/dy|) in horizontal current from the eastern and northern current composants (U and V). The horizontal vorticity (dV/dx-dU/dy) was similarly calculated to represent the local 'eddy potential', with positive values indicating anticlockwise eddy activity and negative values clockwise eddies. In the two expressions dx and dy indicate the horizontal grid spacing in the east and north direction respectively. Frontal strength and eddy potential were calculated at 5 m depth (where possible) in order to represent the conditions centrally in the water column. Grid points at locations shallower than 5 m were flagged as missing values.

Static, topographic predictors have also been shown before to be useful for describing the distribution of pelagic species (e.g. Sonntag et al. 2009). As the processes potentially enhancing the probability of prey encounter are expected to be associated with the slopes of the east-west oriented sands in the estuary, therefore slope of the seabed was included as a static variable. Two pressure variables relating to disturbance from human activities was included, which were distance to land (maximum 5 km) and mean density of ships. The latter was based on AIS data for 28 days from the winter of 2010, which had been gridded to 500 m resolution and scaled to show the number of ships per year per nm^2. Spatial data on densities of fishing vessels operating in the Thames Estuary were not available. Also included was an interaction term between X and Y coordinates as a predictor to account for some of the unexplained variance, not accounted for by the environmental data. See a complete list of the selected variables used in Table 5.

Table 5. *List of variables included in the initial model.*

Predictor	Description	Rationale for inclusion
Slope	Slope (in degrees) of sea floor	Interaction with frontal dynamics which concentrate prey
Water level	Water depth (m)	Diving depth/ Pelagic food resource
Distance to land max 5 km	Euclidian distance (m) to shore of maximum 5 km	Disturbance
Densities of ships	Number of ships/year/km^2	Disturbance
Current gradient	Local horizontal gradient of currents (m/s/m) at 5 m depth	Hydrodynamic structure concentrating prey
U velocity	Local E-W current velocity composant (m/s) at 5 m depth	Water mass characteristics
Vorticity	Eddy activity measured as the local vorticity (m/s/m) of the flow at 5 m depth	Water mass characteristics
V velocity	Local N-S current velocity composant (m/s) at 5 m depth	Water mass characteristics
Vertical velocity (W)	Local upwelling/downwelling measured as vertical velocity (m/s, positive for upward flow) at 5 m depth	Hydrodynamic structure concentrating prey
Current speed	Local magnitude of horizontal current (m/s) at 5 m depth	U and V velocity components combined
X and Y coordiantes	An interaction term between X and Y coordinates	Account for unexplained spatial structure

2.12.2 Model setup, fitting and validation

Setup of the diver distribution models and data preparation

To be able to calculate the detailed distribution patterns and total abundance of Red-throated Divers in the whole Outer Thames Estuary SPA a global model was created, and four stratified models were created to describe the varying spatial distribution patterns in the study area. The setup for the five models was the following:

1) The global model was based on mean diver densities collected during five winters (2003-2004, 2004-2005, 2005-2006, 2009-2010 and 2010-2011) within the study area. By using this model it has been possible to calculate the mean density of divers during the winter period in the Outer Thames Estuary SPA, despite the uneven coverage between the different periods.
2) A stratified model was constructed using data from flow phase 1 (see above, section 2.11.1). This model describes the mean pattern during ebb current during four winters (winter 2009-2010 was not included as the extent of the surveys that specific winter was so small in comparison to the others).
3) The third model that was constructed, was based on observations recorded during flow phase 2. This model describes the mean distribution patterns during low tide (slack water) during the same winters as the in the second model.

4) The fourth model that was constructed, was based on observations recorded during flow phase 3. This model describes the mean distribution patterns during flood current during the four winters (as in model 2 and 3).
5) The fifth model that was constructed, was based on observations recorded during flow phase 4. This model describes the mean distribution patterns during high tide (slack water) during the four winters (as in model 2, 3 and 4).

Before model fitting the distance-corrected diver densities (response variable) were combined with the dynamic environmental variables based on position and time using the DHI Dynamic Data Integration Tool (Figure 18). The tool is written in C#, using the Microsoft .NET Framework. The tool can read one or more tables with survey data, containing locations and timestamps. Spatiotemporal data are extracted from raster series, but the extracted values depend on both the location of the extraction points and their timestamp. This is technically based on the MIKE DFS .NET API, which has been recently developed by DHI and is not yet publicly available.

The output files of the data integration tool were .txt tables containing all original data from the input tables, and additional columns with the values extracted from static rasters and hydrodynamic model results simultaneously (one for each integrated variable, e.g. water depth, current speed). The data was grouped by year and aggregated (mean values within years) into 500 m grid cells. The data was further aggregated (mean values within years) into 500 m grid cells.

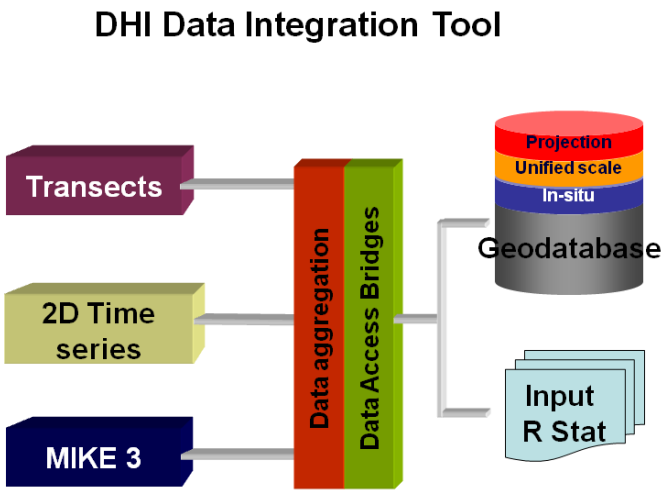

Figure 18. *Dynamic Data Integration Tool.*

Model *formulation*
Because of zero inflation, an excess of zeros in the data set (Potts & Elith 2006), the GAM models were fitted using a two-step approach, a delta model (also called a hurdle model). The first step in the delta model consisted of a presence/absence part, fitted with a binomial error distribution (with a logit link). In the second, positive part, all the zeros were excluded (Le Pape 2004, Potts & Elith 2006) and the density (response variable) was fitted with a gamma error distribution with a log link (Stefánson 1996). Different error distributions were tested, e.g. Tweedie and

quasi Poisson, but the gamma distribution resulted in the best fit. The two model parts were thereafter combined by multiplying the predictions of both model parts. The associated standard error was calculated by using the formula for the variances of the product of two random variables (Goodman 1960), which has also been used by others (e.g. Clark et al. 2009, Webley et al. 2011).

The models were fitted in R version 2.9.0 (R Development Core Team, 2004) and the package "mgcv" (Wood 2006) using thin plate regression splines. The degree of smoothing is in the "mgcv" package chosen automatically based on generalized cross validation (Wood 2006). The default dimension (k = maximum degrees of freedom for each smooth function) is 10 for single covariate smooth functions. To reduce potential overfitting of the GAM models, smooth functions for each of the variables were limited to 5 (k=5). The smoothing was not limited for the interaction term between X and Y coordinates.

An initial model including all variables, chosen prior to the modelling, was first fitted. As highly correlated variables can result in exclusion of important variables, inaccurate model parameterisation and decreased predictive accuracy (Graham 2003, Heikkinen et al. 2006), we checked the pairwise Pearson's correlation between the predictor variables before inclusion in the model. We allowed a high correlation coefficient, 0.70-0.85, between water level and X coordinates as the X coordinates were only included as an interaction term with Y coordinates in the models (and should therefore not cause any problems to model fit). All other variables had a correlation coefficient <0.60. The initial model was further refined in accordance with the recommendations by Wood and Augustin (2002). A variable was dropped if the estimated degree of freedom for the term was close to 1 and if the confidence band included zeros everywhere and further if the GCV/UBRE score dropped when the term was dropped from the model (Wood and Augustin 2002).

Variables displaying ecologically meaningless responses were also removed (Austin 2002, Wintle et al. 2005). The same procedure was used for all five models.

Model diagnostics

The fit of the GAM models were assessed based on deviance (variance) explained. Diagnostic plots, normality and homogeneity of variance (homoscedasticity) of the residuals as well as observed against fitted values were assessed (Zuur et al. 2009). Model residuals were tested for spatial autocorrelation using Moran's I. For the calculations of Moran's I the nearest neighbourhood was defined as 1500 m. To assess the spatial autocorrelation over longer distances a Moran's I correlogram was inspected showing 10 lags where one lag is the defined nearest neighbourhood (1500 m). For the calculations of the spatial statics the R package "spdep" was used (Bivand 2009).

Evaluation of predictive accuracy

The predictive accuracy of the models was assessed by randomly spitting the data into a calibration set (70%) and an evaluation set (30%) (Marini et al. 2010). Usage of data not used in the model development is essential when evaluating the predictive performance (Fielding & Bell 1997, Guisan & Zimmermann 2000, Pearce & Ferrier 2000).

The model, fitted on the calibration data set, was predicted on the evaluation set and the predictions were assessed using evaluation statistics. The presence-absence part of the two-part delta model was assessed using the area under the receiver operating characteristic curve (AUC). AUC is a threshold independent measure. A value of 0.9 means the model is capable of distinguishing between occupied and unoccupied cells 90 % of the time, whereas a value of 0.5 indicates that the model predictions are no better than random (Fielding & Bell 1997). The final

combined predictions were assessed against the observed values using Spearman rank correlation which shows the agreement between the predicted and observed values.

Predictions
Finally the models were used to predict the distribution and density of divers in the whole SPA. For the predictions of the regional density model (global model), one prediction file including mean values during all years of the dynamic environmental predictors as well as the static predictors were constructed (see Figure 19).

For the four stratified models four prediction files were produced, including mean values of the dynamic environmental variables and the static variables for each flow phase during the four winters included in the models. The predictions were then calculated based on the models in R and exported to GIS for visualisation.

Due to the uneven survey coverage of the aerial surveys during the four tidal stages it was necessary to standardise the model predictions in order to avoid the bias introduced when numbers of observed divers in the four flow phases differed significantly. Standardisation was achieved by using percentiles to define the upper and lower thresholds in the suitability of areas to Red-throated Divers. The threshold between Low and Medium habitat suitability was defined by the first quartile (25 %), the threshold between Medium and High habitat suitability was defined by the third quartile (75 %) and the threshold between high and very high habitat suitability was defined by the 90 percentile. The predictions of the stratified models were also clipped with a buffer of 3 km around the survey points to enable an "unbiased" comparison between the tidal phases. Larger degree of extrapolation would lead to higher uncertainty in the flow phases with smaller survey extent.

The predictions were assessed visually. The evaluation statistics used are non-spatial and it is therefore important to assess the spatial distribution of the predictions as well (Ferrier 2002, Wintle et al. 2005). A way of examining the spatial structure of the predictions is to map the observed values on top of the predictions in order to spot unrealistic patterns, which could be driven by missing predictor variables or overfitting, and might require that the model is rejected (Franklin 2009). The whole modelling framework is schematically presented in Figure 19.

To further scrutinise the predictive accuracy of the stratified models the following evaluation was made:

- Comparison of dimensions of predicted high-density areas as compared to the aggregative response scale of observed data as determined by the geostatistical analyses.

Evaluation of model stability, effect of sample size
Further analysis looked into how the sample size affected the stability of the predictions. In other words it was looked at how predicted mean densities fluctuated and how the associated standard errors changed when varying the sample size. Therefore model was fitted (Model 1) with different sample sizes (based on the full data set including average values over all five years) with intervals of 5 %, starting with 5 % up to 100 % which resulted in 20 model results which were plotted and assessed. The different subsets of the data were randomly drawn from the data set used for fitting Model 1, which were mean values for all five years.

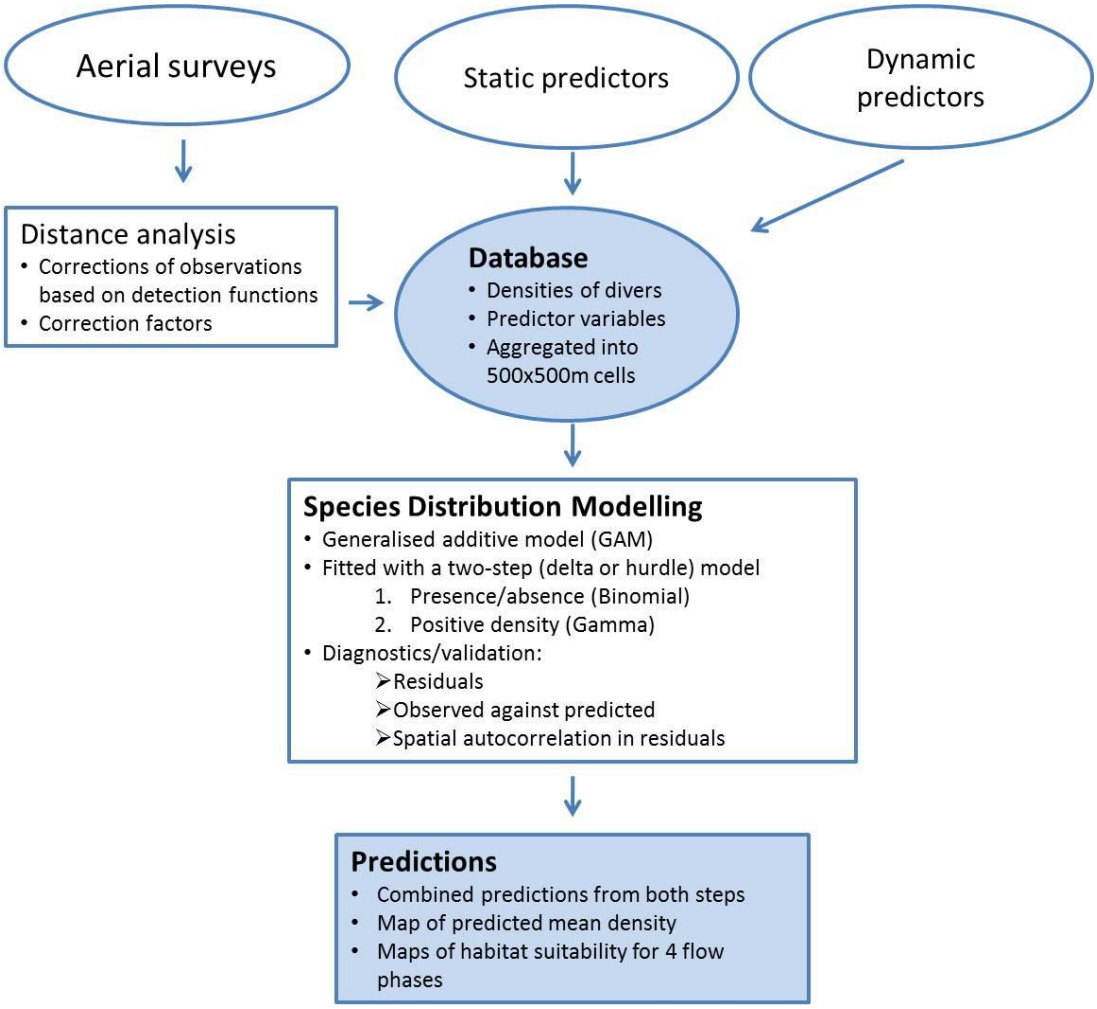

Figure 19. *A summary of the different modelling steps, from surveys to predictions.*

2.13 Comparison of visual and digital survey data

Before densities of Red-throated Divers collected by the visual and digital aerial surveys were combined comparative tests were performed. Two datasets were compared using overlapping time periods collected by APEM and Wildfowl and Wetlands Trust (WWT). For visual data, observation and track file data was processed in the same way as described above for four months over the winter of 2009-2010.

Models were compared on fitted visual and digital survey data to assess potential differences in habitat associations between the two types of survey data. The model setup and methods were the same as for the other models (described above). However, a best set of explanatory variables common for both data set were chosen (the variables were chosen simultaneously for both models), which allowed us to compare the responses between the two types of data.

The models should therefore not be regarded as "best possible models" but as "best models" for a comparison. The models were used to predict the mean density during the whole winter, which allowed the ability to compare differences in density estimates. Also, predicted mean densities were forecast during the different flow phases, and classified into habitat suitability (25, 75 and 90 percentiles), based on the same models but, predicted on the different conditions during the different flow phases.

2.14 Assessment of unsustainable effects on population levels

In order to estimate the threshold for an unstainable displacement of Red-throated Divers in relation to the wintering population in the North Sea the potential biological removal or PBR approach (Wade 1998) was applied. The approach assumes that all displaced birds will suffer mortality, and thus can be seen as a worst case scenario. PBR has been used increasingly to assess effects of additive mortality on bird populations using limited demographic information (Niel & Lebreton 2005, Dillingham & Fletcher 2008, Zador et al. 2008).

PBR is a threshold of additional annual mortality, which could be sustained by the population, and is calculated with minimal demographic information using the following equation:

$$PBR = \frac{1}{2} R_{\max} N_{\min} f \qquad (1)$$

where R_{max} is the maximum annual recruitment rate calculated as

$$R_{max} = \lambda_{max} - 1, \qquad (2)$$

where λ_{max} is the maximum annual population growth rate. By using N_{min} defined as the 20th percentile of the population estimate, and the recovery factor f, ranging between 0.1 and 1 the equation acknowledges uncertainty in the estimates of population size and growth rates (Wade 1998, Niel & Lebreton 2005).

PBR is also a conservative metric and accounts for potential bias due to density dependence, uncertainty in estimates of the population size and stochasticity (Wade 1998, Taylor et al. 2000, Milner-Gulland & Akçakaya 2001). Niel and Lebreton (2005) estimated the maximum annual population growth rate for long-lived bird species using only annual adult survival probability s and the age of first reproduction α in the following equation:

$$\lambda_{\max} = \exp\left(\left(\alpha + \frac{S_{ad}}{\lambda_{\max} - S_{ad}}\right)^{-1}\right) \qquad (3)$$

The main advantage of this approach is that it relies on those demographic parameters which are easiest to obtain for many bird species. The PBR concept is widely used to guide conservation and management of marine mammals (Taylor et al. 2003, Marsh et al. 2004) and has been demonstrated as a useful tool to assess impacts of fisheries by-catch mortality (Niel & Lebreton 2005, Dillingham & Fletcher 2008, Žydelis et al. 2009). Additive mortality exceeding PBR would indicate potentially overexploited populations.

The Red-throated Diver population in NW Europe is believed to be stable or increasing (BirdLife International 2004, Delany & Scott 2006, Dillon et al. 2009), therefore following Dillingham & Fletcher (2008) a recovery factor f = 0.5 was set, as for stable populations.

3 RESULTS

3.1 Assessment of survey data

It was identified that a total of 367 survey days of data (236 boat days and 131 aerial days) between 28/10/2001 and 21/02/2010. However, only a subset of these data (29 % = 105 boat and aerial surveys) was used to focus on winters of 2003/2004, 2004/2005 and 2005/2006. It was relied upon data being available for both observations and survey tracks. However, in many circumstances datasets were either missing or un-extractable from pre-processed files such as GIS dbf files. For Greater Gabbard, 18/54 (33%) of boat survey days either had no tracks or no extractable observation data from processed shapefiles and dbf files. Likewise 3/19 (16%) of DTI aerial bird surveys in London Array suffered the same problems. Duplicate data from aerial surveys of the Gabbard wind farm and some aerial surveys of the Gunfleet Sands wind farm were also contained within Thanet aerial surveys.

In total, the Thanet aerial visual data used in this study covered an area of 8462.63 km^2. These data were already archived on an Access database and thus track and observational data were extracted and processed. Aerial visual data for Thanet covered seven zones. For all Thanet aerial surveys (32, 30/10/2004 - 07/03/2006) there was adequate match-up between observations available throughout 2004, 2005 and 2006. These data therefore encompassed winters of 2003/04, 2004/05 and 2005/06, at a time when Red-throated Divers are at peak abundance within the Greater Thames area. Thanet boat data covered 15 survey days (10/12/2004 - 14/04/2006), over an area of 106.35 km^2, and also had suitable match-up between boat GPS tracks and observations. For Thanet, additional surveys were available for 2008/2009 winter through 2009 and 2009/10 winter during construction of the wind farm (20 survey days).

The use of the Gunfleet Sands aerial visual data proved more problematic. While observational data were easily extractable and thus available, information on survey tracks were not so forthcoming and were either not available or contained within files in which the data proved difficult to extract. Therefore, for those surveys not overlapping Thanet, in total 78 aerial survey days (16/08/2002 - 09/03/2008) were not included. Likewise, boat data from Gunfleet Sands suffered similar issues, including sometimes only having summary information rather than raw observational data, thus exactly 100 boat survey days spanning 28/10/2001 - 13/03/2009 were excluded from further analysis.

DTI aerial bird surveys for London Array were all useable and all but three surveys out of 18 days had suitable observational and track data that matched (21/08/2002 - 05/03/2005). DTI London Array survey data used in this study covered an area of 6561.98 km^2. High-definition digital image survey data collected for London Array by APEM were all available. Boat data from London Array, 45 survey days (03/10/2002 - 09/12/2004), were not used in this study due to lack of GPSU information from boat tracks.

Gabbard data were not contained in original files, but were stored for use from a previous Environmental Impact Assessment carried out by BTO. Aerial visual data were contained within the Thanet group of surveys, however, an additional 54 boat survey days (14/02/2004-16/04/2006) were available, of which 36 (66%) were available and contained both track and observation data. Gabbard Boat data used in this study covered an area of 741.68 km^2.

An optional improvement in processing methods would be to use arbitrary straight line distances through observed geo-referenced bird positions, taking arbitrary selections along the track. However, this would have resulted in a disparity in quality of data and thus was not a favoured approach.

3.2 Distance correction

3.2.1 Thanet and London Array Aerial visual data (no stratification)

For all divers, including Red-throated, Black-throated and unidentified diver species (Figure 20), the best initial detection model was a hazard/cosine function (AICc =17930, Chi-p -1.0, 2.05% CV, df = 8867). Thus, the function was defined as: f(0) = 0.0038432, CI = 0.0036921 - 0.0040004, ESW = 260.20, CI = 249.97-270.85; p = 0.26020, CI = 0.24997 - 0.27085). Truncating the final distance band (i.e. excluding 426-1000 m), the best initial model was a hazard/hermite function (AICc = 17290, Chi-p -1.0, 1.17% CV, df = 8816). Thus the function was defined as: f(0) = 0.0038119, CI = 0.0037256 - 0.0039002, ESW = 262.34, CI = 256.39-268.41; p = 0.61581, CI = 0.60186 - 0.63008)

A

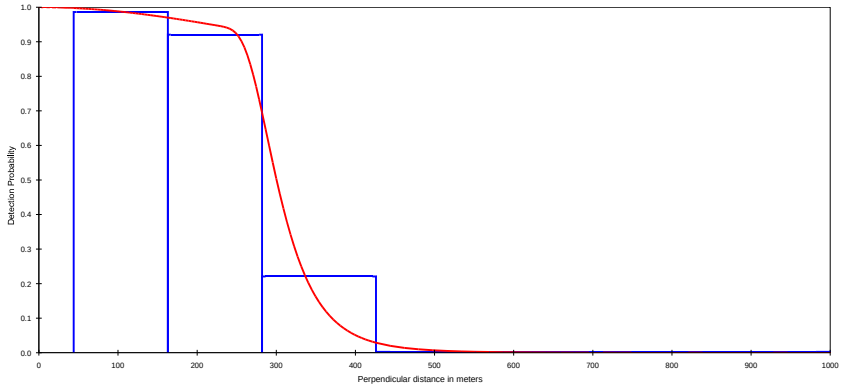

B

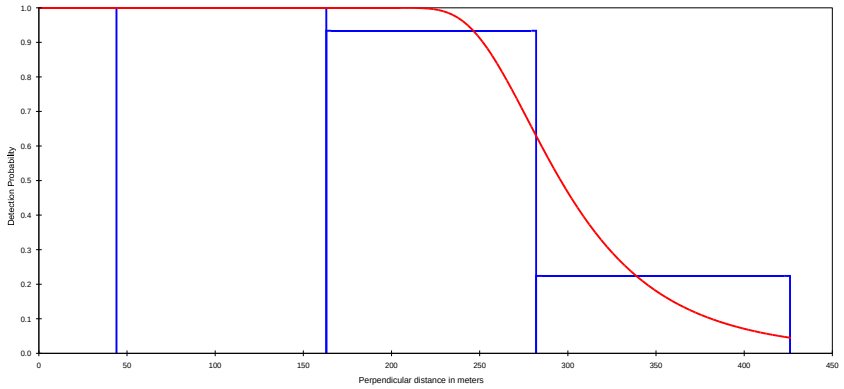

***Figure 20**. Detection functions for all diver species for London Array and Thanet aerial visual data for (A) all distance bands and (B) truncated, 426-1000 m band excluded.*

For the analysis of Red-throated Divers as the only species (Figure 21), the best initial detection model was a hazard/cosine function (AICc = 3779.2, Chi-p -1.0, 3.66% CV, df = 1792). Thus the function was defined as: f(0) = 0.0047451, CI = 0.0044163 - 0.0050983, ESW = 210.74, CI = 196.14-226.43; p = 0.21074, CI = 0.19614 - 0.22643). Truncating the final distance band (i.e. excluding 426-1000 m), the best initial model was a Uniform/Cosine function (AICc = 3385.9, Chi-p -1.0, 5.03% CV, df = 1752). Thus the function was defined as: f(0) = 0.0048130, CI

= 0.0043613- 0.0053116, ESW = 207.77, CI = 188.27-229.29; p = 0.48772, CI = 0.44195 - 0.53824).

A

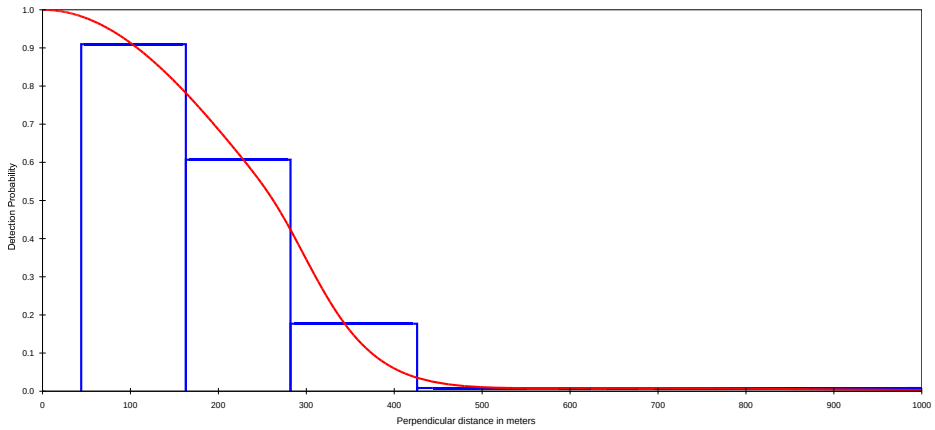

B

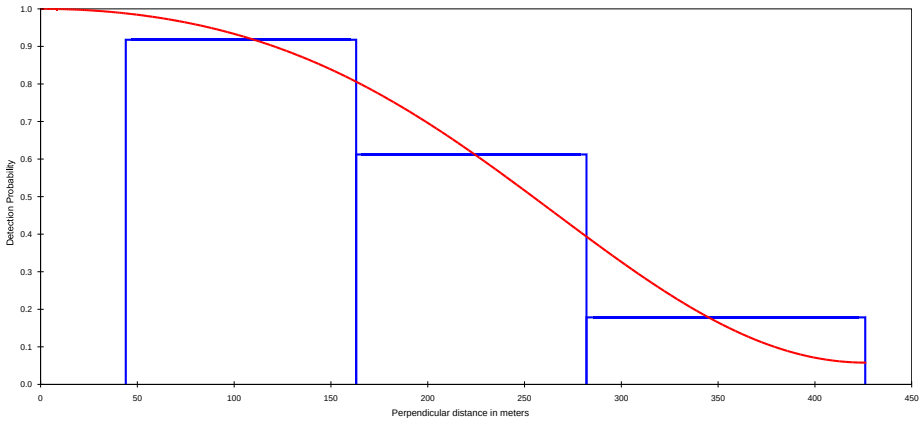

***Figure 21**. Detection functions for Red-throated Divers only for London Array and Thanet aerial visual data for (A) all distance bands and (B) truncated, 426-1000 m band excluded.*

3.2.2 Gabbard and Thanet Boat data (no stratification)

The best initial detection model was a uniform/cosine function (AICc = 332.30, Chi-p 0.43780), with a single straight line and no apparent drop of detectability. Thus the function was: f(0) = 0.0033, 0% CV, df = 126, CI = 0.0033-0.0033, and ESW = 300.0, 0% CV, df = 126, CI = 300-300)

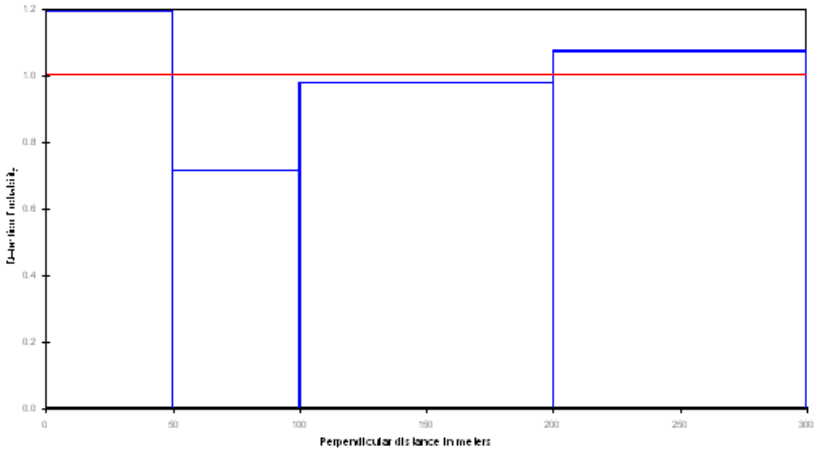

***Figure 22**. Detection function for Gabbard and Thanet boat data combined, n.b. truncation of final distances band and separation of Red-throated Divers from the rest of the divers gave similar results.*

3.3 Final corrections and stratifying for wave data

For final application to the aerial visual data, the wave-stratified detection function was used for all diver species due to lower CV (Figure 23). The final distance band was also retained, owing to greater inflation of CV from truncation – see below.

3.3.1 Thanet and London Array (wave corrected)

Approximately 7-8% fewer divers were observed when maximum wave heights were higher than 1.2 m. The final best model was one with a hazard/cosine function. The detection function was defined as follows for stratum 1: f(0) = 0.0032897, CI = 0.0032376 - 0.0033425, ESW = 303.98, CI = 299.17-308.87; p = 0.30398, CI = 0.29917 -0.30887 (AIC = 9622.7, Chi-p -0.0017134, % CV 0.81, df = 4346).

For stratum 2, the detection function was defined as follows: f(0) = 0.0044013, CI = 0.0041752 - 0.0046395, ESW = 227.21, CI = 215.54-239.51; p = 0.22721, CI = 0.21554-0.23951 (AIC = 1742.9, Chi-p -0.0046526, % CV 2.69, df = 1060).

The apparent drop in the probability of detection ("p") for divers was notable, decreasing from 0.30 to 0.23 with no overlap in confidence limits, suggesting a significant difference. Therefore this model was retained and applied this function to the aerial density data.

3.3.2 Gabbard and Thanet Boat data

After investigation, no wave stratification was applied to the boat data since there was no apparent drop off in detectability. This could have been caused by a sampling bias, with observers adding birds from outside the transect causing heaping in the outer two bands.

A; Stratum 1

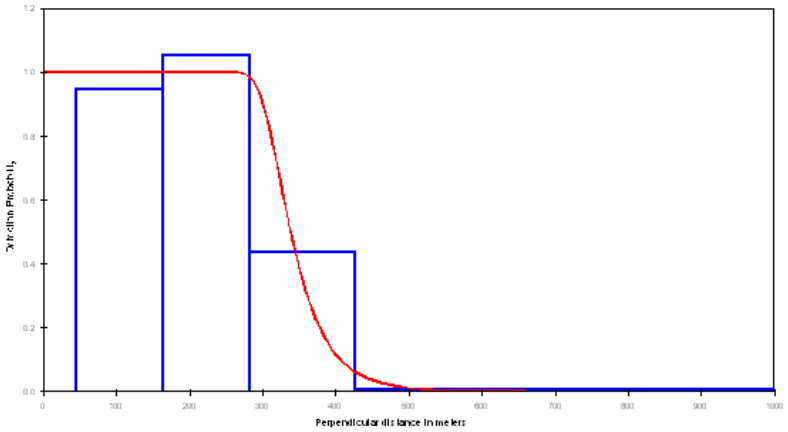

B; Stratum 2

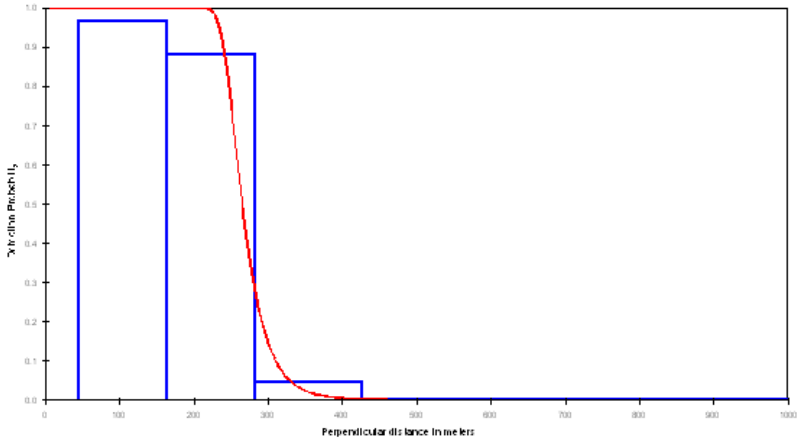

***Figure 23**. Detectability function incorporating wave data; data were stratified into (A) those days where surveys were conducted in conditions of less than 1.2 m wave height, and (B) those days where maximum wave heights exceeded 1.2 m.*

3.4 Comparison between visual and digital survey data

Two, two-part GAMs were fitted for comparison between visual and digital survey data. One model was fitted based on visual data and the other based on digital data, collected during the winter 2009-2010. The approximate significance of the smooth terms included in the models is shown in table 6 and table 7, and the response curves are displayed in Figure 24. The same set of variables was chosen for both models. In the presence/absence part current velocities U and V, current speed, current gradient, water level, ship densities and an interaction term between X and Y coordinates were included. In the positive part, current velocities U and V, current speed, vorticity, water level, and an interaction term between X and Y coordinates were included. The resulting response curves are very similar in both data sets (Figure 24).

Table 6. *Smooth terms with associated approximate significance and chi-square/F statistics for the model based on visual data. Variables not included in the final model are indicated with a dash.*

Smooth terms	Presence/absence		Positive denstiy	
	chi-sqr	p	F	p
Velocity U	7.677	0.05	5.470	0.02
Velocity V	19.474	<0.01	2.150	0.14
Current speed	0.469	0.49	0.225	0.64
Vorticity	-	-	3.282	0.01
Current gradient	1.928	0.16	-	-
Water level	14.955	<0.01	6.174	0.01
Ship densities	2.774	0.10	-	-
X,Y	45.254	<0.01	2.565	0.01

Table 7. *Smooth terms with associated approximate significance and chi-square/F statistics for the model based on digital data. Variables not included in the final model are indicated with a dash.*

Smooth terms	Presence/absence		Positive denstiy	
	chi-sqr	p	F	p
Velocity U	7.198	0.09	5.826	<0.01
Velocity V	9.556	0.03	4.162	<0.01
Current speed	3.444	0.06	3.414	0.01
Vorticity			1.963	0.16
Current gradient	0.640	0.49		-
Water level	8.928	0.17	0.097	0.76
Ship densities	2.126	0.14		-
X,Y	28.327	<0.01	9.172	<0.01

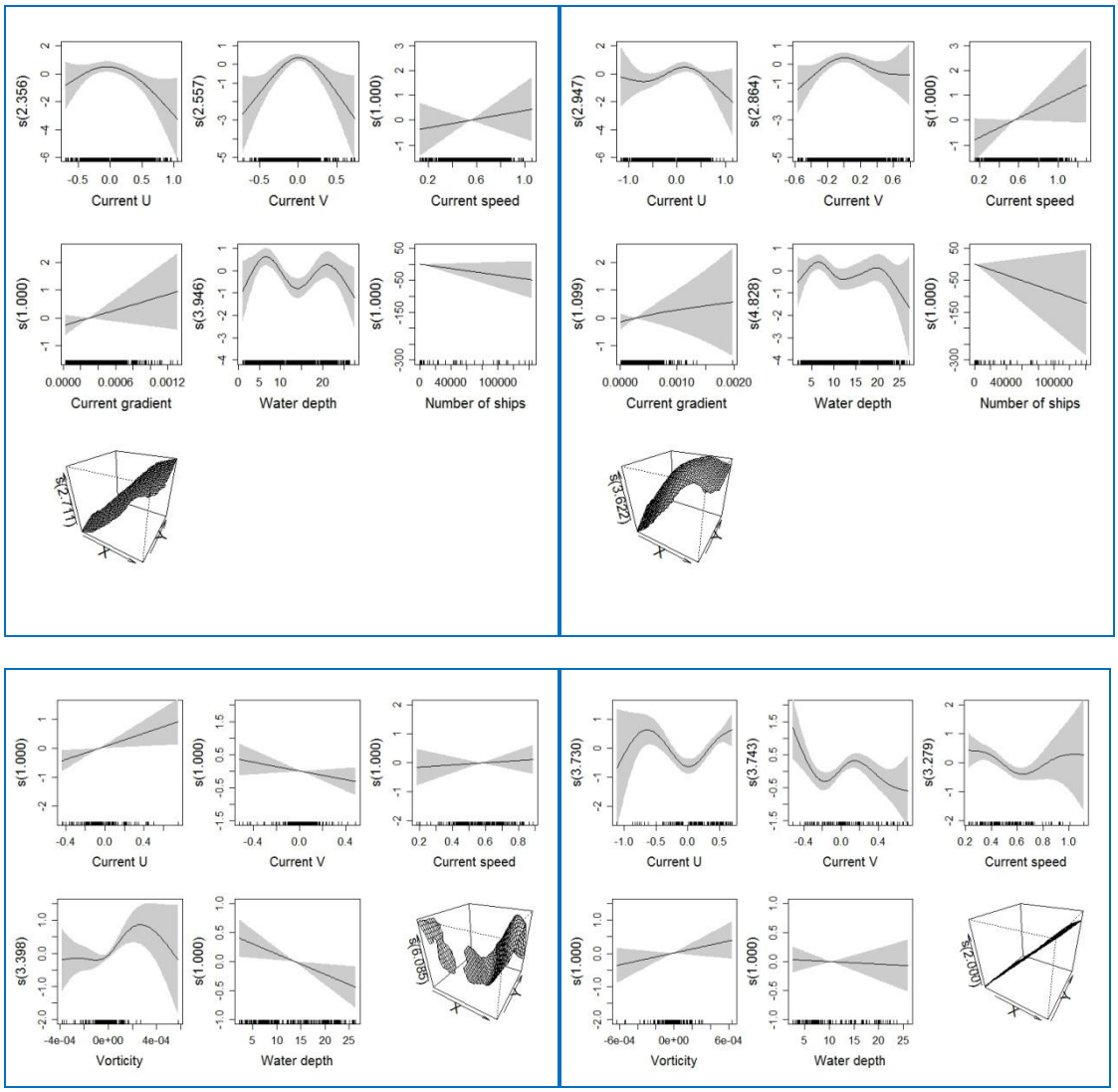

***Figure 24**. Partial GAM plots for the visual model (to the left) and digital model (to the right). The presence/absence parts are shown above and the positive part below. The values of the environmental variables are shown on the X-axis and the probability on the Y-axis in logit scale. The degree of smoothing is indicated in the legend of the Y-axis. The dotted lines and shaded areas show±1standard errors. For the 2-d term (X,Y) a perspective plot is shown, with the degree of smoothing indicated as a label to the Z-axis.*

Spatial autocorrelation was tested for in the model residuals by defining the nearest neighbourhood to 1500 m and calculating the Moran's I value over 10 lag (1 lag = 1500 m). It was found only significant spatial autocorrelation in one lag in the presence/absence part of the model based on the visual data. The Moran's I value was very low, however, only 0.046 (Moran's I ranges from -1 to 1). It was therefore concluded that spatial autocorrelation in model residual did not affect the model results.

The predictive ability of the models was tested by withdrawing 30% of the data for evaluation. Following this, the predictive ability of the presence-absence part was tested by using AUC and the final combined models by Spearman's correlation coefficient. Both models had a reasonable predictive accuracy, with the digital data displaying the highest predictive power both for the P/A part and for the positive (density) part (Table 8).

Table 8. *Evaluation statistics for the two models based on visual respectively digital data. Deviance explained for the presence/absence part of the model and for the positive (density) part. AUC values are shown for the presence/absence part and the Spearman Rank correlation for the final combined model.*

	Dev. Exp. P/A	Dev. Exp. positive	AUC	Spearman Rank correlation
Visual model	36.8	25.7	0.694	0.24
Digital model	13.8	48.4	0.848	0.44

Finally the predictions of the two models were compared, both regarding spatial patterns and estimated densities. The spatial patterns were similar (Figures 26-27), but the model based on digital data produced higher densities (Figure 25). Higher densities were expected as more birds were counted by the digital surveys in comparison to the visual surveys.

To visualise the agreement between the predictions the predicted densities (and probabilities) were plotted based on visual surveys against the digital surveys (Figure 28). Spearman's correlation between the presence/absence predictions was 0.864 and between predicted densities 0.894. It can therefore conclude that the two types of data produce similar patterns and order of the predictions although the digital data produce higher densities. As also the responses to the environmental data are very similar in the models based on both types of data, it can be concluded that the inclusion of both types of data in further analyses would be correct.

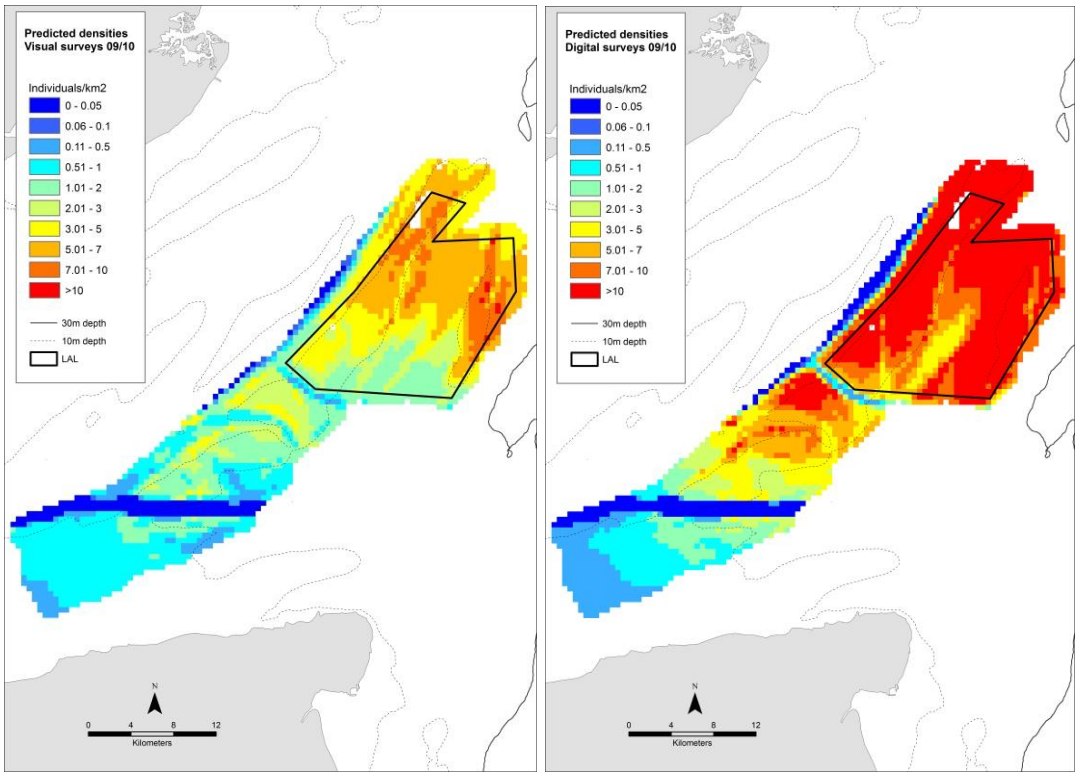

Figure 25*. Predicted densities based on visual data to the left and based on digital data to the right.*

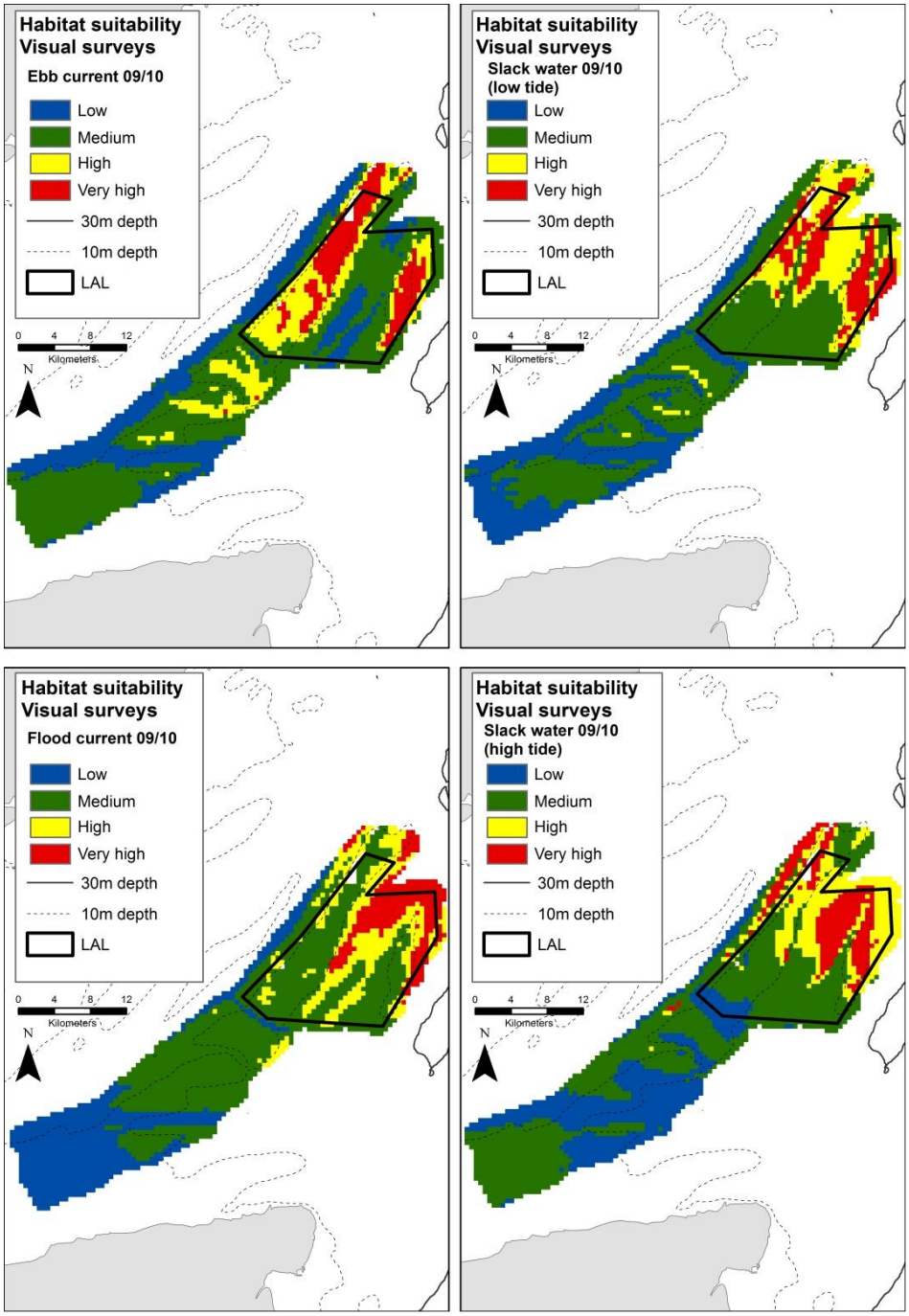

***Figure 26**. Habitat suitability during the four different flow phases based on visual data.*

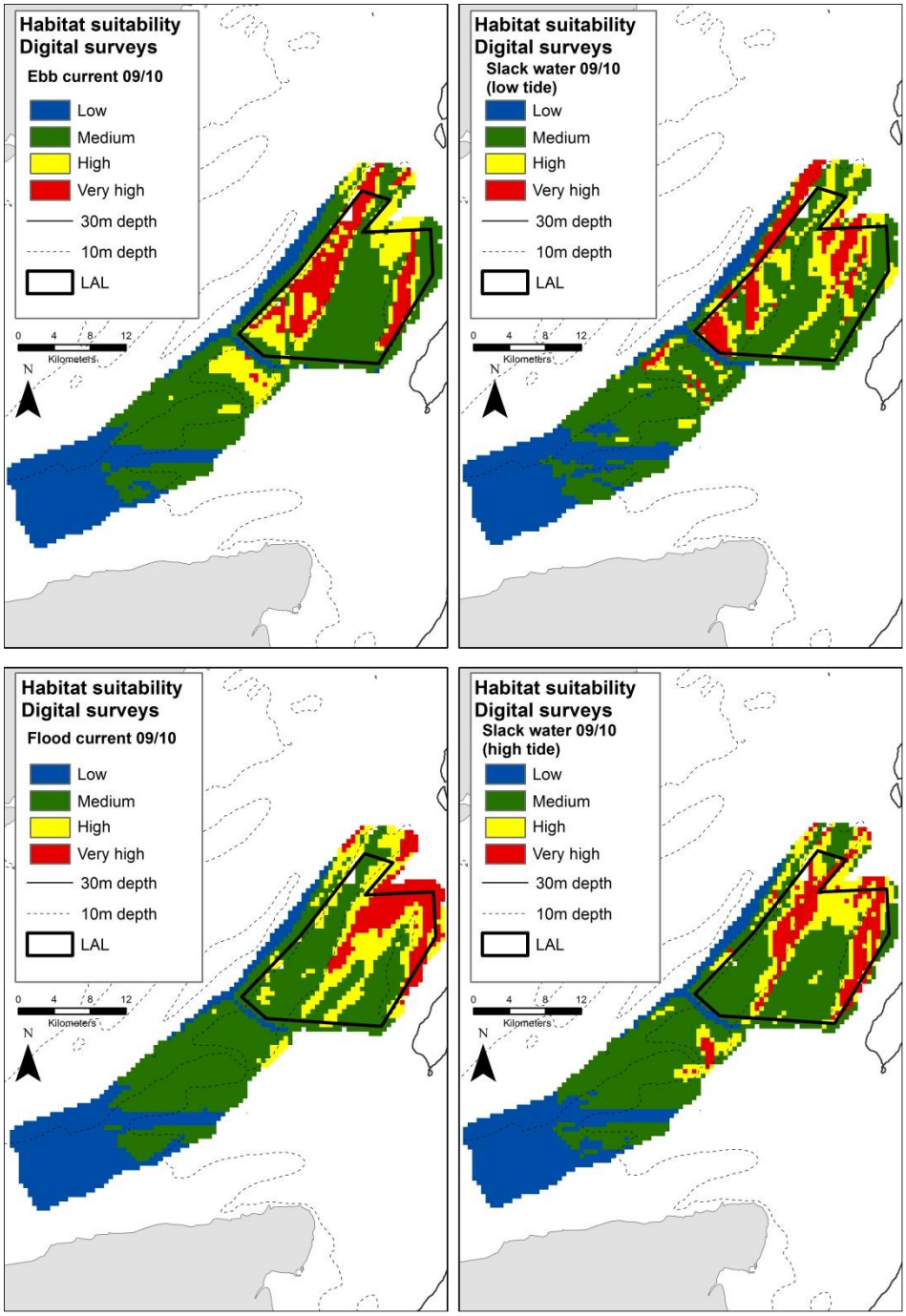

***Figure 27**. Habitat suitability during the four different flow phases based on digital data.*

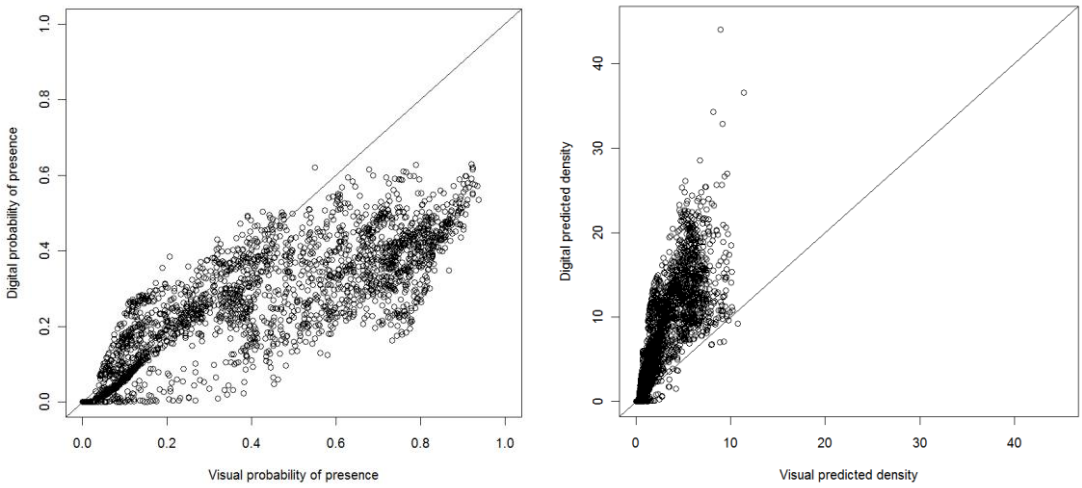

***Figure 28**. The predicted probability based on visual data is plotted (to the left) against the predicted probability modelled based on digital data. The same with predicted density is plotted to the right. The straight 45 degree line indicates perfect agreement.*

3.5 Aggregative responses in survey data

The geo-statistical analyses of the aerial diver data in the southern part of the Outer Thames Estuary revealed rather consistent results in terms of the spatial structures at lower scales. The structures deduced from variograms of aerial surveys in this region between 2003 and 2006 have been listed in Table 9. Range values indicated aggregative responses at spatial scales between 1400 and 2300 m, and prominent anisotropies present in the data, - mostly with main directions between north and east. The discrete scale of the aggregative response indicates a high degree of patchiness, and aggregations occurring mainly within small-scale habitats. Examples of the dispersion of diver observations and related variograms are shown in Figure 29.

16.2. 2004

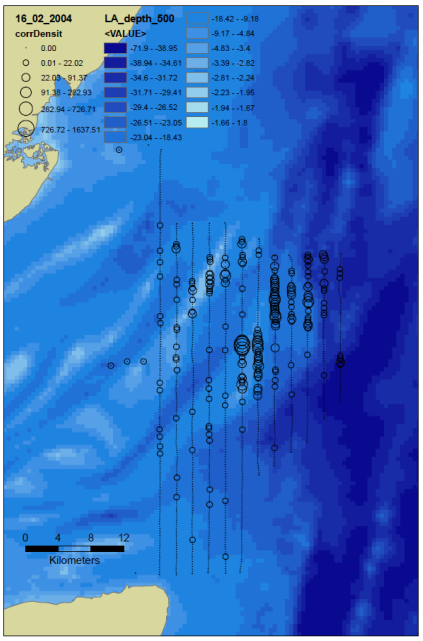

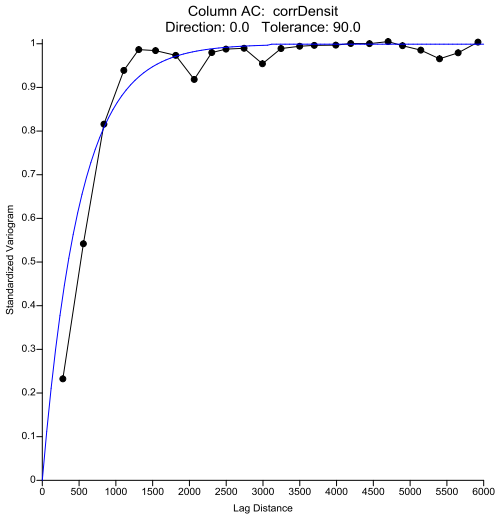

Anisotropy: ratio 2, angle 79.79 (N)

7.3.2005

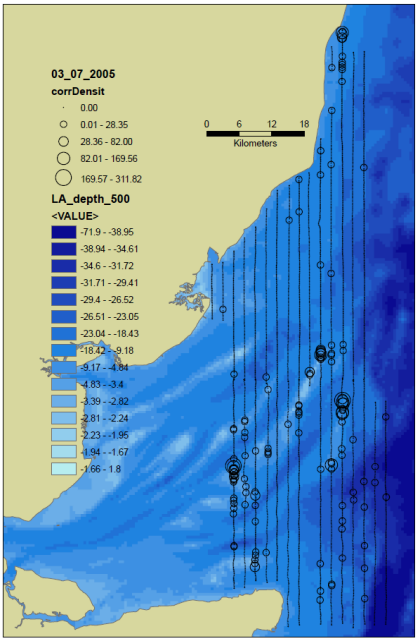

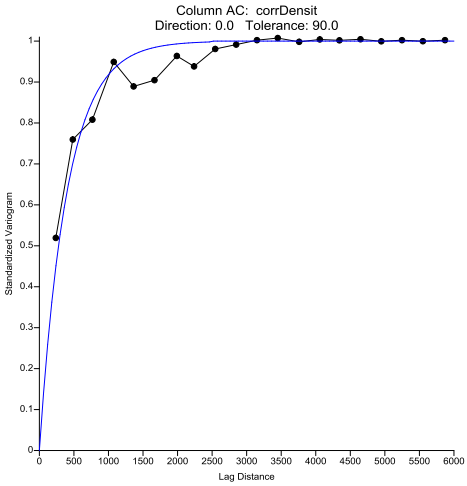

Anisotropy: ratio 2, angle 90 (N)

Figure 29. *Examples of variagrams for two surveys around the LAOWF site.*

***Table 9**. Range, anisotropy ratio and angle of aerial survey data of divers from 2003 to 2006 determined by geo-statical analysis. Surveys covering the main part of the Outer Thames Estuary were selected.*

Day	Range	Anisotropy ratio	Anisotropy angle
27/11 2003	1200	1.2	50
17/12 2003	1500	2	70
15/2 2004	1500	2	5
16/2 2004	1500	2	10
12/4 2004	2100	2	0
12/5 2004	1500	2	7
14/1 2005	2100	2	27
15/1 2005	2100	2	0
13/3 2005	2000	2	31
15/3 2005	1800	2	0
7/3 2005	2300	2	0
13/1 2006	2000	2	61
14/1 2006	1500	0	-
3/2 2006	2200	1.3	58
18/2 2006	1400	1.2	35

3.6 Pure tidal model prediction performances

As it has been mentioned previously, it is necessary to ensure that the propagation of the pure tidal wave along the North Sea and the English Channel is represented accurately enough to provide a good basis to model the dynamics in the region, including tide and surge and integrating data assimilation. Consequently, the pure tidal predictions of the 2D regional model have been analysed through the derivation of the tidal constituents from the harmonic decomposition of a 6-month tidal period using the IOS method (by Foreman et al. (1977, 1978).

For tidal periods shorter than 1 year, a number of main constituents cannot be analysed and the amplitude and phase of the calculated main constituents will include, in addition to the effect of their satellite, inference of the non-analysed main constituents. However, using a 6-month tidal period yields to a relatively accurate analysis of 48 constituents out of 69, which accounts for about 95% of the total tidal-raising force. Table 10 describes the main constituents taken into account for the tidal decomposition.

Table 10. *Description of main tidal constituents.*

Constituents		Period
Name	**Symbol**	**(hrs)**
Principal Lunar	M2	12.42
Principal Solar	S2	12
Larger Elliptical Lunar	N2	12.66
Luni-Solar Declinational	K2	11.97
Luni-Solar Declinational	K1	23.93
Principal Lunar	O1	25.82
Principal Solar	P1	24.07

The main semi-diurnal and diurnal tidal constituents, M2, N2, S2, K1 and O1 resulting from the decomposition of the modelled tidal signal have been compared against measured tidal constituents at ten stations located within the North Sea and the English Channel. Figure 30 indicates their location and Table 11 to 15 indicate measured and predicted amplitudes and phases of the five constituents.

From a general perspective, the predicted semi-diurnal constituents' characteristics fit fairly well with the measurements. Their amplitudes are on average captured properly with a maximum difference compared to the measurements of 0.06m, and phases fit reasonably well with measurements except for N2, which presents an averaged deviation in phase lag of 27 degree. At the southern part of the North Sea, the M2 component is governed by the presence of an amphidromic point located slightly south of K-13, a small spatial deviation of this point and the tidal signal within this area is automatically disturbed, but Table 7 indicates clearly that the latter has been well captured.

It can be observed that along the English Channel; at Cherbourg and Newlyn, the tidal predictions are good with a difference in amplitude and phase not exceeding 0.06m and 7 degree respectively. Along the east coast of UK; at Lerwick, Wick, North Shields and Aberdeen, the results are reasonable presenting, however, a tendency to over-predict the phase is evident. In deep water, at K-13 and Ekofisk, predictions match perfectly with the measurements and at Lowestoft and Dover, the maximum amplitude and phase difference between predictions and measurements are 0.05m and 8 degree.

Regarding the diurnal constituents, the amplitude of K1 is reduced by a factor of about 1.5 compared to the measurements, and phases are poorly captured with an averaged deviation of about 40 degree for O1 and K1. This might result in a small diurnal reduction of the amplitude and phase lag of the water level predictions. However, these errors are not crucial as the modelled domain is strongly dominated by semi-diurnal tide: impacts on the tidal forcing of K1 and O1 are less than 10% compared to the three main semi-diurnal constituents.

Thus, it can be concluded that the 2D regional model captures reasonably well the pure tidal propagation.

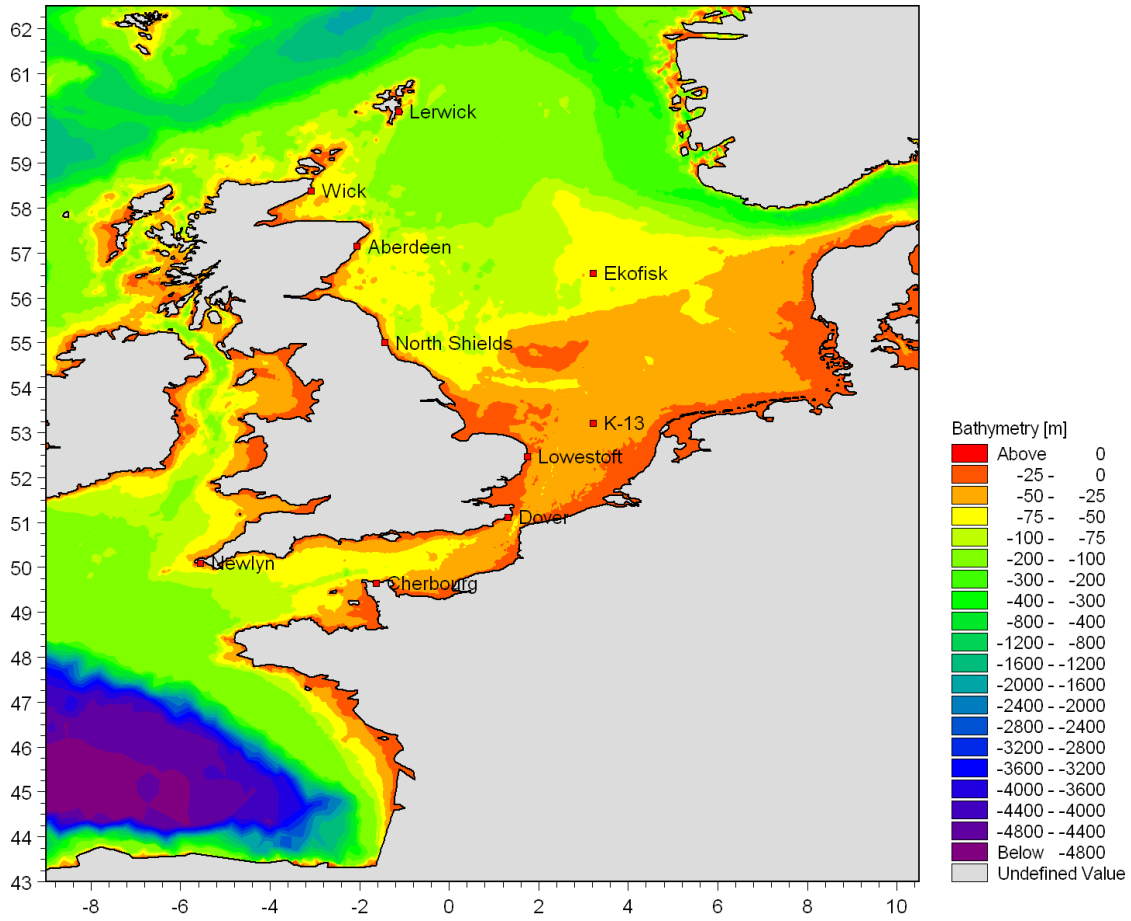

Figure 30. *Locations of the stations used for comparison between measured and modelled tidal components.*

Table 11. *Measured and modelled amplitude and phase of the M2 constituent at 10 stations.*

	M2-Amplitude (m)		M2-Greenwich Phase (deg)	
Station Name	Measured	Modelled	Measured	Modelled
Lowestoft	0.71	0.66	258	254
North Shields	1.56	1.58	89	93
Aberdeen	1.30	1.33	23	30
Ekofisk	0.28	0.27	78	80
Lerwick	0.58	0.58	312	319
Cherbourg	1.86	1.91	229	229
Dover	2.26	2.23	332	337
Wick	1.01	1.06	322	331
Newlyn	1.72	1.78	135	130
K-13	0.52	0.51	178	178
Averaged	1.18	1.19	196	211
Averaged difference	0.01		15	
Maximum difference	0.06		9	

Table 12. *Measured and modelled amplitude and phase of the S2 constituent at 10 stations.*

	S2-Amplitude (m)		S2-Greenwich Phase (deg)	
Station Name	**Measured**	**Modelled**	**Measured**	**Modelled**
Lowestoft	0.21	0.21	298	293
North Shields	0.53	0.53	130	134
Aberdeen	0.45	0.45	60	69
Ekofisk	0.08	0.08	111	117
Lerwick	0.21	0.21	346	355
Cherbourg	0.70	0.70	271	272
Dover	0.71	0.69	24	29
Wick	0.35	0.38	0	9
Newlyn	0.58	0.60	179	173
K-13	0.19	0.18	234	234
Averaged	0.40	0.40	165	169
Averaged difference	0.00		0	
Maximum difference	0.03		9	

Table 13. *Measured and modelled amplitude and phase of the N2 constituent at 10 stations.*

	N2-Amplitude (m)		N2-Greenwich Phase (deg)	
Station Name	Measured	Modelled	Measured	Modelled
Lowestoft	0.14	0.13	230	222
North Shields	0.32	0.31	35	67
Aberdeen	0.25	0.27	0	5
Ekofisk	0.06	0.06	51	52
Lerwick	0.12	0.12	290	297
Cherbourg	0.36	0.39	210	209
Dover	0.41	0.40	310	313
Wick	0.2	0.22	301	308
Newlyn	0.33	0.35	116	109
K-13	0.1	0.10	162	162
Averaged	0.23	0.23	184	211
Averaged difference	0.00		27	
Maximum difference	0.03		32	

Table 14. *Measured and modelled amplitude and phase of the K1 constituent at 10 stations.*

	K1-Amplitude (m)		K1-Greenwich Phase (deg)	
Station Name	Measured	Modelled	Measured	Modelled
Lowestoft	0.12	0.20	332	287
North Shields	0.11	0.21	240	205
Aberdeen	0.11	0.19	204	173
Ekofisk	0.03	0.04	273	233
Lerwick	0.08	0.15	164	143
Cherbourg	0.08	0.16	117	111
Dover	0.05	0.06	43	316
Wick	0.11	0.18	175	148
Newlyn	0.06	0.10	112	100
K-13	0.08	0.15	332	295
Averaged	0.08	0.14	240	201
Averaged difference	0.06		39	
Maximum difference	0.10		87	

Table 15. *Measured and modelled amplitude and phase of the O1 constituent at 10 stations.*

	O1-Amplitude (m)		O1-Greenwich Phase (deg)	
Station Name	Measured	Modelled	Measured	Modelled
Lowestoft	0.14	0.17	159	204
North Shields	0.14	0.18	81	126
Aberdeen	0.14	0.16	48	94
Ekofisk	0.03	0.04	104	163
Lerwick	0.08	0.10	31	63
Cherbourg	0.06	0.10	351	351
Dover	0.06	0.08	177	256
Wick	0.08	0.15	28	68
Newlyn	0.1	0.08	341	353
K-13	0.1	0.12	166	210
Averaged	0.09	0.12	149	189
Averaged difference	0.03		40	
Maximum difference	0.07		79	

3.7 Tide and surge prediction performances

Performances of the tide and surge hydrodynamic model assimilating water levels are examined in this section. Figure 31-34 represent 1-month comparisons between measured and predicted water levels at ten stations. Table 16 shows the root mean square error (RMSE) which has been calculated for the same stations over the entire hindcast period. This quality index used as a measure of the accuracy of the regional model is defined as follows:

$$RMSE = \sqrt{\frac{1}{N}\sum_{i=1}^{N}(Hp_i - Ho_i)^2}$$

Where H_o and H_p represent the observed and predicted water level and N is the number of time steps.

These results indicate clearly that the hydrodynamic predictions are accurate within the project area where the maximum RMSE of water level is found to be around 0.17m.

Along the North Sea water levels present a small diurnal amplification of the signal which tends to disappear further to the south of the North Sea. This pattern can also be seen from the RMSE calculated over the entire hindcast period evolving from 0.13m at Wick to 0.06m at Cromer. At Aberdeen, which has not been assimilated, the quality index remains below 0.15m indicating that the assimilation scheme is robust.

In the English Channel, water levels match perfectly with the measurements, which is confirmed by a computed RMSE of approximately 0.07m within the area.

Closer to the Thames Estuary, at the three validation stations the results are fairly reasonable. Despite Lowestoft and Felixstowe are characterised by a small bias and a slight amplification of the water levels, results are satisfying especially at Dover where a RMSE of approximately 0.1m has been calculated.

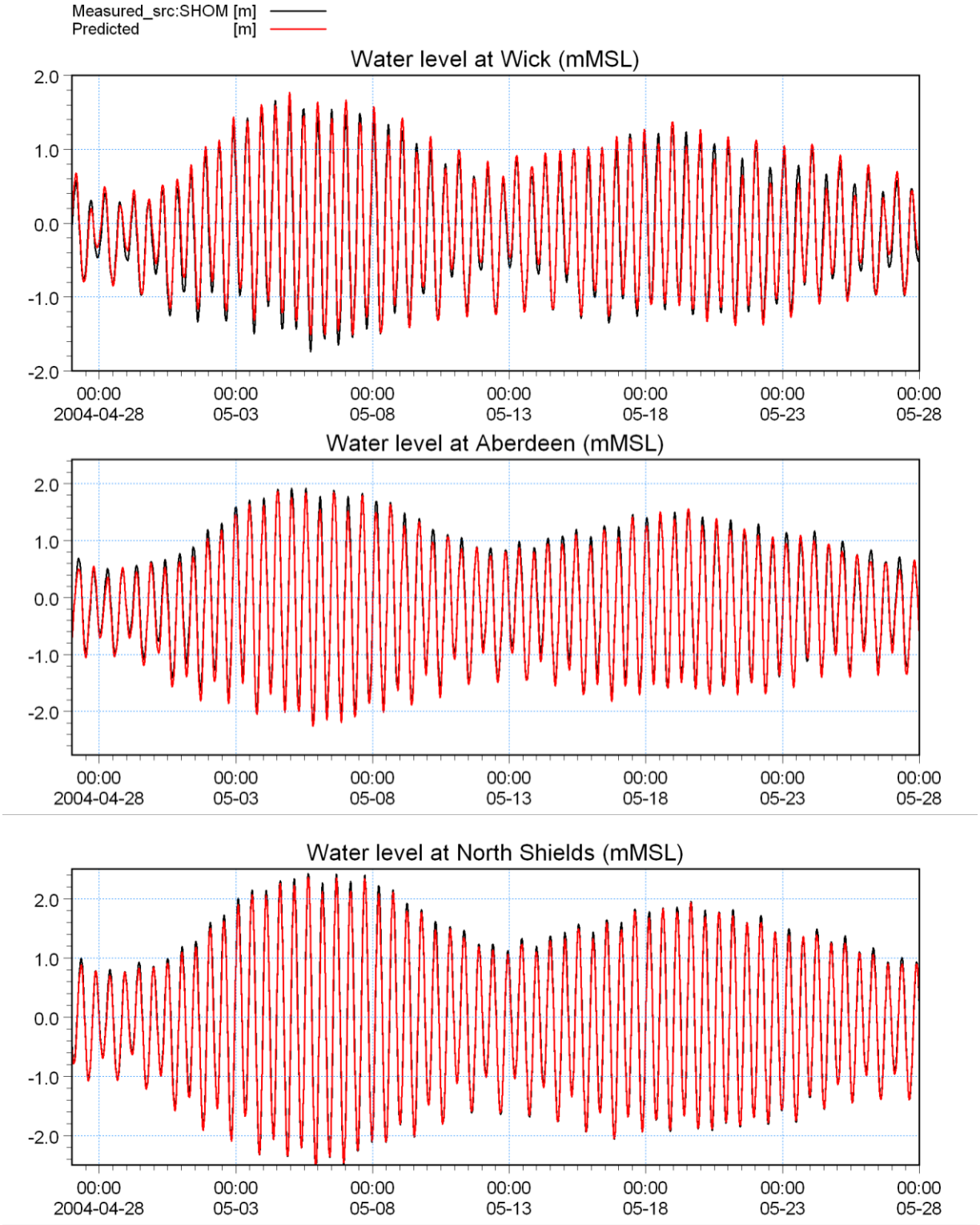

Figure 31. *Comparison of predicted (in red) and measured (in black) water levels at Wick, Aberdeen and North Shields from top to bottom.*

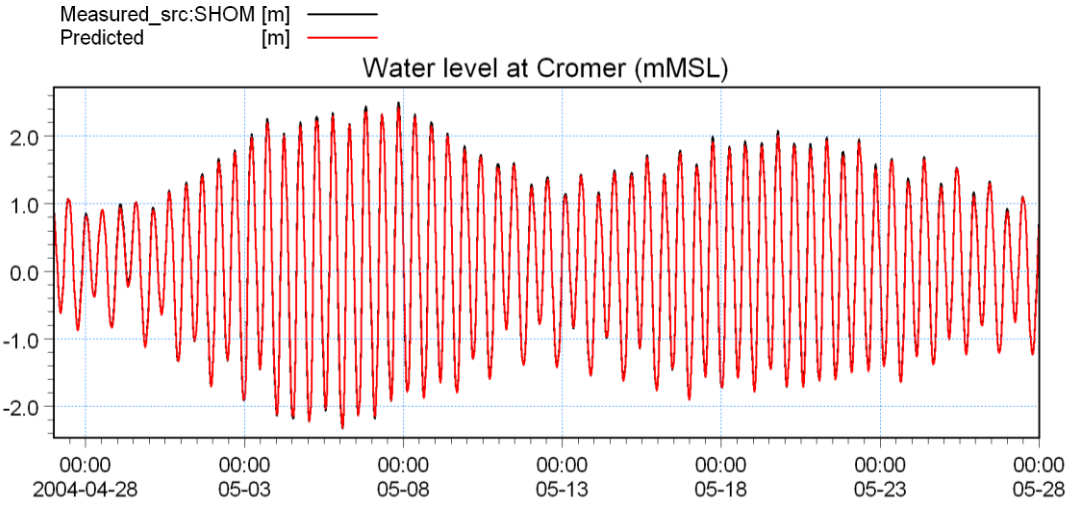

Figure 32. *Comparison of predicted (in red) and measured (in black) water levels at Cromer.*

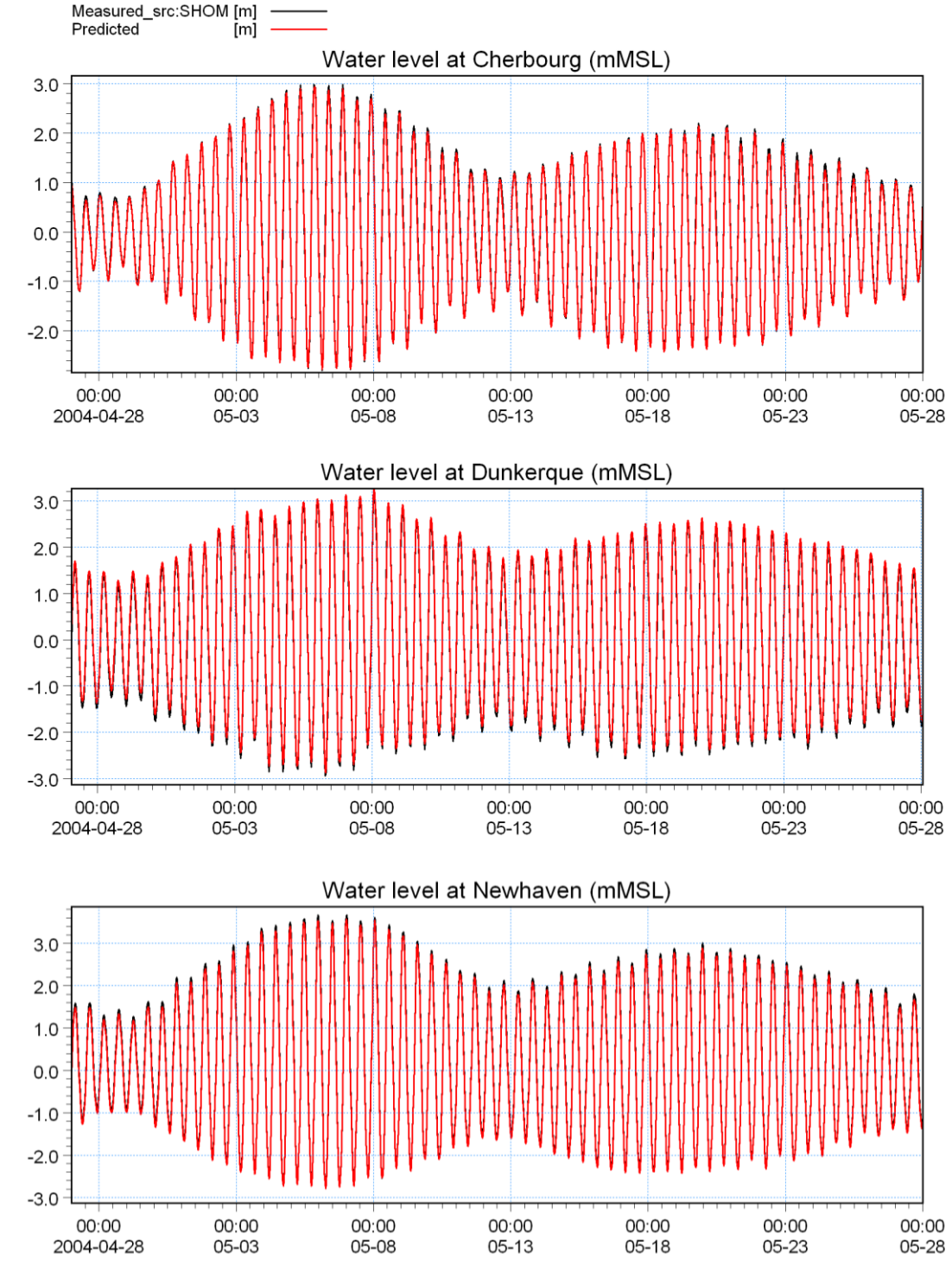

Figure 33. *Comparison of predicted (in red) and measured (in black) water levels at Cherbourg, Dunkerque and Newhaven from top to bottom.*

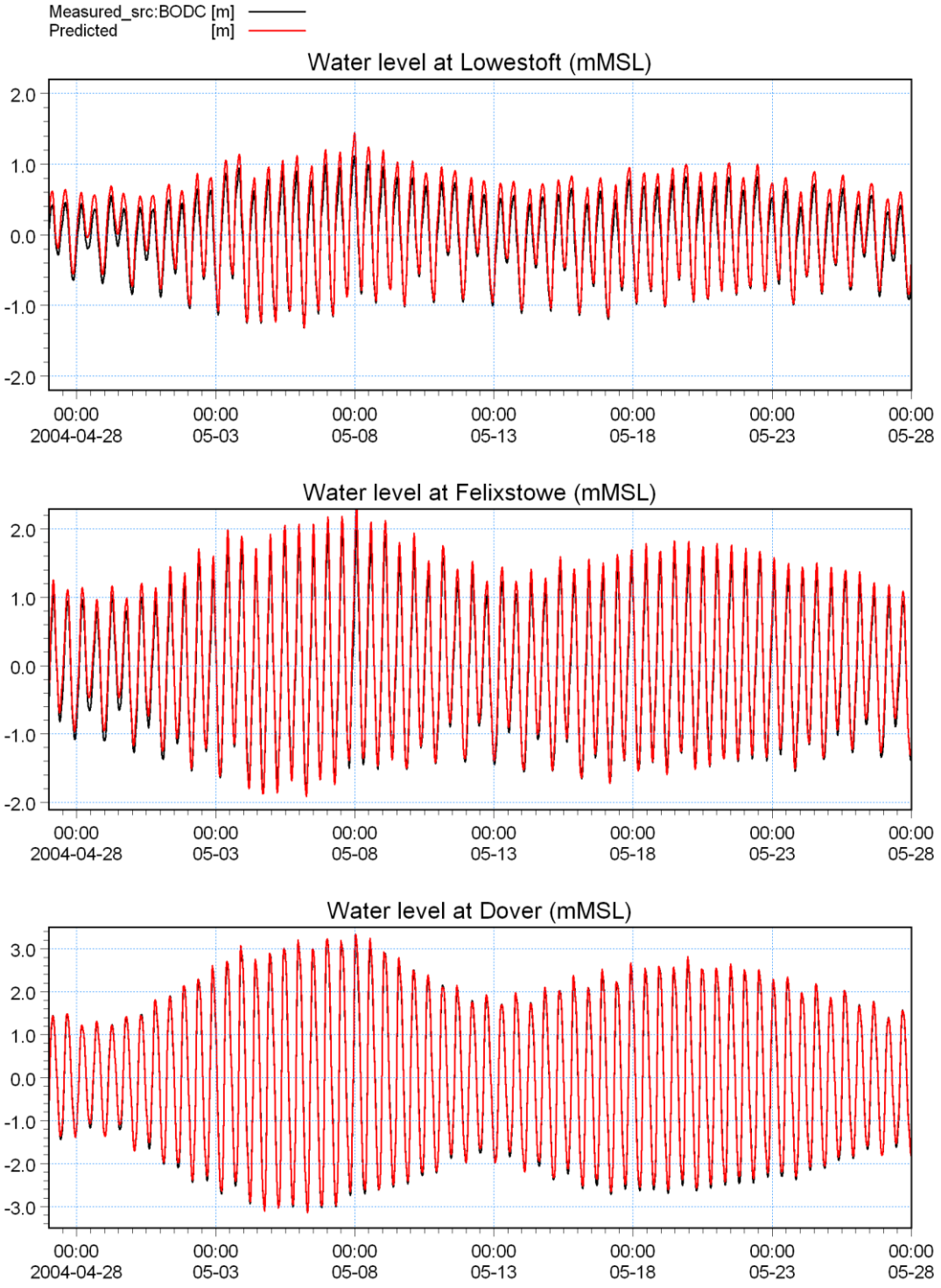

Figure 34. *Comparison of predicted (in red) and measured (in black) water levels at Lowestoft, Felixstowe and Dover from top to bottom.*

Table 16. *RMSE of the water levels predicted by the 2D regional model calculated over January 2002 to March 2006.*

Station	2002	2003	2004	2005	January 2006 - March 2006	January 2002 - March 2006
Aberdeen	0.12	0.11	0.13	0.13	0.14	0.12
Cherbourg	0.07	0.09	0.07	0.06	0.07	0.07
Cromer	0.06	0.05	0.05	0.06	0.06	0.06
Dover	0.12	0.11	0.10	0.09	0.11	0.10
Dunkerque	0.05	0.05	0.09	0.08	0.11	0.07
Felixstowe	0.17	0.15	0.17	0.17	0.16	0.16
Lowestoft	0.17	0.15	0.16	0.17	0.17	0.16
Newhaven	0.06	0.04	0.08	0.07	0.10	0.06
North Shields	0.06	0.05	0.06	0.07	0.07	0.06
Wick	0.12	0.13	0.12	0.14	0.14	0.13

3.8 Model Validation

Current measurements recorded within the LAOWF development area are available at Long Sand, Kentish Knock and Knock Deep for a number of periods. Based on this list, the period from 15 April to 2 June 2004 was selected as the validation period of the 3D local hydrodynamic model.

Figure 35 indicates comparisons between measured (black curve) and predicted (blue curve) water levels at Dover, Felixstowe and Lowestoft. Similar comparisons for the depth-averaged current intensity and direction as well as water levels at Kentish Knock, Knock Deep and Long Sand are shown in Figures 36-38. In addition, the statistic parameter RMSE defined previously has been computed for the water levels and current speeds at the six stations for the validation period, results are indicated in Table 17.

Water levels at Dover, Felixstowe and Lowestoft are reasonably predicted in terms of phase and amplitude. The RMSE is in the order of 0.15m - 0.25m at these three stations with a bias component of about 0.15m. Similar tendencies can be observed for water level predictions at Long Sand, Kentish Knock and Knock Deep which present a RMSE inferior to 0.3m. The hydrodynamic complexity within the Outer Thames Estuary induced by the presence of sand bars and channels is also well represented.

Indeed within the deep channel Knock Deep (Figure 37), ebb and flood tidal currents are oriented along a SW-NE axis, during the reverse of the tide, the flow follows a clockwise rotation which is well represented by the model. The channel is ebb-dominated and the maximum ebb-current reaches 1.2m/s, while during flood its magnitude presents a maximum of 1m/s. The predicted ebb-dominance within Knock Deep tends to be slightly smoothed out compared to the measurements, but a reasonable RMSE of less than 0.1m/s has been estimated for the validation period.

At Kentish Knock sand bank, the asymmetry current pattern characterised by a significantly higher ebb current peak is correctly reproduced by the model in terms of phase and magnitude characterised by a RMSE of less than 9cm/s. The predicted temporal current direction variation cycle matches well with measurements. At Long Sand bank, the flow is rotating during the entire tidal cycle. During fully developed flood and ebb currents at the adjacent channels, the flow at the Long Sand station is oriented WSW and ESE due to refraction of the current on the flank of the sand bank. The water moves almost perpendicularly to the bank during the current

reverse at the channels. Current peaks are well depicted in time but present, however, a slight difference in amplitude, the RMSE calculated for the current intensity is about 0.15m/s for the validation period.

From the above considerations, it can be concluded that the predictive power of the hydrodynamic model complex is strong and accurate hydrodynamic parameters have been supplied to the diver distribution models.

Table 17. *RMSE of the water levels and depth-averaged current intensity predicted by the 3D local model calculated over the validation period.*

	Water level	Current Speed
Station	**(m)**	**(m/s)**
Felixstowe	0.228	-
Lowestoft	0.141	-
Dover	0.2	-
Knock Deep	0.231	0.096
Kentish Knock	0.217	0.089
Long Sand	0.293	0.136

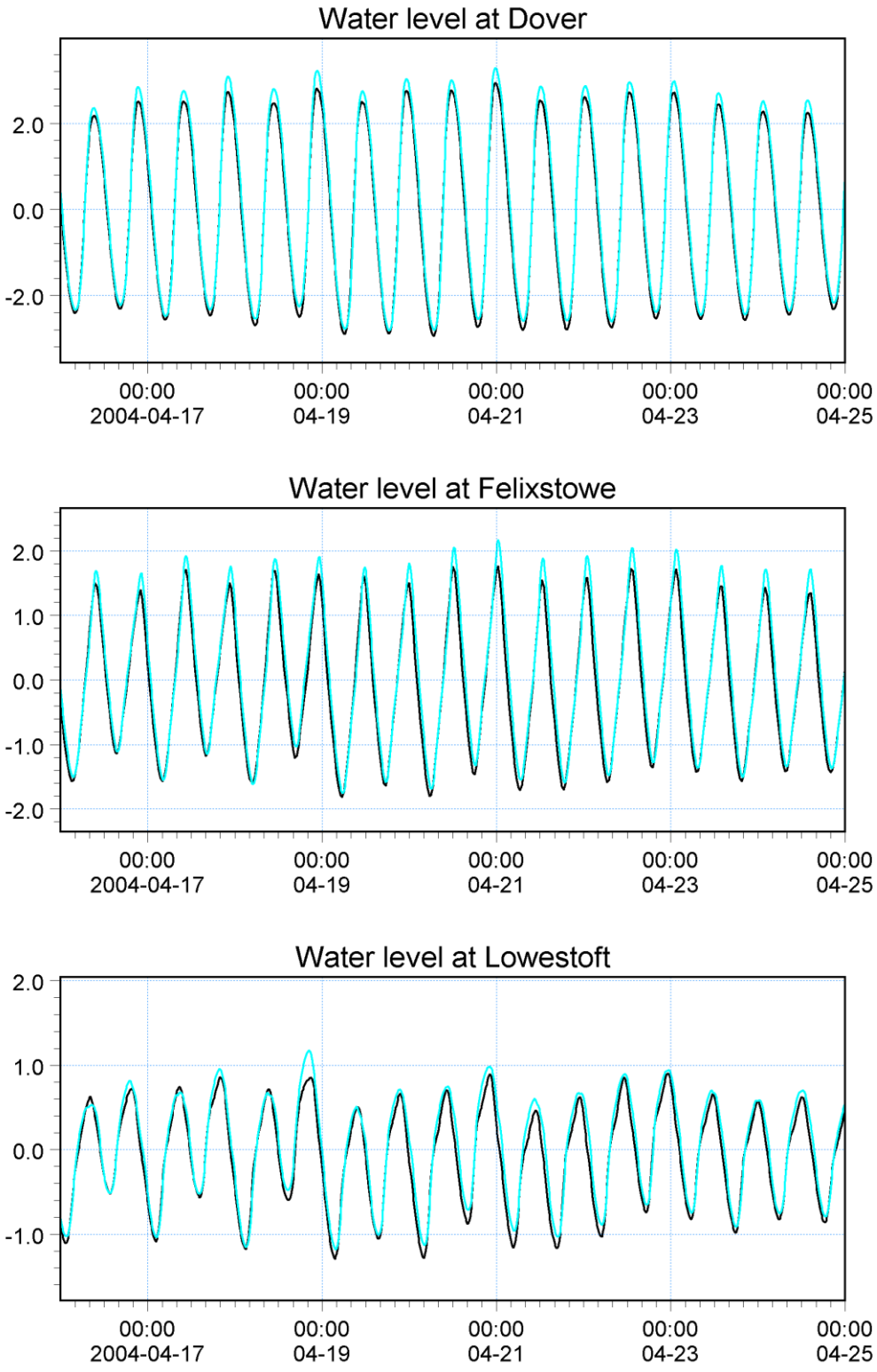

Figure 35. *Comparison of measured (black line) and predicted (blue line) water levels during validation period.*

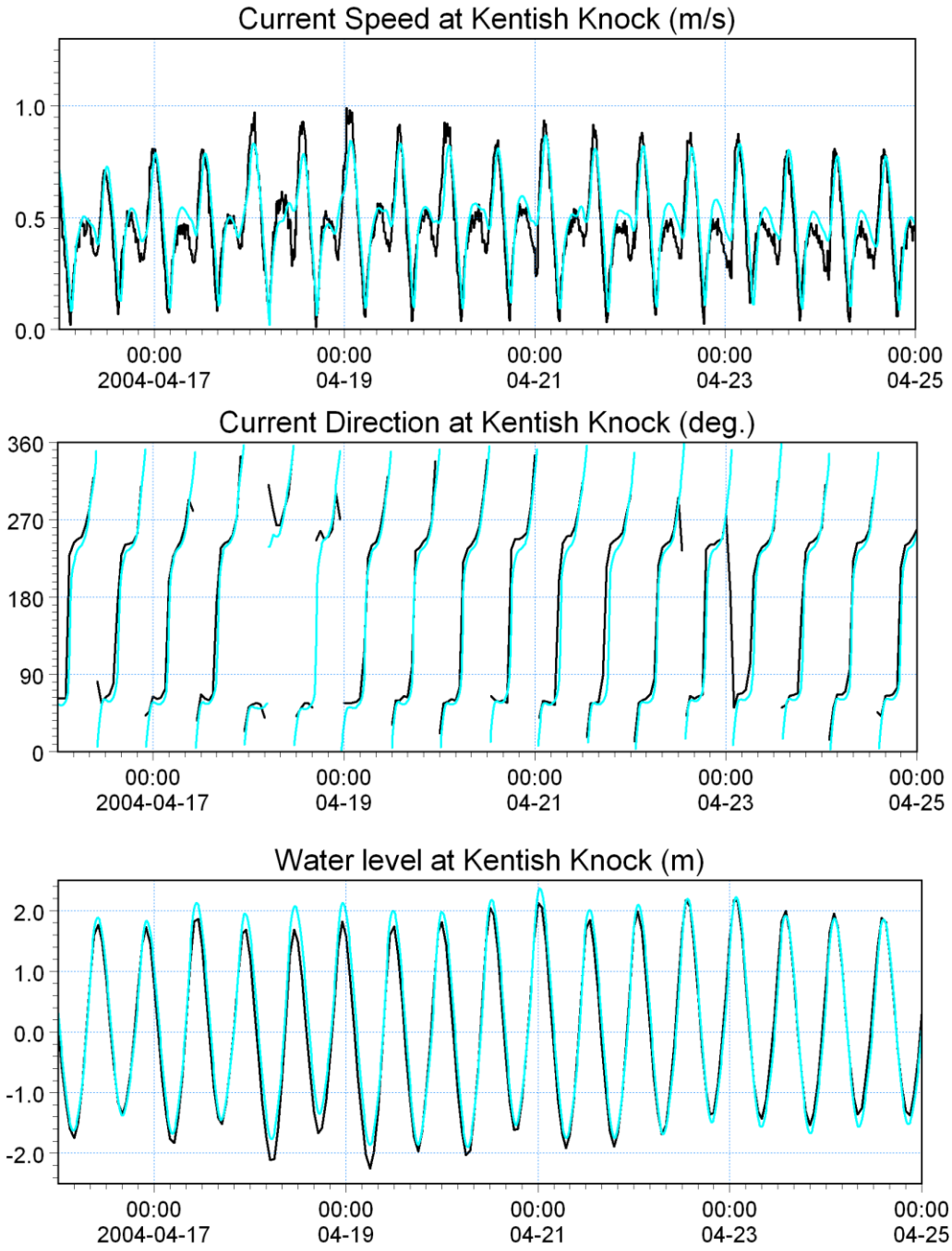

Figure 36. *Comparison of measured (black line) and predicted (blue line) water levels and currents during validation period at Kentish Knock.*

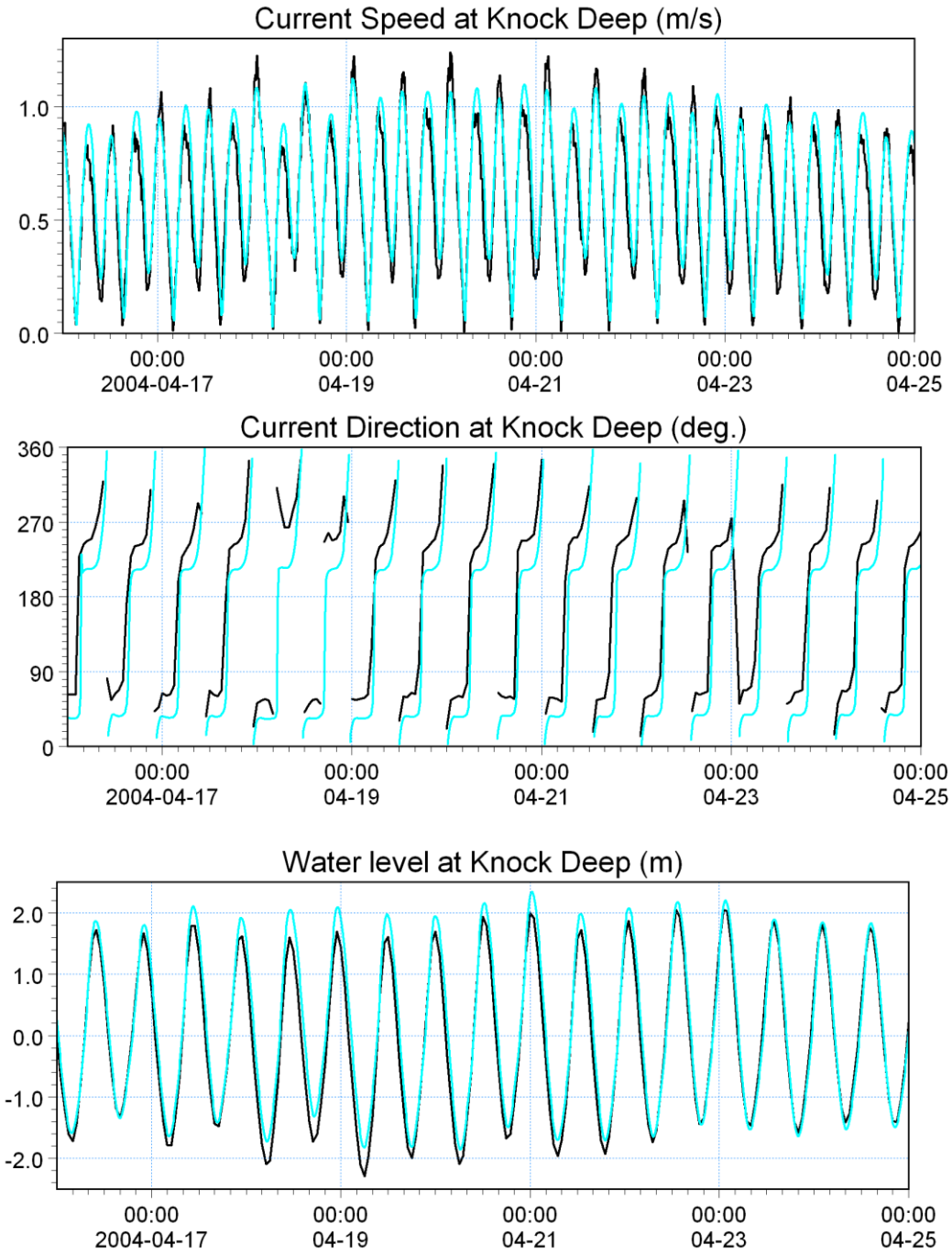

Figure 37. *Comparison of measured (black line) and predicted (blue line) water levels and currents during validation period at Knock Deep.*

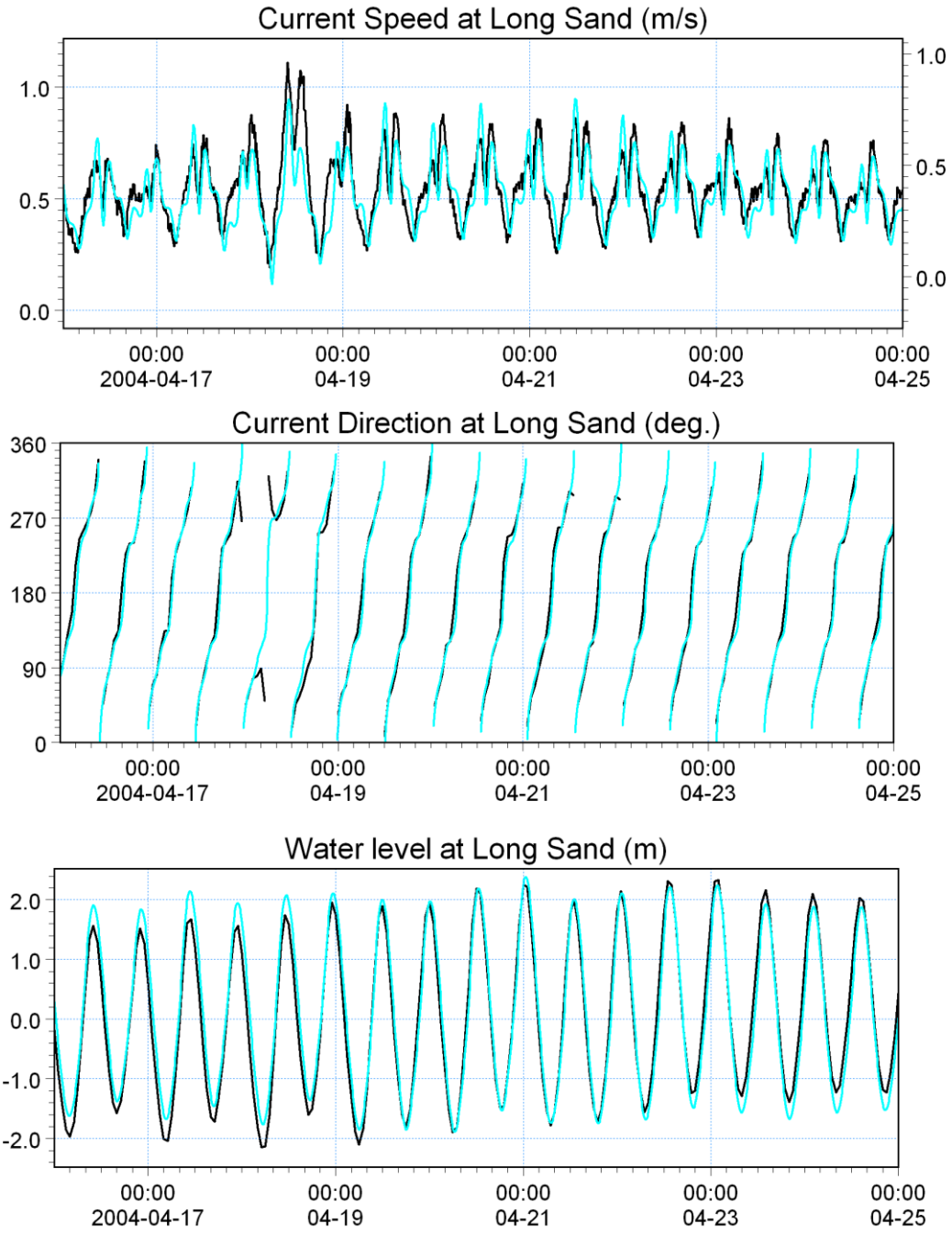

Figure 38. *Comparison of measured (black line) and predicted (blue line) water levels and currents during validation period at Long Sand.*

3.9 Fitting the Diver distribution models

3.9.1 Model 1: Global model

All data, aggregated into 500 m (mean values), from all five winters were used for fitting Model 1. The model data set included 14,682 samples with 3,176 diver occurrence (21.6%) and the mean diver density was 1.26 individuals/km^2 within the modelled region, and 1.53 individuals/km^2 within the Outer Thames SPA. The approximate significance of the smooth terms included in the model is shown in table 18, and the response curves are displayed in Figure 39. Current velocities U and V, current speed, vorticity, water level, slope, distance to land, ship densities and the

interaction term between X and Y coordinates were all shown to be important in the presence/absence part of the model. The model indicates a higher probability of presence in slope areas away from the coast and shipping lanes characterised by high current speeds, eddy activity and low water levels. Diagnostics for all five diver models are given in Appendix 1.

In the positive density part of the model current velocities U and V, current speed, vorticity, current gradient, water level, ship densities and the interaction term between X and Y coordinates were important. Thus, the model indicates higher densities of divers in general in the parts of the Outer Thames Estuary housing the above characteristics but with lower current velocities and strong current gradients.

Significant ($p<0.01$) but low spatial autocorrelation was found in the residuals of both model parts. In the presence-/absence part autocorrelation was present in 3 out of 10 lags (1 lag = 1500 m which was the defined nearest neighbourhood). The Moran's I values were, however, really low, ranging from 0.03 to 0.008 (Moran's I range from -1.0 to 1.0). In the positive part significant spatial autocorrelation in the residuals was found in 4 out of 10 lags, however, again with low Moran's I values ranging from 0.08 to 0.02).

Table 18. *Smooth terms with associated approximate significance and chi-square/F statistics for model 1. Variables not included in the final model are indicated with a dash.*

Smooth terms	Presence/absence		Positive denstiy	
	chi-sqr	p	F	p
Velocity U	125.3	<0.01	16.0	<0.01
Velocity V	95.8	<0.01	23.3	<0.01
Velocity W	-	-	-	-
Current speed	172.9	<0.01	14.4	<0.01
Vorticity	38.5	<0.01	16.7	<0.01
Current gradient	-	-	6.8	<0.01
Water level	88.5	<0.01	15.3	<0.01
Slope	17.9	<0.01	-	-
Land 5 km	43.1	<0.01	-	-
Ship densities	13.27	<0.01	10.2	<0.01
X,Y	566.2	<0.01	48.4	<0.01

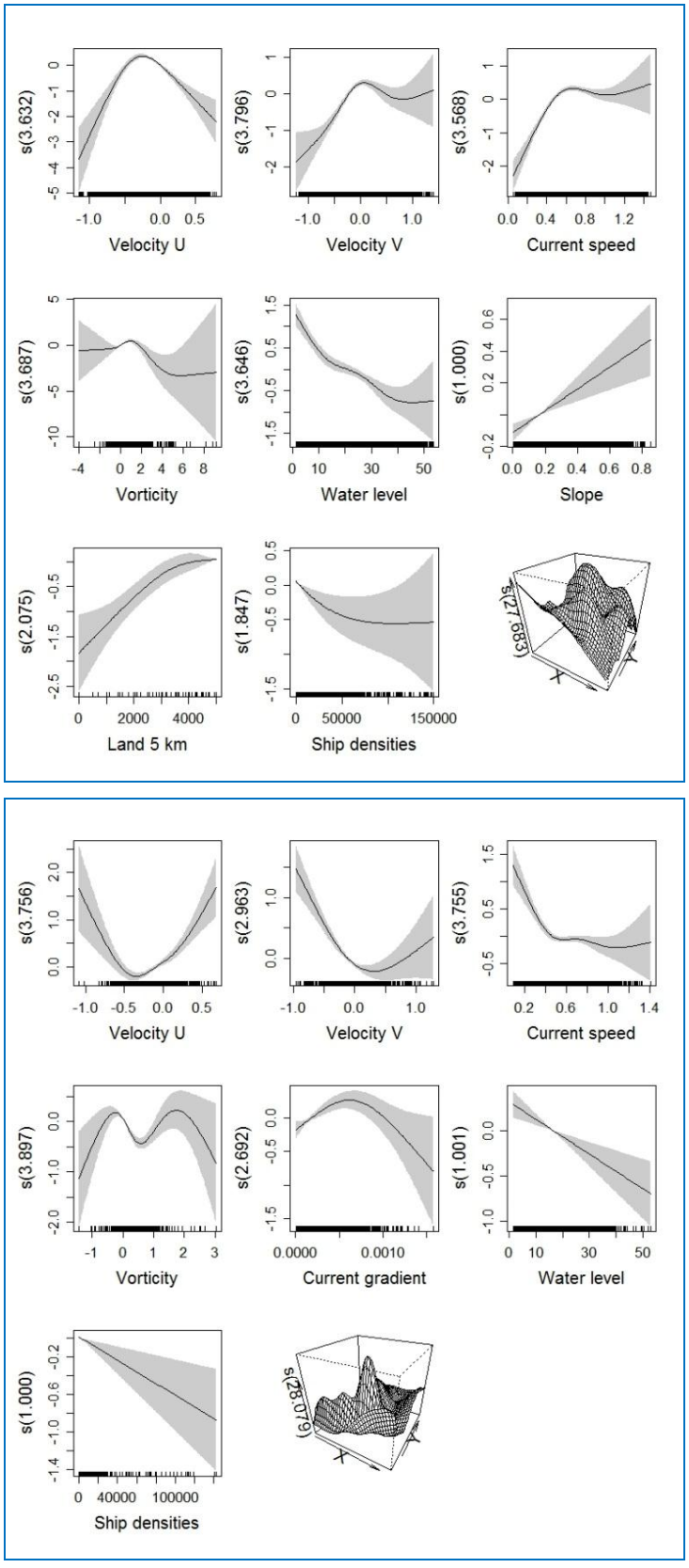

Figure 39. *Partial GAM plots for presence/absence (upper) and positive (lower) parts for the global model. The values of the environmental variables are shown on the X-axis and the probability on the Y-axis in logit scale. The degree of smoothing is indicated in the legend of the Y-axis. The dotted lines and shaded areas show ±1standard errors. For the 2-d term (X,Y) a perspective plot is shown, with the degree of smoothing indicated as a label to the Z-axis.*

3.9.2 *Model 2: Stratified distribution model for flow phase 1 (ebb current)*

Data recorded during flow phase 1 was used for fitting the model and the model is therefore capable of predicting the mean distribution and abundance of divers during this phase. As the aims of the stratified models were to describe and explain the changes in distribution during the different tidal flow phases, we did not include U and V velocities as separate predictors in these models. U and V velocity is confounded with the predictor current speed and leaving them out makes the interpretation of the model results clearer. The aim of the global model, however, was to estimate the densities as accurately as possible and we therefore included all possible variables in the global model to achieve the best predictive model possible, at the expense of interpretability. The aggregated model data set included 6,444 samples with 706 diver occurrences (11.0 %) and the mean diver density was 4.86 individuals/km^2. The approximate significance of the smooth terms included in the model is shown in Table 19, and the response curves are displayed in Figure 40.

The results for the presence/absence part indicated that current speed, water level and vertical current velocity as well as the interaction term between X and Y coordinates were important variables. The model indicates a higher probability of presence in areas with low water levels, moderate current speeds and upwelling/downwelling activity.

In the positive density part of model 2 vertical velocity and current speed were important (Figure 40). Model 2 therefore indicates higher densities of divers in the Outer Thames Estuary during ebb current in areas housing the above characteristics but having low current speed and strong upwelling.

Significant ($p<0.01$) but low spatial autocorrelation was found in the residuals of both model parts. In the presence/absence part autocorrelation was present in the first lag (1 lag = 1500 m which was the defined nearest neighbourhood). The Moran's I value was, however, very low (Moran's I = 0.01). In the positive part significant spatial autocorrelation was found only in the first lag (Moran's I = 0.23), indicating that not all of the spatial variation in the data could be accounted for by the model.

We also considered and tried to include year as a categorical variable in the models. However, we chose to average the densities during all years due to the uneven survey coverage and density estimates during the different years. Winter 2010/2011 for example had higher densities of divers within a smaller survey extent while winter 2005/2006 had a wider survey extent. Using year as predictor might therefore have reflected the differences in survey rather than actual differences in the distribution and abundance of the divers.

Table 19. *Parametric and smooth terms for model 2. The z-values and significance for the parametric terms are shown and for the smooth terms the approximate significance and chi-square/F statistics. Variables not included in the final model are indicated with a dash.*

Smooth terms	Presence/absence		Positive denstiy	
	chi-sqr	p	F	p
Velocity W	16.14	<0.01	6.176	0.01
Current speed	28.57	<0.01	43.464	<0.01
Vorticity^2	-	-	-	-
Current gradient	-	-	-	-
Water level	20.13	<0.01	-	-
Slope	-	-	-	-
Ship densities	-	-	-	-
Land 5 km	-	-	-	-
X,Y	508.86	<0.01	36.225	<0.01

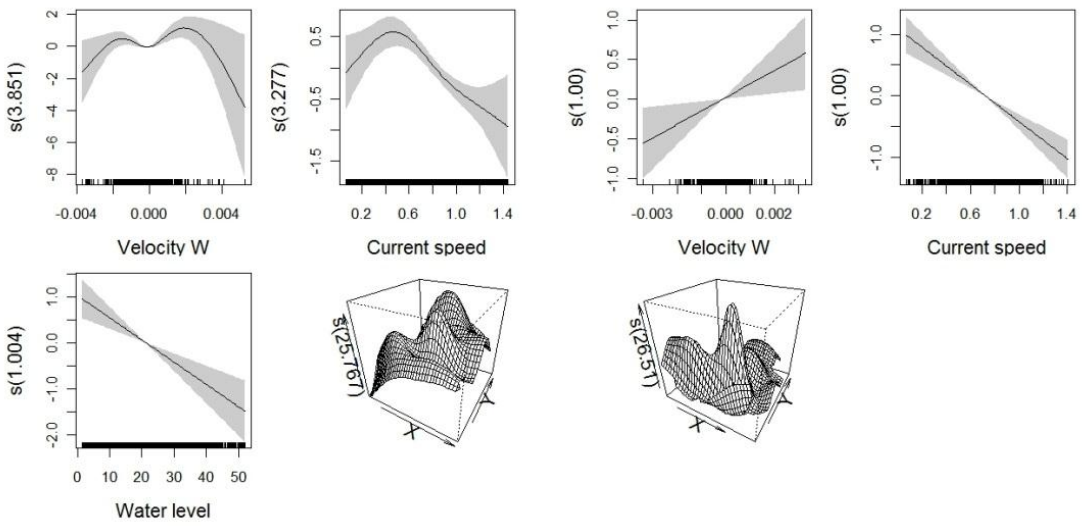

Figure 40. *Partial GAM plots for presence/absence (left) and positive (right) parts for model 2. The values of the environmental variables are shown on the X-axis and the probability on the Y-axis in logit scale. The degree of smoothing is indicated in the legend of the Y-axis. The dotted lines and shaded areas show ±1standard errors. For the 2-d term (X,Y) a perspective plot is shown, with the degree of smoothing indicated as a label to the Z-axis.*

3.9.3 *Model 3: Stratified distribution model for flow phase 2 (low tide)*

Data recorded during flow phase 2 was used for fitting the model and the model is therefore capable of predicting the mean distribution and abundance of divers during this phase. The model data set included 7,766 samples with 770 diver occurrences (9.9 %) and the mean diver density was 1.14 individuals/km^2. The approximate significance of the smooth terms included in the model is shown in Table 20, and the response curves are displayed in Figure 41. The results for the presence/absence part were comparable to the results for flow phase 1, and showed a higher probability of presence in areas with low water levels, moderate currents speeds and steep slopes of the seafloor.

The preference for the shallow offshore parts of the area with which the divers are associated are also apparent for flow phase 2 with the positive parts of model 3 indicating higher densities of divers in shallow, slope areas with strong current gradients. Current speed was also important in the positive part of model 3.

Significant spatial autocorrelation in model residuals was found in the first two lags of the presence/absence part of model 3. The Moran's I values were, however, really low indicating weak correlation. In the positive part significant but moderate spatial autocorrelation was found in the two first lags (Moran's I 0.19 and 0.14), indicating that not all of the spatial variation in the data could be accounted for by the model.

Table 20. *Parametric and smooth terms for model 3. The z-values and significance for the parametric terms are shown and for the smooth terms the approximate significance and chi-square/F statistics. Variables not included in the final model are indicated with a dash.*

Smooth terms	Presence/absence		Positive denstiy	
	chi-sqr	p	F	p
Velocity W	-	-	-	-
Current speed	33.17	<0.01	2.692	0.04
Vorticity^2	-	-	-	-
Current gradient			3.532	0.03
Water level	34.47	<0.01	10.402	<0.01
Slope	18.18	<0.01	5.142	<0.01
Ship densities	-	-	-	-
Land 5 km	-	-	-	-
X,Y	343.12	<0.01	12.766	<0.01

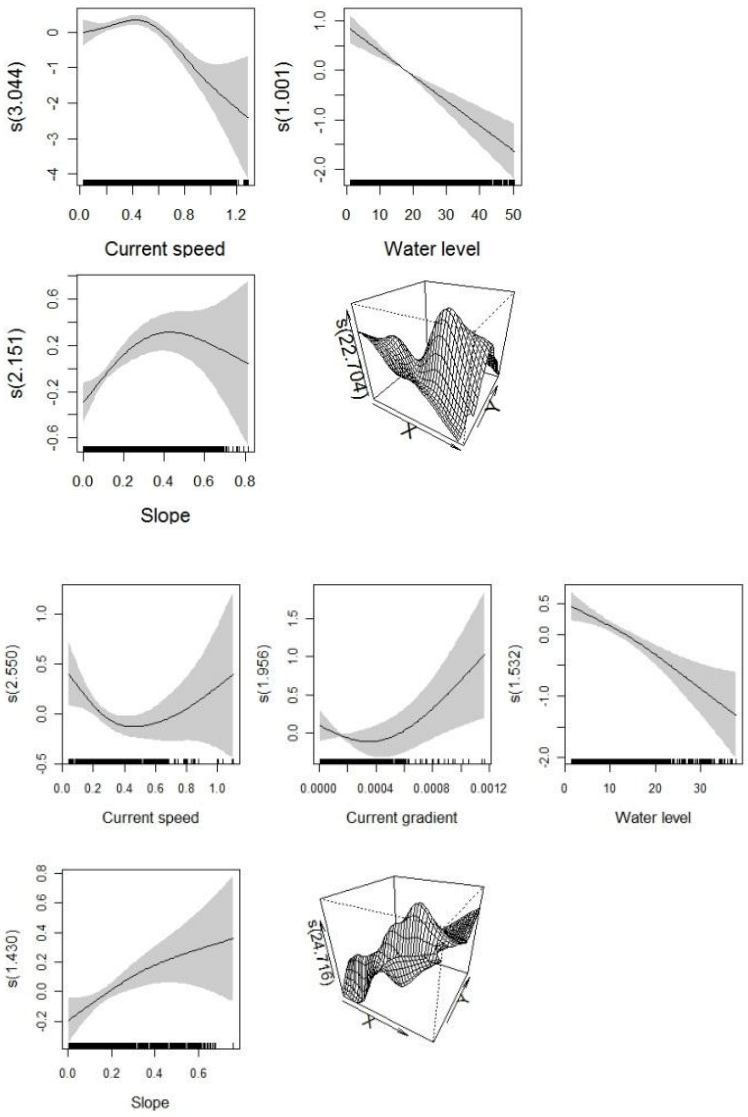

Figure 41. *Partial GAM plots for presence/absence (upper) and positive (lower) parts for model 3. The values of the environmental variables are shown on the X-axis and the probability on the Y-axis in logit scale. The degree of smoothing is indicated in the legend of the Y-axis. The dotted lines and shaded areas show ±1standard errors. For the 2-d term (X,Y) a perspective plot is shown, with the degree of smoothing indicated as a label to the Z-axis.*

3.9.4 Model 4: Stratified distribution model for flow phase 3 (flood current)

Data recorded during flow phase 3 was used for fitting the model and the model is therefore capable of predicting the mean distribution and abundance of divers during this phase. The model data set included 9,269 samples with 1,042 diver occurrences (11.2 %) and the mean diver density was 0.89 individuals/km^2. The approximate significance of the smooth terms included in the model is shown in Table 21, and the response curves are displayed in Figure 42.

The results for the presence/absence part were highly comparable to the results for the ebb current, as the model indicated a higher probability of presence in areas

with low water levels, moderate currents speeds and upwelling/downwelling activity.

Model 4 indicated higher densities of divers in the Outer Thames Estuary during flood current in areas housing the above characteristics but having high current speed and low density of ships. Significant ($p<0.01$) but low spatial autocorrelation was found in the residuals of both model parts. In the presence/absence part autocorrelation was present in seven lags and in the positive part significant in the three first lags. The Moran's I values were, however, very low (<0.082).

Table 21. *Parametric and smooth terms for model 2. The z-values and significance for the parametric terms are shown and for the smooth terms the approximate significance and chi-square/F statistics. Variables not included in the final model are indicated with a dash.*

Smooth terms	Presence/absence		Positive denstiy	
	chi-sqr	p	F	p
Velocity W	47.955	<0.01	4.308	<0.01
Current speed	-	-	24.445	<0.01
Vorticity^2	-	-	-	-
Current gradient	-	-	-	-
Water level	19.231	<0.01	-	-
Slope	6.342	0.01	-	-
Ships densities	-	-	8.563	<0.01
Land 5 km	-	-	-	-
X,Y	241.165	<0.01	13.106	<0.01

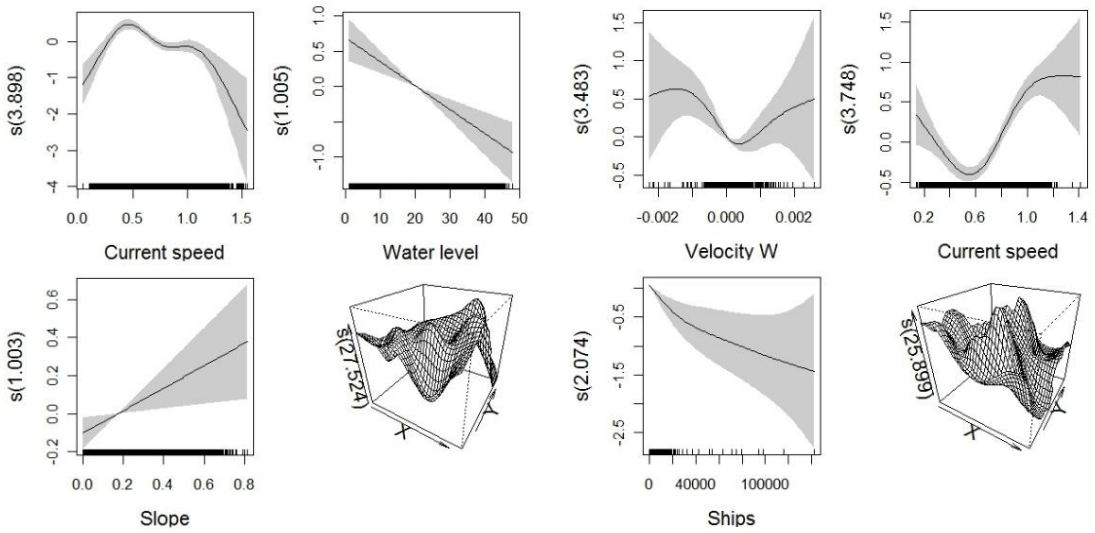

Figure 42. *Partial GAM plots for presence/absence (left) and positive (right) parts for model 2. The values of the environmental variables, depth and current speed (CS) are shown on the X-axis and the probability on the Y-axis in logit scale. The degree of smoothing is indicated in the legend of the Y-axis. The dotted lines and shaded areas show ±1standard errors. For the 2-d term (X,Y) a perspective plot is shown, with the degree of smoothing indicated as a label to the Z-axis.*

3.9.5 *Model 5: Stratified distribution model for flow phase 4 (high tide)*

Data recorded during flow phase 4 was used for fitting the model and the model is therefore capable of predicting the distribution and abundance of divers during this phase. The model data set included 11,684 samples with 1,242 diver occurrences (10.6 %) and the mean diver density was 0.64 individuals/km^2. The approximate significance of the smooth terms included in the model is shown in Table 22, and the response curves are displayed in Figure 43. The results for the presence/absence part were comparable to the results for the flood current phase, and showed a higher probability of presence in areas with low water levels, moderate currents speeds and steep slopes of the seafloor. In addition, the presence-absence part of model 5 indicated a higher probability of occurrence in offshore areas of low ship density.

The resemblance with the results for the high tide phase model was also apparent for the positive part of model 5 indicating higher densities of divers in shallow, slope areas with strong current gradients. Additionally, low current speed, eddy activity, high slopes and low ship density were also important parameters in the positive part of the high tide phase model.

Significant but very low spatial autocorrelation in model residuals was found only in the first lag of both the presence/absence and positive parts of model 5 (Moran's I <0.038).

Table 22. *Parametric and smooth terms for model 3. For the parametric terms (winter 1, 2003-2004 is the reference term), winter 2=2004-2005, winter 3 =2005-2006, winter 4 = 2009-2010 and winter 5 = 2010-2011. The z-values and significance for the parametric terms are shown and for the smooth terms the approximate significance and chi-square/F statistics. Variables not included in the final model are indicated with a dash.*

Smooth terms	Presence/absence		Positive denstiy	
	chi-sqr	p	F	p
Velocity W	-	-	-	-
Current speed	70.957	<0.01	16.580	<0.01
Vorticity^2	-	-	4.026	<0.01
Current gradient	-	-	7.065	<0.01
Water level	32.070	<0.01	7.605	<0.01
Slope	8.624	<0.01	4.193	0.01
Ship densities	5.334	0.03	6.752	<0.01
Land 5 km	17.250	<0.01	-	-
X,Y	272.004	<0.01	10.419	<0.01

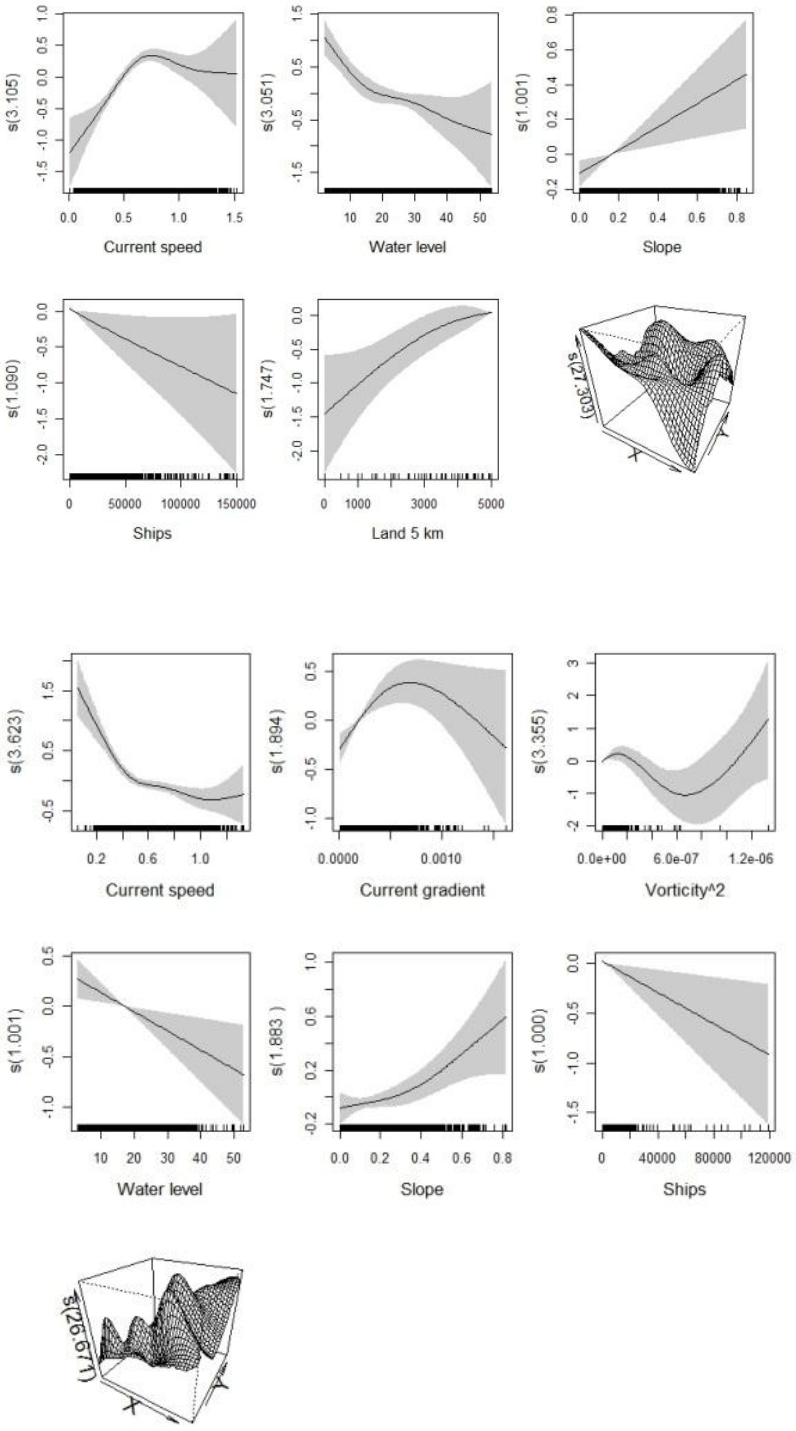

Figure 43. *Partial GAM plots for presence/absence (upper) and positive (lower) parts for model 3. The values of the environmental variables are shown on the X-axis and the probability on the Y-axis in logit scale. The degree of smoothing is indicated in the legend of the Y-axis. The dotted lines and shaded areas show ±1standard errors. For the 2-d term (X,Y) a perspective plot is shown, with the degree of smoothing indicated as a label to the Z-axis.*

3.10 Validation of the fit and predictive ability of the Diver models

The predictive accuracy of the models was tested on withdrawn data (30%) by using AUC (only presence/absence part) and Spearman's correlation (final combined predictions). The results are shown in table 21. Model 2 had the highest proportion of explained variance, 19.3, in the presence/absence models. While model 2 had the highest proportion explained variance, 65.6, in the positive part. The positive parts of all the models had generally much higher explained variances.

The AUC values indicate the models are capable of distinguishing presence from absence about 75 % of the time which is quite low, but acceptable given the high resolution of the model. The Spearman's correlation of the combined models indicates that there is a clear agreement between predicted and observed values.

Table 21. *Evaluation statistics of the five models, Model 1 = all data, Model 2 = data from flow phase 1, Model 3 = data from flow phases 2, Model 4 =data from flow phase 3 and Model 5 data from flow phase 4. Deviance explained for the presence/absence part of the model and for the positive density part. AUC is the evaluation results for the presence absence part and the Spearman Rank correlation is the evaluation of the final combined model.*

	Dev. Exp. P/A	Dev. Exp. positive	AUC	Spearman Rank correlation
Model 1	17.7	48.2	0.774	0.345
Model 2	19.3	65.6	0.768	0.261
Model 3	14.8	45.1	0.749	0.239
Model 4	9.39	41.6	0.731	0.195
Model 5	10.5	31.3	0.746	0.232

3.11 Stability of the Diver models, effect of sample size

Model 1 was fitted on varying sample size (randomly selected) to assess whether the data could be regarded as large enough for obtaining a reliable density estimate. As the mean density estimate with associated standard error seems to stabilise after including about 55% (Figure 44) of the data it seemed like there was a sufficient sample size to obtain a reliable density estimate.

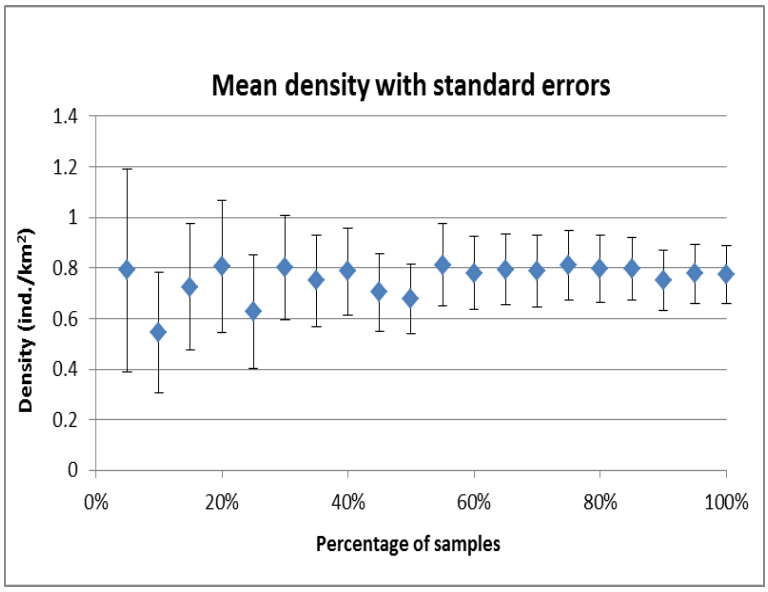

Figure 44. *Mean density predicted by model 1 when varying the sample size from 5 to 100 %.*

3.12 Estimation of Diver distribution

The result, mean density of divers, of the deployment of the global model is depicted in Figure 45. The mapped model deployments show areas of high densities (≥ 3 birds/km^2) extending across the eastern parts of the Outer Thames Estuary over Sunk Sand, Long Sand and Kentish Knock. Multiple fine-scale high-density patches are predicted along these sand bars with a spatial scale matching the estimated scale of aggregative response observed during single surveys (see Chapter 3.5).

A large patch (approximately 12 * 12 km) of very high densities (≥ 5 birds/km^2) is estimated at the eastern end of Long Sand and Kentish Knock. A smaller patch of higher densities is depicted in the northern parts of the Outer Thames Estuary SPA. Areas in the North Sea deeper than 30 m, several inshore areas and the shipping lanes are estimated supporting virtually no or very few divers. The parts between the high-density and low-density areas and the coastal areas of Suffolk and Norfolk representing the northern parts of the Outer Thames Estuary SPA are indicated as having medium densities (< 3 birds/km^2) of divers.

Figure 46 depicts the results of the stratified model deployments for each of the four flow scenarios. The density model results have been standardised into four classes of habitat suitability to enhance comparability between model deployments and overcome biased density levels due to uneven survey coverage during the dif-

ferent tidal phases. The habitat suitability models which have been deployed in a 500 m grid outline striking patterns of suitable habitat, and consistent systematic changes in these patterns with the intensity of the flow.

In all current scenarios the major part of the Outer Thames Estuary has been classified as either of low or medium habitat suitability. The lowest habitat suitability is indicated for the areas deeper than 20 m, the shipping lanes and areas close to the coast. The suitable habitats are associated with the three SW-NE protruding sands: Sunk Sand, Long Sand and Kentish Knock, the coastal area of Suffolk and Norfolk as well as with the shallow area off the southwest coast of the estuary. The areas of suitable habitat change systematically with the flow regime. During ebb current and low tide phases areas in the south-western part of the estuary generally show low habitat suitability, while during flood current and high tide phases prominent patches of very high habitat suitability are estimated in this part of the estuary. Thus, a westward extension of the main distribution of divers in the estuary seems to take place during the two tidal phases dominated by westward flowing currents. Superimposed on the east-west oscillation changes in the north-south location of the most suitable habitats can be observed around the sand bars. During the flow phases with slack water (low tide, high tide) divers display a more concentrated distribution along the slopes of the sands than during the phases with stronger currents (ebb current, flood current). The patch off the Suffolk-Norfolk coast is most extensive during flood current and high tide.

Accordingly, depending on flow phase the LAOWF site experiences both medium, high and very high habitat suitability to divers, with the proportion of the site having very high suitability changing between 51 % and 79 % (Table 22). The largest area of suitable habitat to divers in the LAOWF footprint is predicted during low and high tide, when high densities of divers coincide with the shallow, slope areas with strong current gradients found over Long Sand.

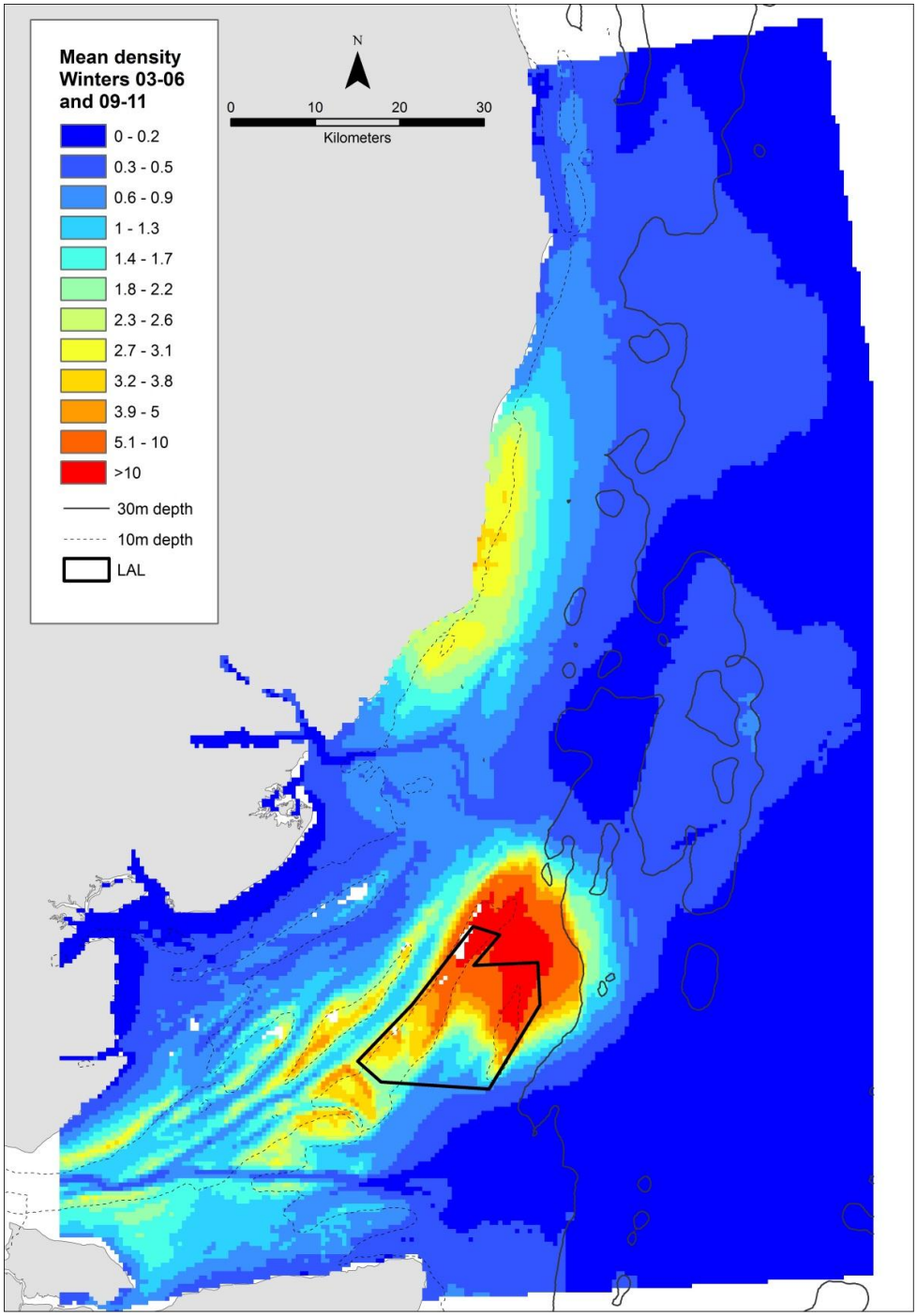

Figure 45. *Modelled mean densities of divers during all five winters (2003-2004, 2004-2005, 2005-2006, 2009-2010 and 2010-2011). The spatial resolution is 500 m.*

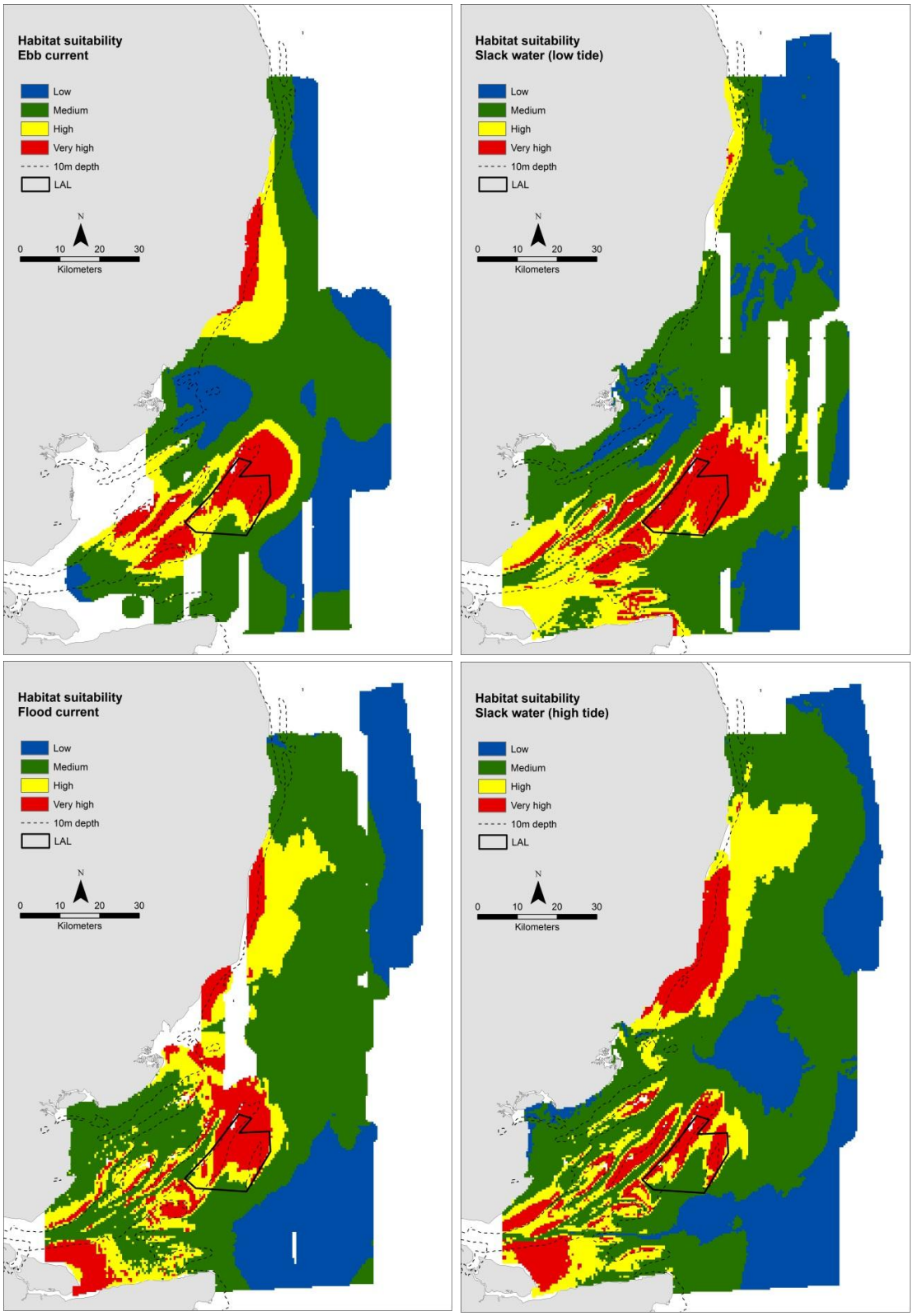

Figure 46. *Modelled stratified habitat suitability for divers in the southern part of the Outer Thames Estuary during all five winters (2003-2004, 2004-2005, 2005-2006, 2009-2010 and 2010-2011). White areas indicate missing values. The spatial resolution is 500 m.*

Table 22. *Areas and proportion of areas (km^2) covered by the modelled stratified habitat suitability classes. The table shows mean values for each current scenario for the area occupied by the footprint of London Array.*

	Habitat suitability – London Array footprint							
	Low		Medium		High		Very high	
Current Scenario	**Area**	**%**	**Area**	**%**	**Area**	**%**	**Area**	**%**
Ebb current	0	0	45	20	53	23	134	58
Slack water (low)	0	0	10	4	40	17	182	79
Flood current	0	0	44	19	70	30	118	51
Slack water (high)	0	0	14	6	46	20	171	74

Figures 47 and 48 show standard errors for the global model and for the four different stratified models. The errors are generally largest for the areas with higher diver densities, however the relative standard errors (% of the predictions) are generally lower in the high density areas. For the global model (Figure 47), the errors are mostly well below 0.3 birds/km^2, and below 0.7 birds/km^2 in the high-density areas (density ≥ 3 birds/km^2, see Figure 45). Thus, it can be concluded that the modelled densities have a moderate amount of uncertainty associated with them, with the patterns of errors mirroring the distribution of densities. The relative standard errors are generally below 30 %. The relative standard errors (%) are generally highest in areas with very low densities which means that the errors are also low and not very influential.

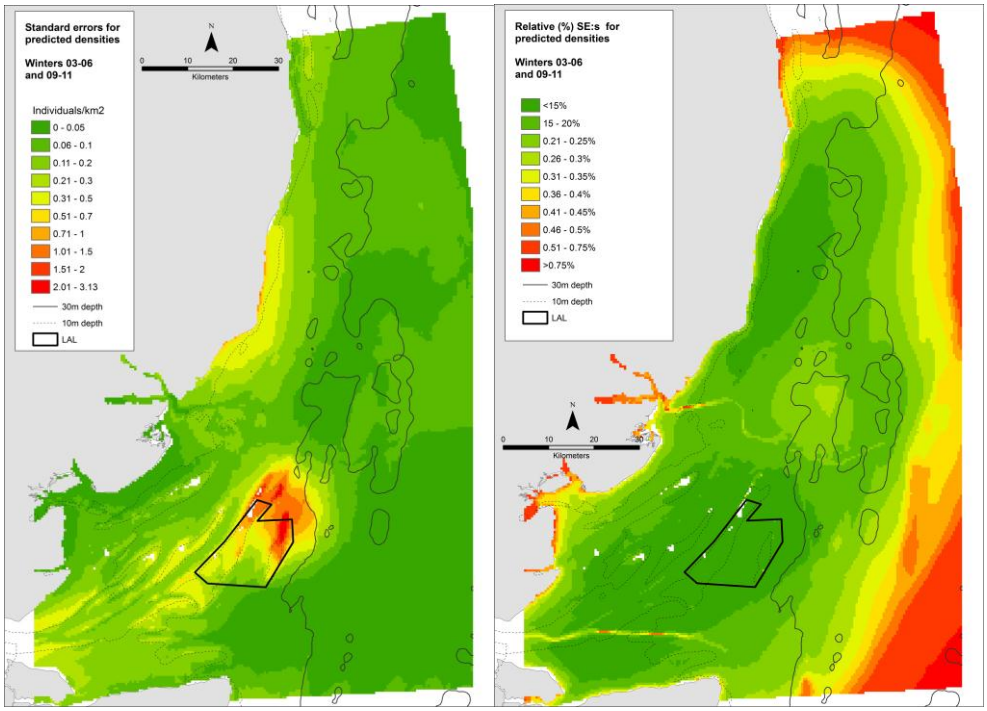

Figure 47. *Standard errors (left) and relative standard errors (right) for the combined predictions of mean density (Models 1). The largest errors are found in the high density areas, where the % error (relative SE:s) of the predictions are, however, low.*

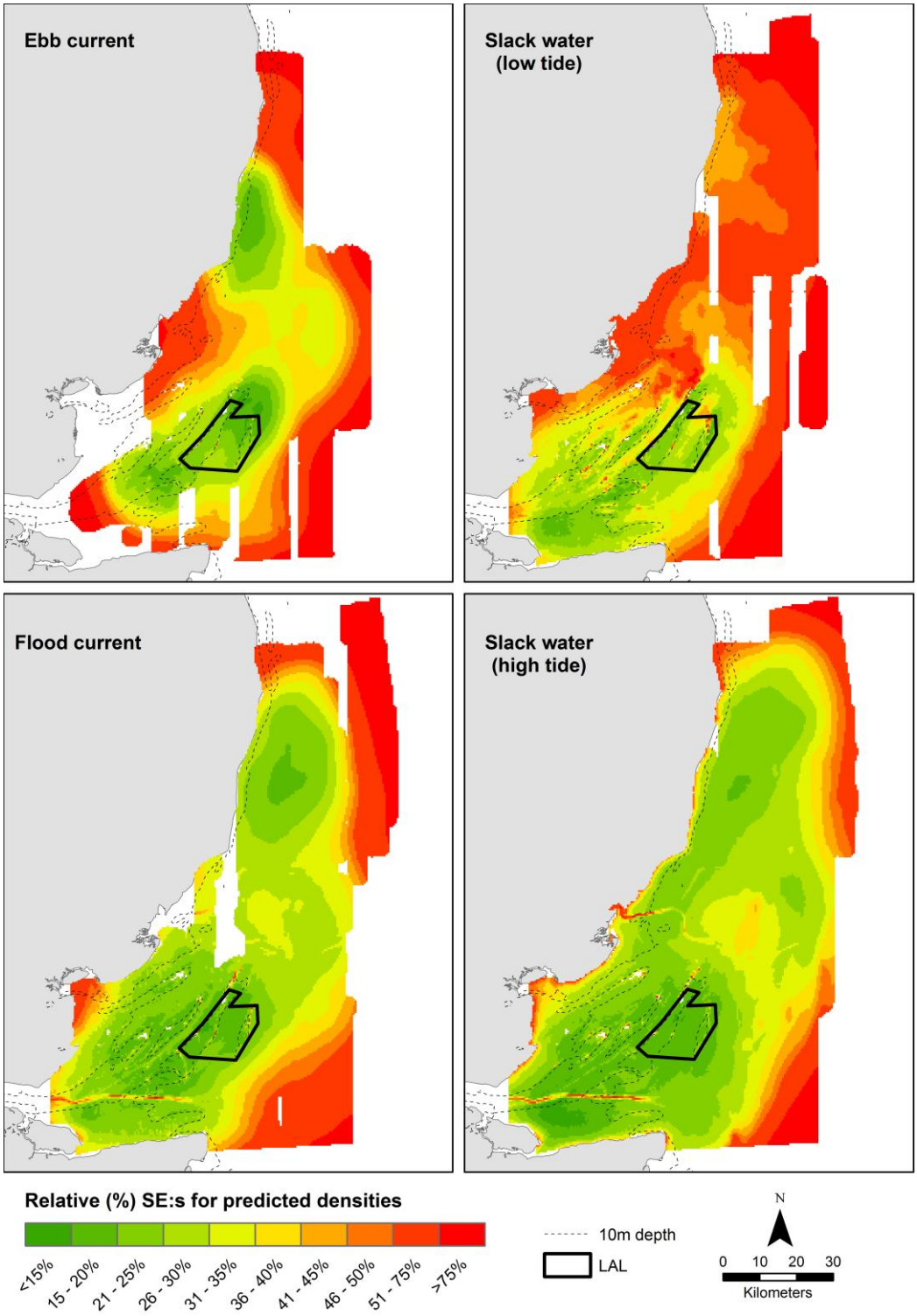

Figure 48. *Relative standard errors (% of the predictions) for the combined predictions of the stratified models (Model 2-5).*

3.13 Estimation of Diver abundance

On the basis of the regional model (Figure 45) for the five investigated survey winters total abundance of divers within the Outer Thames Estuary could be estimated for the whole area of 9,180 km^2. The mean abundance within the estuary was

7,100 (±1045) birds (mean density was 0.773). The confidence interval was calculated based on the standard errors (Figure 47). The mean density estimated within the Outer Thames SPA was 1.53 with an estimated mean abundance of 6,025 divers.

3.14 Assessment of unsustainable impacts on diver population levels

The Red-throated Diver is a widespread circumpolar species, but in this assessment it was considered only a population wintering in the North Sea, which consists of approximately 65,200 birds (Table 23). Because this estimate lacks a measure of uncertainty, it can be assumed a coefficient of variation $CV_{\hat{N}} = 0.5$ (Wade 1998, Dillingham & Fletcher 2008) to estimate the minimum population size N_{min}. Further, it was assumed an age of first reproduction being $\alpha = 2$ and annual adult survival s = 0.84 (Hemmingsson & Eriksson 2002). Considering that the population trend of the species in NW Europe seems to be declining (Skov et al. 2011) a recovery factor f of 0.3 was used (Niel & Lebreton 2005).

Table 23. *Estimates of wintering Red-throated Diver numbers in the North Sea.*

Region	Number	Source
UK	14,000	O'Brien et al. 2008
Netherlands	7,500	Skov et al. 1995
Germany	23,000	Skov et al. 1995
Denmark North Sea	9,000	Skov et al. 1995
Denmark Kattegat	1,500	Skov et al. 2011
Sweden Kattegat	1,000	Skov et al. 2011
Norway	500	Guesstimate
SUM	**65,200**	

Considering all the assumptions above, the PBR for Red-throated Divers wintering in the North Sea was estimated at 1,915 birds (Table 23; 95% confidence intervals were not calculated as variability measure of adult survival is unknown). This estimate refers to annual additive mortality the current population could sustain. If a recovery factor f of 0.5 was used (recommended for species with stable populations) the PBR threshold would be 3,191 birds.

Table 24. *Demographic parameter values and calculation of potential biological removal of Red-throated Divers from the North Sea wintering population.*

Parameters	Value	Source
Minimum population size, N_{min}	42,840	20th percentile of population estimate (Table 1)
Age of first reproduction, α	2	Hemmingsson & Eriksson 2002
Adult survival, s	0.84	Hemmingsson & Eriksson 2002
Maximum population growth rate, λ_{max}	1.30	Equation (3) in the text
Recovery factor, f	0.3	see text above
Potential Biological Removal, PBR	1,915	

4 DISCUSSION AND CONCLUSIONS

4.1 Comparability of survey data

The quality check of the available aerial and boat survey data indicated no major problems in the standardisation of the aerial survey techniques in the region. Neither should combining visual and digital aerial survey data cause major problems. The modelling comparison between visual and digital data indicated very similar responses in both types of data although digital data resulted in higher density estimates. Problems related to the task of assessing diver density and distribution in the Outer Thames Estuary were mainly due to the presence of imperfect databases and a high degree of variability in the survey effort between months and years. However, several issues with the boat surveys were highlighted.

The conglomerate of aerial transect surveys used for the modelling of diver distribution and area use represents a well-standardised methodology, both in terms of transect design, relative coverage, survey height, transect and strip widths as well as survey conditions. The problems in terms of lack of matching information on survey tracks which was observed with some of the databases were unfortunate. However, as revealed by the tests of the robustness of the diver distribution models relative to the amount of empirical survey data inclusion of more data is unlikely to have enhanced the performance of the models significantly.

The uneven survey coverage by aircraft between months and years made it necessary to split the model applications into abundance and distribution. And due to almost twice as many divers being seen during flow phases 1 and 3 as compared to 2 and 4, standardisation of densities into indices of habitat suitability was necessary to allow for direct comparisons between current scenarios. Using habitat suitability indices, on the other hand, may comprise a robust basis for future monitoring of divers at LAOWF using high-resolution image technology.

The quality of the available boat survey data was uncertain. Despite the fact that the surveys from the different wind farm projects have been carried out using the same standard survey technique (Tasker et al. 1984, Camphuysen et al. 2004), there were issues related to the application of snap-shot counts of flying birds and the continuous use of binoculars.

Snap-shot counts of flying birds are necessary to avoid overestimation of the density of flying divers. Since an ample proportion of the boat surveys did not apply snap-shot counts the density of divers sampled during these surveys may have been inflated. Counter to this the lack of continuous use of binoculars may have led to biases in the sampled densities which go in the opposite direction (MacLean et al. 2008). Continuous use of binoculars during boat surveys of divers is not routinely applied in these surveys, although it is a prerequisite for sampling birds, which like divers react strongly on approaching boats (Durinck et al. 1993).

Thus, given the uncertain reliability of sampled densities of divers from the boat surveys, the use of data from the aerial surveys for modelling purposes seemed the safer option.

The tests of the agreement between aerial visual and digital data on diver densities during the winter 2009/10 documented a high degree of correspondence. The spearman's correlation between the predicted presence of divers from the two platforms was 0.864 and between predicted densities 0.894. It can therefore be concluded that the two types of data produce similar distribution patterns and order of the predictions although the digital data produce higher densities. As also the re-

sponses to the environmental data are very similar in the models based on both types of data the combination of both types of data in the models seems logical.

4.2 Reliability of the hydrodynamic model

The validation of the Outer Thames Estuary hydrodynamic model showed that the predictive power of the model complex is strong, and that accurate hydrodynamic parameters have been supplied to the diver distribution models. One of the key parameters in order to stratify the diver models by tidal current stages is the reliability of the modelled decomposition of the tidal signal and the main semi-diurnal and diurnal tidal constituents.

The comparisons with measurements at ten stations in the North Sea and the English Channel showed that the 2D regional model captures reasonably well the pure tidal propagation. The predicted semi-diurnal constituents' characteristics fit fairly well with the measurements, with amplitudes on average captured properly with a maximum difference compared to the measurements of 0.06 m, and the phases fitting reasonably well with the measurements.

Performances of the tide and surge predictions by 1-month comparisons between measured and predicted water levels at ten stations indicate clearly that the hydrodynamic predictions are accurate within the Outer Thames Estuary. The maximum RMSE of water level was found to be around 0.17 m. Along the North Sea water levels present a small diurnal amplification of the signal which tends to disappear further to the south of the North Sea. This pattern can also be seen from the RMSE calculated over the entire hindcast period evolving from 0.13 m at Wick to 0.06 m at Cromer.

In the English Channel, water levels match perfectly with the measurements which are confirmed by a computed RMSE of approximately 0.07 m within the area. Closer to the Thames Estuary, at the three validation stations the results are fairly reasonable. Despite Lowestoft and Felixstowe are characterised by a small bias and a slight amplification of the water levels, results are satisfying especially at Dover where a RMSE of approximately 0.1 m has been calculated.

The validation of the modelled water levels and currents is especially important in relation to the diver distribution model, as water levels and several current parameters were used as potential habitat drivers. The comparisons between measured and predicted water levels at Dover, Felixstowe and Lowestoft showed that the water levels are reasonably well predicted in terms of phase and amplitude, with a RMSE in the order of 0.15 m - 0.25 m and a bias component of about 0.15 m.

Similar tendencies were observed for water level predictions at Long Sand, Kentish Knock and Knock Deep which present a RMSE inferior to 0.3 m. The hydrodynamic complexity within the Outer Thames Estuary induced by the presence of sand bars and channels was also well represented. Within the deep channel Knock Deep ebb and flood tidal currents are oriented along a SW-NE axis, during the reverse of the tide, the flow follows a clockwise rotation which is well represented by the model.

At Kentish Knock, the asymmetry current pattern characterised by a significantly higher ebb current peak is correctly reproduced by the model in terms of phase and magnitude characterised by a RMSE of less than 9 cm/s. The predicted temporal current direction variation cycle matches well with measurements.

At Long Sand the flow is rotating during the entire tidal cycle. During fully developed flood and ebb currents at the adjacent channels, the flow at the Long Sand is

oriented WSW and ESE due to refraction of the current on the flank of the sand bank. The water moves almost perpendicularly to the bank during the current reverse at the channels. Current peaks are well depicted in time but present, however, a slight difference in amplitude, the RMSE calculated for the current intensity is about 0.15 m/s for the validation period.

4.3 Quality of Diver distribution models

The five diver distribution models were mainly created on the basis of the parameters from the hydrodynamic model. Overall, a high degree of consistency was seen with respect to the predicted distribution patterns from the five models. With respect to important variables, the highest degree of consistency was seen in the stratified models when comparing flow phases with strong currents with flow phases representing slack water.

The important parameters in the global model indicated a higher probability of presence in offshore slope areas with low density of ships characterised by high current speeds, eddy activity and low water levels. The important parameters for densities of divers in the global models were (low) current velocity and (strong) current gradients. As the global model was established on all data across the tidal flow phases these parameters reflect a mixture of the key parameters determined by the stratified models. The two stratified distribution models for strong tidal flows both indicated a higher probability of presence of divers in the shallower areas with high vertical velocities, - a characteristic of most of the Outer Thames where divers were recorded (see overview of the distribution of key parameters in Appendix 2). The two stratified distribution models for weak tidal flows both indicated a higher probability of presence of divers over the shallow slopes with moderate currents, - indicating more discrete patterns of distribution during low and high tide as displayed by the deployed models in Figure 46 and by the well-defined small areas of fronts developed along the slopes during these flows (Appendix 2).

The parameters in the positive density parts of the stratified models described a large amount of the variability in the surveyed densities of divers, and the interaction term between X and Y coordinates was less important than in the presence parts.

The parameters in the positive density part of the stratified models stressed the importance of current gradients and shallow slopes to high densities of divers during the low velocity phases. Additionally, low current speed, eddy activity, high slopes and low ship density were also important parameters in the positive part during high tide. During ebb current low current speed and strong upwelling were important parameters to high densities, while during flood current high current speed and low density of ships were important. Accordingly, the key parameters for the positive part of the models representing strong flows further indicated the use of wider areas during these scenarios (Appendix 2). As the parameter current gradient marks horizontal frontal activity the results of the stratified models suggest that divers in the Thames Estuary primarily use these supposedly high-productive sites during weak tidal flows.

Differences between the four stratified models were apparent, and the areas of estimated suitable habitat changed systematically with the flow regime. During ebb current and low tide, - areas in the south-western part of the estuary generally showed low habitat suitability, while during flood current and high tide, prominent patches of very high habitat suitability were estimated in this part of the estuary. Superimposed on the east-west oscillation changes in the north-south location of the most suitable habitats can be observed around the sand bars. During the flow phases with slack water (low tide, high tide) divers display a more concentrated

distribution along the slopes of the sands than during the phases with stronger currents (ebb current, flood current). Finally, the patch off the Suffolk-Norfolk coast is most extensive during flood current and high tide. Accordingly, without the application of stratified models the estimation of detailed distribution patterns and associated variability would not have been possible. The tests for spatial autocorrelation in the model residuals indicated that despite some spatial autocorrelation remained in the residuals most of the spatial structure could be explained by the environmental variables. Autocorrelations in both the presence/absence parts and positive parts were very low which indicates the spatial autocorrelation did not have an influential effect on the results.

The predictive accuracy of the models as tested on withdrawn data indicated that the models are capable of distinguishing presence from absence more than 75 % of the time which is quite low, but acceptable given the high resolution of the model. The Spearman's correlation coefficients of the combined models indicated that there is a clear agreement between predicted and observed values the Spearman's correlation coefficient for the global model (model 1) was 0.35.

Given that the validation of accuracy was undertaken at a high spatial resolution (500 m) this result is satisfactory (many "suitable" samples will be unoccupied for example), and indicates that the predicted densities and habitat suitabilities are reliable. The deviance explained (variance explained) was higher in the positive part of all models, ranging between 31.3 % and 65.6 %. This indicates that the environmental variables are better at describing the distribution of densities than the simple probability of occurrence.

A moderate amount of error was associated with the predicted densities of wintering divers by the three models. The errors are generally below 30 %. For the global model, the errors are mostly well below 0.3 birds/km^2, and below 0.7 birds/km^2 in the high-density areas (density ≥ 3 birds/km^2).

5 REFERENCES

Andersen, O., Baltazar; E., G.D; Erofeeva, S.Y.; Ray, R.D. 2006. Mapping nonlinear Shallow-water tides: a look at the past and future. Ocean Dynamics (ISSN: 1616-7341); Vol: 56; issue: 5-6, pages;:416-429. Springer Heidelberg.

Andrews, W.R.H. & Hutchings, L. 1980. Upwelling in the southern Benguela Current. Prog. Oceanogr. 9: 1-81.

Armstrong, D.A., Mitchell-Innes, B.A., Verhaye-Due, F., Waldron, H. & Hutchings, L. 1987. Physical and biological features across the upwelling front in the southern Benguela. South African Journ. Mar. Sci. 5: 171-190.

Austin, M. P. 2002. Spatial prediction of species distribution: an interface between ecological theory and statistical modelling. Ecological Modelling 157: 101-118.

Banks, A.N., Burton, N.H.K., Austin, G.E., Carter, N., Chamberlain, D.E., Holt, C., Rehfisch, M.M., Wakefield, E. & Gill, P. 2005. The potential effects on birds of the Greater Gabbard Offshore Windfarm: Report for February 2004 to March 2005. BTO Research Report No. 419, BTO, Thetford.

Banks, A.N., Maclean, I.M.D., Burton, N.H.K., Austin, G.E., Carter, N., Chamberlain, D.E., Holt, C., Rehfisch, M.M., Pinder, S., Batty, A., Wakefield, E. & Gill, P. 2006. The potential effects on birds of the Greater Gabbard Offshore Windfarm: Report for February 2004 to March 2005. BTO Research Report No. 440, BTO, Thetford.

Bivand, R. 2009. Spatial dependencies: weighting schemes, statistics and models. R package version 0.4-34.

Birdlife International. 2004. Birds in Europe: Population Estimates, Trends and Conservation Status. Birdlife International, Cambridge.

Blayo, E.; Debreu, L., 2005: Revisiting open boundary conditions from the point of view of characteristic variables. Ocean Modelling, 9: 231–252.

Buckland, S.T., Anderson, D.R., Burnham, K.P. & Laake, J.L. 1993. Distance Sampling: Estimating Abundance of Biological Populations. Chapman and Hall, London.

Camphuysen, C.J., Fox, A.D., Leopold, M.F. & Petersen, I.K. 2004. Towards standardised seabirds at sea census techniques in connection with environmental impact assessments for offshore wind farms in the U.K. A comparison of ship and aerial sampling methods for marine birds, and their applicability to offshore wind farm assessments. Koninklijk Nederlands Instituut voor Onderzoek der Zee Report commissioned by COWRIE.

Clark, C.J., Poulsen, J.R, Malonga, R. and Elkan, P.W. 2009. Logging concessions can extend the conservation estate for central African tropical forests. Conservation Biology, 23: 1281-1293.

Delany, S., Scott, D., 2006. Waterbird Population Estimates, fourth ed. Wetlands International, Wageningen, The Netherlands.

Dillingham, P.W., Fletcher, D., 2008. Estimating the ability of birds to sustain additional human-caused mortalities using a simple decision rule and allometric relationships. Biological Conservation 141, 1783–1792.

Durinck, J., Skov, H. & P. Andell. 1993. Seabird distribution and numbers in selected Offshore parts of the Baltic Sea, winter 1992. Ornis Svecica 3: 11-26.

Elith, J., Graham, C. H., Anderson, R. P., Dudý´k, M., Ferrier, S., Guisan, A., Hijmans, R. J., Huettmann, F., Leathwick, J. R., Lehmann, A., Li, J., Lohmann, L. G., Loiselle, B. A., Manion, G., Moritz, C., Nakamura, M., Nakazawa, Y., Overton, J. McC., Peterson, A. T., Phillips, S. J., Richardson, K., Scachetti-Pereira, R., Schapire, R. E., Soberón, J., Williams, S., Wisz, M. S. & Zimmermann, N. E. 2006. Novel methods improve prediction of species' distributions from occurrence data. Ecography 29: 129-151.

Elith, J. & Leathwick, J. R. 2009. Species distribution models: ecological explanation and prediction across space and time. Annual Review of Ecology, Evolution, and Sys tematics 40: 677-697.Emu. 2002. Kentish Flats Environmental Statement. Volume 1, August 2002. Global Renewable Energy Partners.

Fauchald, P., K. E. Erikstad, & H. Skarsfjord. 2000. Scale-dependent predator-prey interactions: the hierarchical spatial distribution of seabirds and prey. Ecology 81:773-783.

Fauchald, P., Skov, H., Skern-Mauritzen, M., Hausner, V.H., Johns, D. & Tveraa, T. 2010. Scale-dependent response diversity of seabirds to prey in the North Sea. Ecology (In press).
Ferrier, S., Watson, G. Pearce, J. & Drielsma, M. 2002. Extended statistical approaches to modelling spatial pattern in biodiversity in northeast New South Wales. I. Species-level modelling. Biodiversity and Conservation 11: 2275-2307.
Fielding, A.H. & Bell, J.F., 1997. A review of methods for the assessment of prediction errors in conservation presence/absence models. Environ. Conserv. 24: 38–49.
Follestad, A. 1990. The pelagic distribution of Little Auk Alle alle in relation to a frontal system off central Norway, March/April 1988. Polar Research. 8: 23 - 28.
Foreman, M.G., 1977. Manual for Tidal Heights Analysis and Prediction. Pacific Marine Science Report 77-10, Institute of Ocean Sciences.
Foreman, M.G., 1978. Manual for Tidal Heights Analysis and Prediction. Pacific Marine Science Report 78-6, Institute of Ocean Sciences.
Franklin, J. 2009. Mapping species distributions: spatial inference and prediction. Cambridge University Press, Cambridge.
Gill, J.P., Sales, D., Pinder, S. & R. Salazar. 2008. Draft Kentish Flats wind farm fifth ornithological monitoring report. ESS 2008.
Goodman, L.A. 1960. On the exact variance of products. Journal of the American Statistical Association, 55: 708-713.
Graham, M. H. 2003. Confronting multicollinearity in ecological multiple regression. Ecology 84: 2809-2815.
Guisan, A. & Zimmermann, N.E. 2000. Predictive habitat distribution models in ecology. Ecological Modelling 135: 147-86.
Guisan, A., Edwards, T. C. & Hastie, T. 2002. Generalized linear and generalized additive models in studies of species distributions: setting the scene. Ecological Modelling 157: 89-100.
Guisan, A. & Thuiller, W. 2005. Predicting species distribution: offering more than simple habitat models. Ecology Letters 8: 993-1009
Hastie, T. & Tibshirani, R. 1990. Generalized additive models. Chapman & Hall, London.
Heikkinen, R. K., Luoto, M., Araújo, M. B., Virkkala, R., Thuiller, W. & Sykes, M. T. 2006. Methods and uncertainties in bioclimatic envelope modelling under climate change. Progress in Physical Geography 30: 751-777.
Hemmingsson, E. & Eriksson, M. O. G. 2002. Ringing of redthroated diver *Gavia stellata* and black-throated diver *Gavia arctica* in Sweden. Diver/Loon Specialist Group, Wetlands International, Newsletter, Vol 4.
Jensen, A. 2006. Thanet Offshore Wind Farm Environmental Statement Addendum Report. Section 8 - Ornithology. Royal Haskoning Report to Thanet Offshore Wind Limited.
Kinder, T.H., Hunt, G.L. Jr., Schneider, D. & Schumacher, J.D. 1983. Correlations between seabirds and oceanic fronts around the Pribilof Islands, Alaska. Est. Coast. Shelf Sci. 16: 309-319.
Le Pape, O., Guérault, D. & Désaunay, Y. 2004. Effect of an invasive mollusc, American slipper limpet Crepidula fornicata, on habitat suitability for juvenile common sole Solea solea in the Bay of Biscay. Mar. Ecol. Prog. Ser. 277: 107-115.
Maclean, I.M.D, Wright, L.J., Showler, D.A. & Rehfisch, M.M. 2009. A Review of Assessment Methodologies for Offshore Windfarms. British Trust for Ornithology Report Commissioned by Cowrie Ltd.
Marsh, H., Lawler, I.R., Kwan, D., Delean, S., Pollock, K., Alldredge, M., 2004. Aerial sur veys and the potential biological removal technique indicate that the Torres Strait dugong fishery is unsustainable. Animal Conservation 7, 435–443.
Marini, M. Â., Barbet-Massin, M., Lopes, L. E. & Jiguet, F. 2010. Predicting the occurrence of rare Brazilian birds with species distribution models. Journal of Ornithology 151: 857-866.
Milner-Gulland, E.J., Akçakaya, H.R., 2001. Sustainability indices for exploited populations. Trends in Ecology and Evolution 16, 686–692.
Moisen, G. G. & Frescino, T. S. 2002. Comparing five modelling techniques for predicting forest characteristics. Ecological modelling, 157, 209-225.

Niel, C., Lebreton, J.-D., 2005. Using demographic invariants to detect overharvested bird populations from incomplete data. Conservation Biology 19, 826–835.
Natural England. 2009. Departmental Brief: Outer Thames Estuary. Potential Special Protection Area. Natural England. Peterborough
O'Brien, S. H., Wilson, L. J., Webb, A. & Cranswick, P. A. 2008. Revised estimate of numbers of wintering Red-throated Divers *Gavia stellata* in Great Britain. Bird Study 55, 152-160.
Pearce, J. & Ferrier, S. 2000. Evaluating the predictive performance of habitat models developed using logistic regression. Ecological Modelling 133: 225-245.
Petersen, I.K., Pihl, S., Hounisen, J.P., Holm, T.E., Clausen, P., Therkildsen, O. & Christensen, T.K. 2006. Landsdækkende optællinger af vandfugle, januar og februar 2004. Danmarks Miljøundersøgelser. 76 s. – Faglig rapport fra DMU nr. 606. http://www.dmu.dk/Pub/FR606.pdf
Petersen et al. 2006. Final results of bird studies at the offshore wind farms at Nysted and Horns Rev, Denmark. Report request. Commissioned by DONG energy and Vattenfall A/S. National Environmental Research Institute. Ministry of the Environment, Denmark.
PMSS. 2005. Greater Gabbard Offshore Wind Farm Environmental Statement. Airtricity and Fluor.
Potts, J. M. & Elith, J. 2006. Comparing species abundance models. Ecological Modelling 199: 153-163.
R Development Core Team. 2004. A language and environment for statistical computing. R Foundation for Statistical Computing, Vienna, Austria. http://www.R-project.org.
R Development Core Team. 2010. R: A Language and Environment for Statistical Computing. R Foundation for Statistical Computing, Vienna. http://www.R-project.org.
Rasmussen, E.B. 1991. A finite difference scheme for three dimensional modelling of fluid dynamics. Proceedings of IAHR, Madrid, Spain: 339-348.
Royal Haskoning. 2005. Thanet Offshore Wind Farm Environmental Statement. Thanet Offshore Wind Limited and Warwick Energy Limited.
RPS. 2005. London Array Environmental Statement. Volume 1: Offshore Works London Array Ltd. Shell WindEnergy, Farm Energy, Energie2.
Schneider, D.C. 1982. Fronts and seabird aggregations in the southeastern Bering Sea. Mar. Ecol. Prog. Ser. 10: 101-103.
Schneider, D.C. & Duffy, D.C. 1985. Scale-dependent variability in seabird abundance. Mar. Ecol. Prog. Ser. 25: 211-218.
Schneider & Hunt 1982: Carbon flux to seabirds in waters with different mixing regimes in the southeastern Bering Sea. Mar.Biol. 67: 337-344.
Sonntag, N., Garthe, S. & Adler, S. 2009. A freshwater species wintering in a brackish environment: Habitat selection and diet of Slavonian grebes in the southern Baltic Sea. Estuarine, Coastal and Shelf Science 84: 186-194.
Skov, H., Durinck, J., Leopold, M.F., Tasker, M.L., 1995. Important Bird Areas for Seabirds in the North Sea. BirdLife International, Cambridge, United Kingdom.
Skov, H. & Prins, E. 2001. Impact of estuarine fronts on the dispersal of piscivorous birds in the German Bight. Mar. Ecol. Prog. Ser. 214: 279-287.
Skov, H., Piper, W., Leonhard, S.B.L. 2008. Horns Rev II wind farm. Monitoring of waterbirds. Baseline Studies 2007-08. Report request. Commissioned by DONG Energy. Orbicon A/S & DHI.
Skov, H. Krogsgaard, J., Piper, W., Durinck, J. 2009. Anholt Offshore Wind Farm. Birds. Report commissioned by EnergiNet.dk.
Skov, H., Heinänen, S, Zydelis, R. et al. 2011. Waterbird populations and pressures in the Baltic Sea. TemaNord 2010. DHI Report.
Stefánsson, G. 1996. Analysis of groundfish survey abundance data: combining the GLM and delta approaches. ICES Journal of Marine Science, 53: 577-588.
Sørensen, J.V.T.; Madsen H.; Madsen H., 2004. Efficient Sequential techniques for the assimilation of tide gauge data in three dimensional modeling of the North Sea and Baltic Sea system, J. Geophysic. Res. (Oceans).
Tasker, M.L., Jones, P.H., Dixon, D.J. & Blake, B.F. 1984. Counting seabirds at sea from

ships: a review of methods employed and a suggestion for a standardized approach. Auk 101: 567-577.
Taylor, B.L., Wade, P.R., de Master, D.P., Barlow, J., 2000. Incorporating uncertainty into management models for marine mammals. Conservation Biology 14, 1243–1252.
Teague, W.J., M.J. Carron, & P.J. Hogan, A comparision between the Generalized Digital Environmental Model and Levitus climatologies, *J. Geophys. Res., 95 C5*, 7167-7183, 1990.
Thomas, L., Buckland, S.T., Rexstad, E.A., Laake, J.L., Strindberg, S., Hedley, S.L., Bishop, J.R.B., Marques, T.A. & Burnham, K.P. 2010. Distance software: design and analysis of distance sampling surveys for estimating population size. Journal of Applied Ecology 47 (1): 5-14.
Trembley, Y., Bertrand, S., Henry, R. W., Kappes. M. A., Costa. D. P & Shaffer, S. A. 2009. Analytical approaches to investigating seabird – environment interactions: a review. Mar Ecol Prog Ser 391: 153-163.

Wade, P.R., 1998. Calculating limits to the allowable human-caused mortality of cetaceans and pinnipeds. Marine Mammal Science 14, 1–37.
Webley, J.A.C, Mayer, D.G. and Taylor, S.M. 2011. Investigating confidence intervals generated by zero-inflated count models: Implications for fisheries management. Fisheries Research, 110: 177-182.
Wilhelmsson, D., Malm, T., Thompson, R., Tchou, J., Sarantakos, G., McCormick, N., Luitjens, S., Gullström, M., Patterson, Edwards, J.K., Amir, O. & Dubi, A. (eds.) (2010). Greening Blue Energy: Identifying and managing the biodiversity risks and opportunities of offshore renewable energy. Gland, Switzerland: IUCN. 102pp.
Wintle, B. A., Elith, J. & Potts, J. M. 2005. Fauna habitat modelling and mapping: A review and case study in the Lower Central Coast Region of NSW. Austral Ecology 30: 719–738.
Wood, S. N. & Augustin, N. H. 2002. Gams with integrated model selection using penalized regression splines and applications to environmental modeling. Ecological Modelling 157: 157-177.
Wood, S. N. 2006. Generalized Additive Models: An Introduction with R. Chapman and Hall, London.
http://www.space.dtu.dk/English/Research/Scientific_data_and_models/Global_Ocean_Tide_Model.aspx
Zador, S.G., Punt, A.E., Parrish, J.K., 2008. Population impacts of endangered shorttailed albatross bycatch in the Alaskan trawl fishery. Biological Conservation 141, 872–882.
Zipkin, E. F., Gardner, B., Gilbert, A. T., O'Connel Jr., A. F., Royle, J. A. & Silverman, E. D. 2010. Distribution patterns of wintering sea ducks in relation to the North Atlantic Oscillation and local environmnetla characteristics. Oecologia, 163, 893-902.
Zuur, A. F., Ieno, E. N., Walker, N. J., Saveliev, A. A. & Smith, G. M. 2009. Mixed effect models and extensions in ecology. Springer, New York.
Žydelis, R., Bellebaum, J., Osteblom, H., Vetemaa, M., Schirmaister, B., Stipniece, A., Dagys, M., van Eerden, M. & Garthe, S. 2009. Bycatch in gillnet fisheries – an overlooked threat to waterbird populations. Biological Conservation 142, 1269-1281.

6 APPENDICES

APPENDIX 1: DIAGNOSTICS FOR SPECIES DISTRIBUTION MODELS

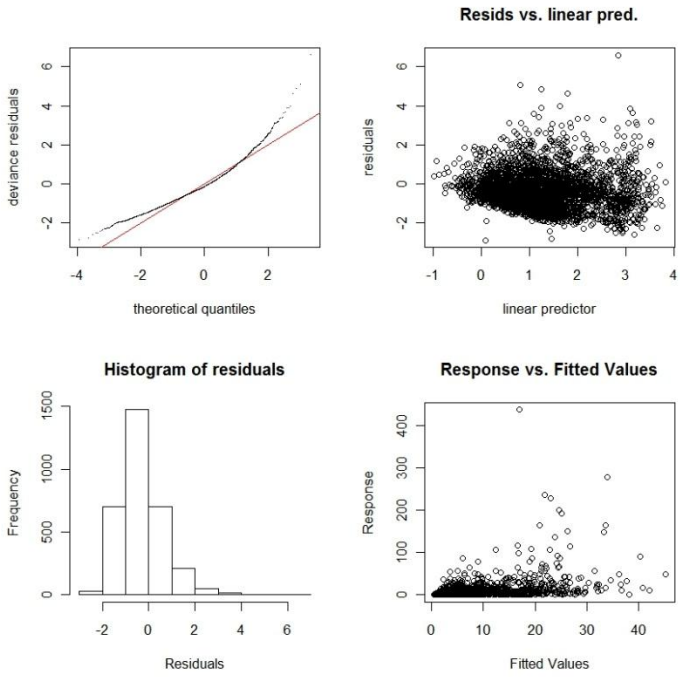

Diagnostic plots for the positive part of the global two-part GAM (Model 1). Normality of the residuals is displayed in a Q-Q plot (upper left) and in a histogram (lower left). The spread of the residuals is displayed in the upper right plot whereas the predicted against the observed values are plotted in the lower right plot.

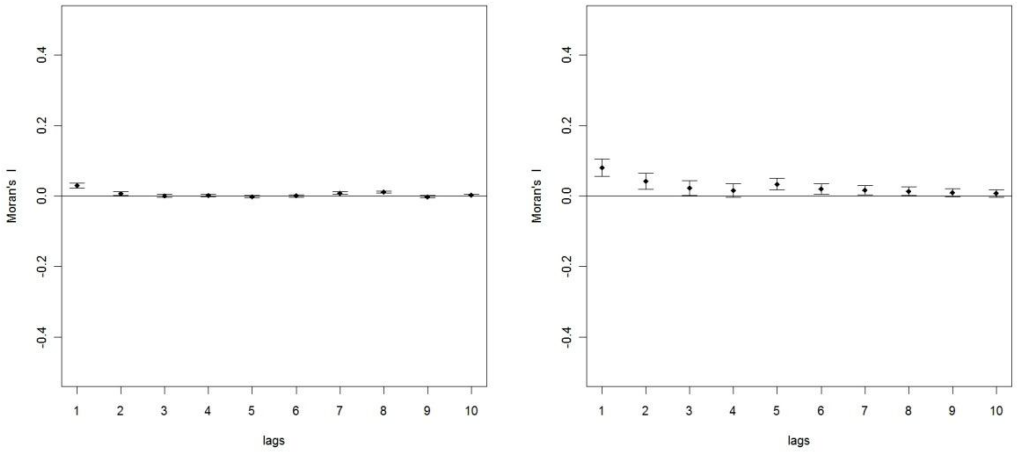

Spatial correlograms displaying the spatial autocorrelation over 10 lags in the residuals for the global two-part GAM model (Model 1). The correlogram for the presence/absence part is shown to the left and the positive part to the right The dots indicate the estimated Moran's I value and the bars show twice the square root of the variance from the estimated Moran's I value. 1 lag equals the defined nearest neighborhood of 1500 meters.

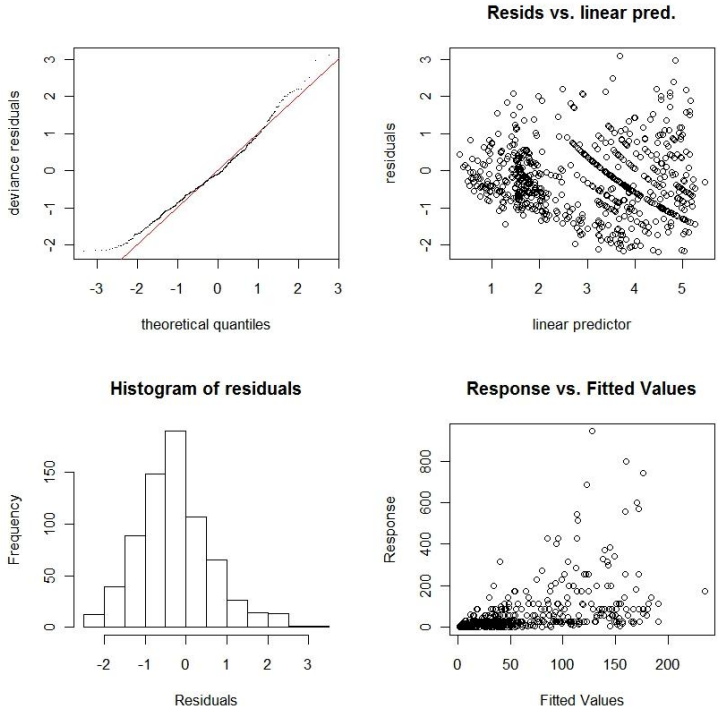

Diagnostic plots for the positive part of the two-part GAM for flow phase 1 (Model 2). Normality of the residuals is displayed in a Q-Q plot (upper left) and in a histogram (lower left). The spread of the residuals is displayed in the upper right plot whereas the predicted against the observed values are plotted in the lower right plot.

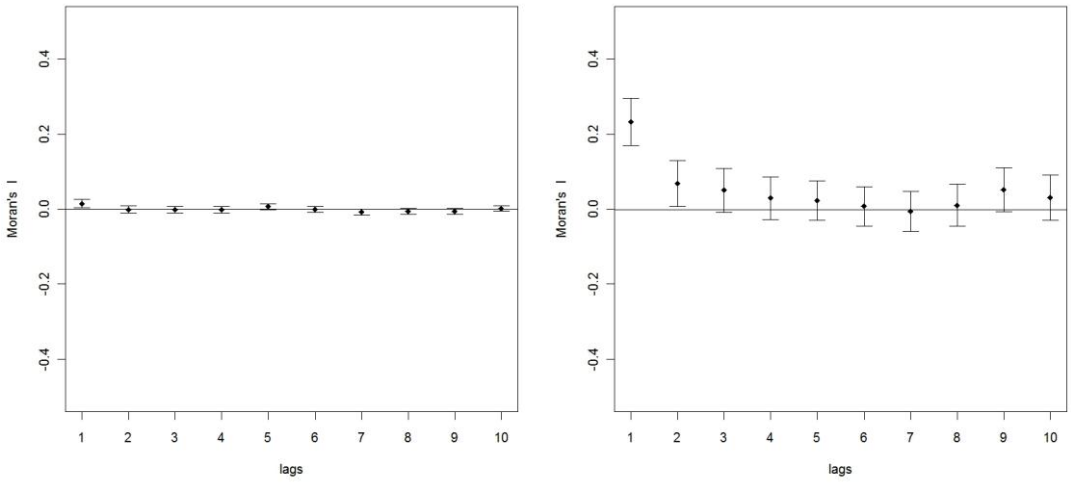

Spatial correlograms displaying the spatial autocorrelation over 10 lags in the residuals for the two-part GAM for flow phase 1 (Model 2). The correlogram for the presence/absence part is shown to the left and the positive part to the right The dots indicate the estimated Moran's I value and the bars show twice the square root of the variance from the estimated Moran's I value. 1 lag equals the defined nearest neighborhood of 1500 meters.

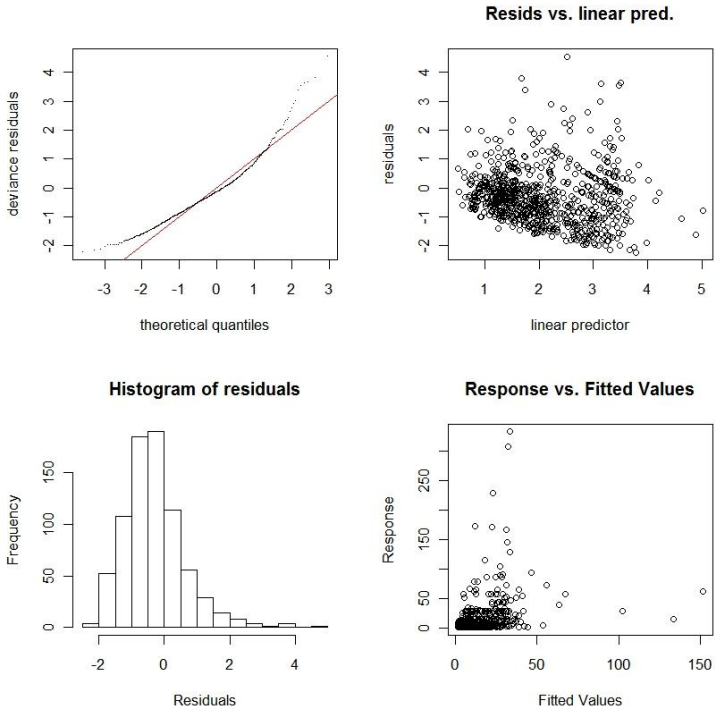

Diagnostic plots for the positive part of the two-part GAM for flow phase 2 (Model 3). Normality of the residuals is displayed in a Q-Q plot (upper left) and in a histogram (lower left). The spread of the residuals is displayed in the upper right plot whereas the predicted against the observed values are plotted in the lower right plot.

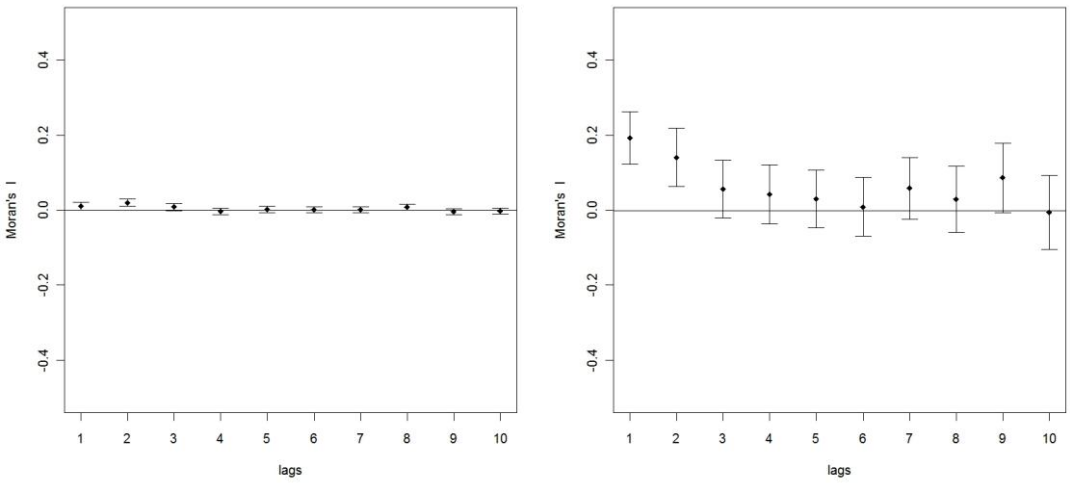

Spatial correlograms displaying the spatial autocorrelation over 10 lags in the residuals for the two-part GAM for flow phase 2 (Model 3). The correlogram for the presence/absence part is shown to the left and the positive part to the right The dots indicate the estimated Moran's I value and the bars show twice the square root of the variance from the estimated Moran's I value. 1 lag equals the defined nearest neighborhood of 1500 meters.

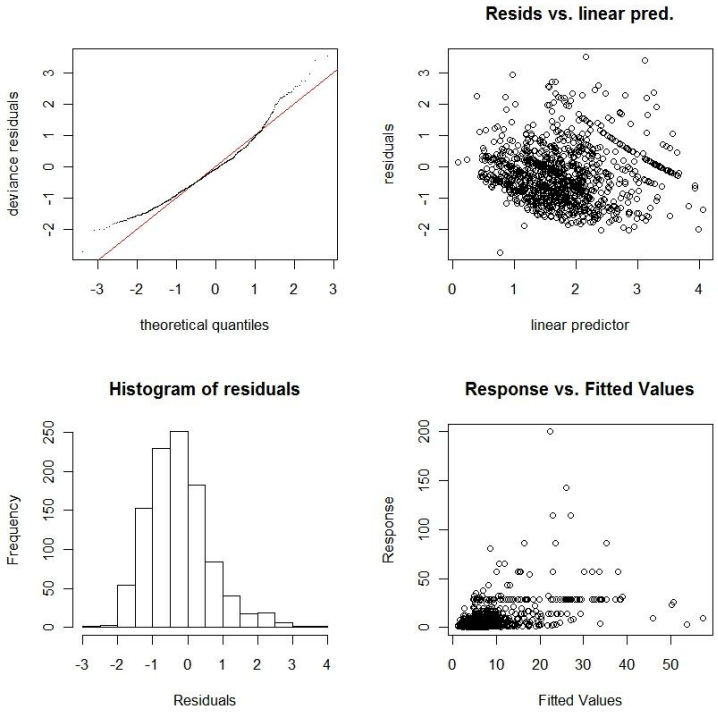

Diagnostic plots for the positive part of the two-part GAM for flow phase 3 (Model 4). Normality of the residuals is displayed in a Q-Q plot (upper left) and in a histogram (lower left). The spread of the residuals is displayed in the upper right plot whereas the predicted against the observed values are plotted in the lower right plot.

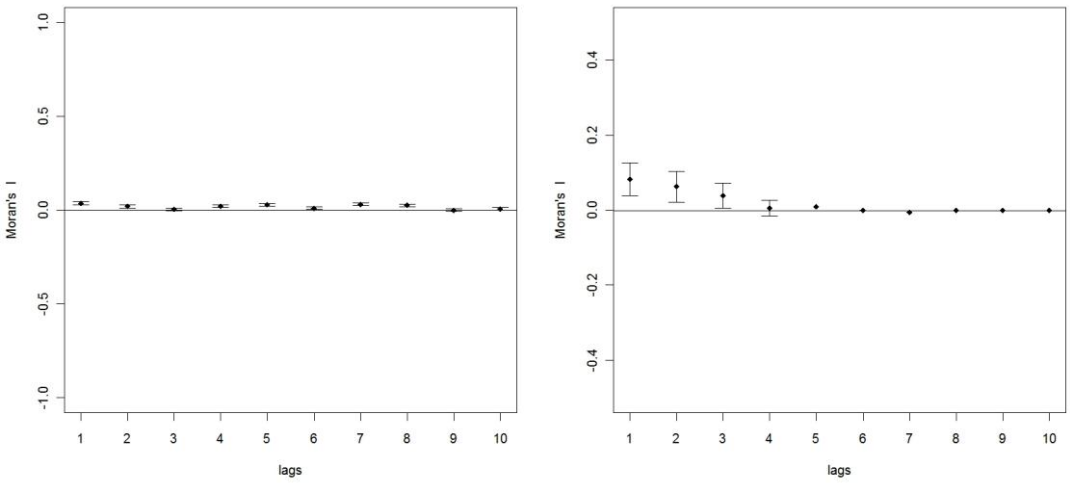

Spatial correlograms displaying the spatial autocorrelation over 10 lags in the residuals for the two-part GAM for flow phase 3 (Model 4). The correlogram for the presence/absence part is shown to the left and the positive part to the right The dots indicate the estimated Moran's I value and the bars show twice the square root of the variance from the estimated Moran's I value. 1 lag equals the defined nearest neighborhood of 1500 meters.

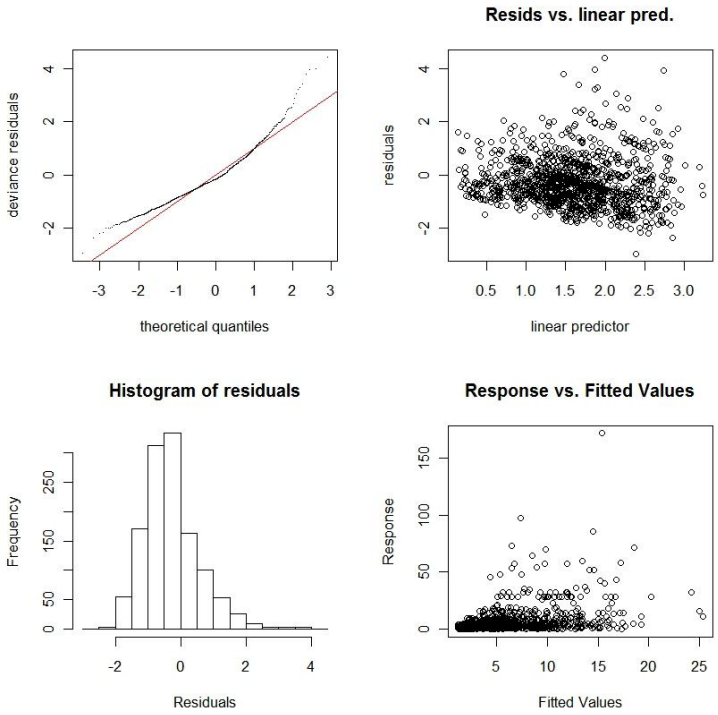

Diagnostic plots for the positive part of the two-part GAM for flow phase 4 (Model 5). Normality of the residuals is displayed in a Q-Q plot (upper left) and in a histogram (lower left). The spread of the residuals is displayed in the upper right plot whereas the predicted against the observed values are plotted in the lower right plot.

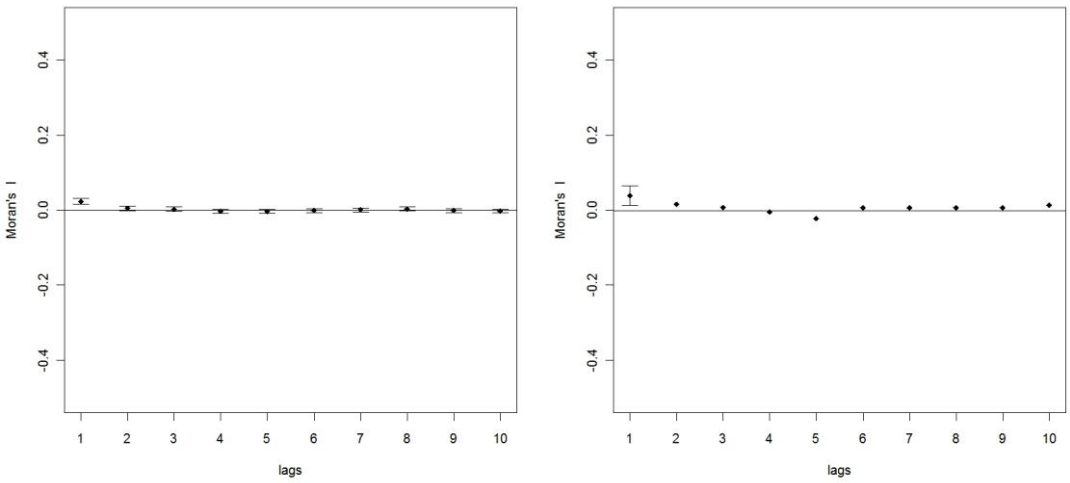

Spatial correlograms displaying the spatial autocorrelation over 10 lags in the residuals for the two-part GAM for flow phase 4 (Model 5). The correlogram for the presence/absence part is shown to the left and the positive part to the right The dots indicate the estimated Moran's I value and the bars show twice the square root of the variance from the estimated Moran's I value. 1 lag equals the defined nearest neighborhood of 1500 meters.

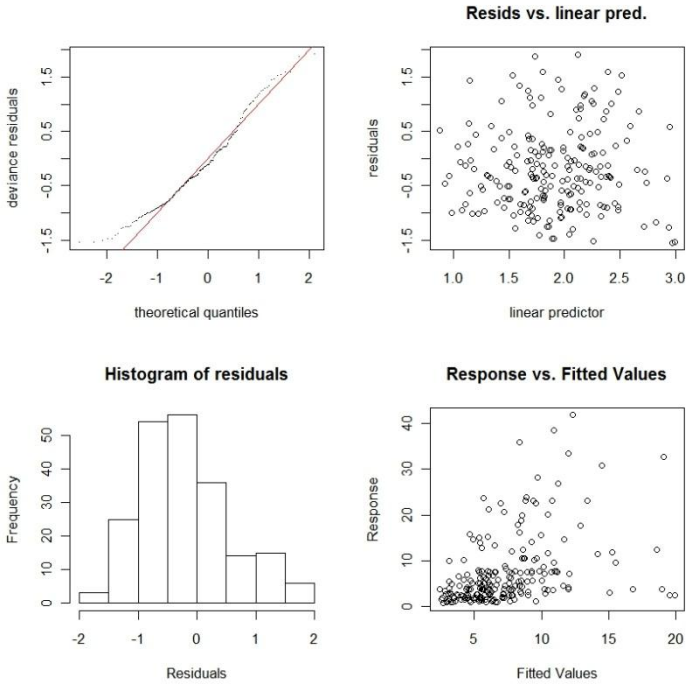

Diagnostic plots for the positive part of the two-part GAM based on visual data for the comparison between visual and digital survey data. Normality of the residuals is displayed in a Q-Q plot (upper left) and in a histogram (lower left). The spread of the residuals is displayed in the upper right plot whereas the predicted against the observed values are plotted in the lower right plot.

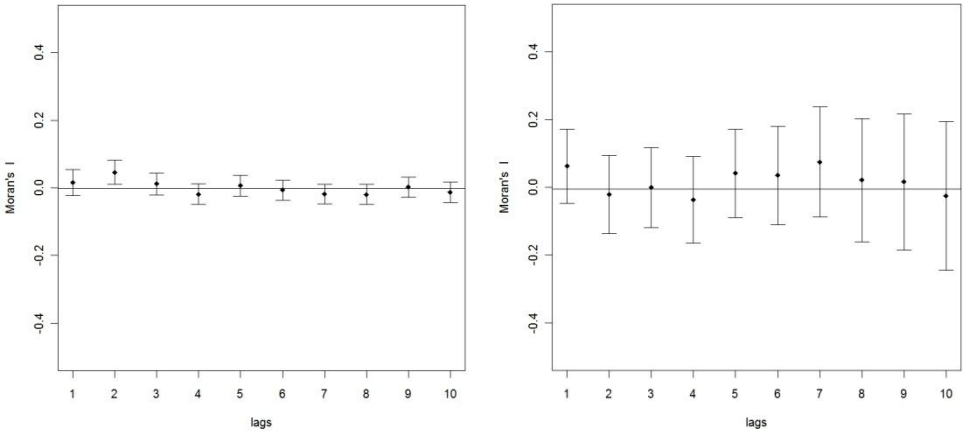

Spatial correlograms displaying the spatial autocorrelation over 10 lags in the residuals for the two-part GAM based on visual data for the comparison between visual and digital survey data. The correlogram for the presence/absence part is shown to the left and the positive part to the right The dots indicate the estimated Moran's I value and the bars show twice the square root of the variance from the estimated Moran's I value. 1 lag equals the defined nearest neighborhood of 1500 meters.

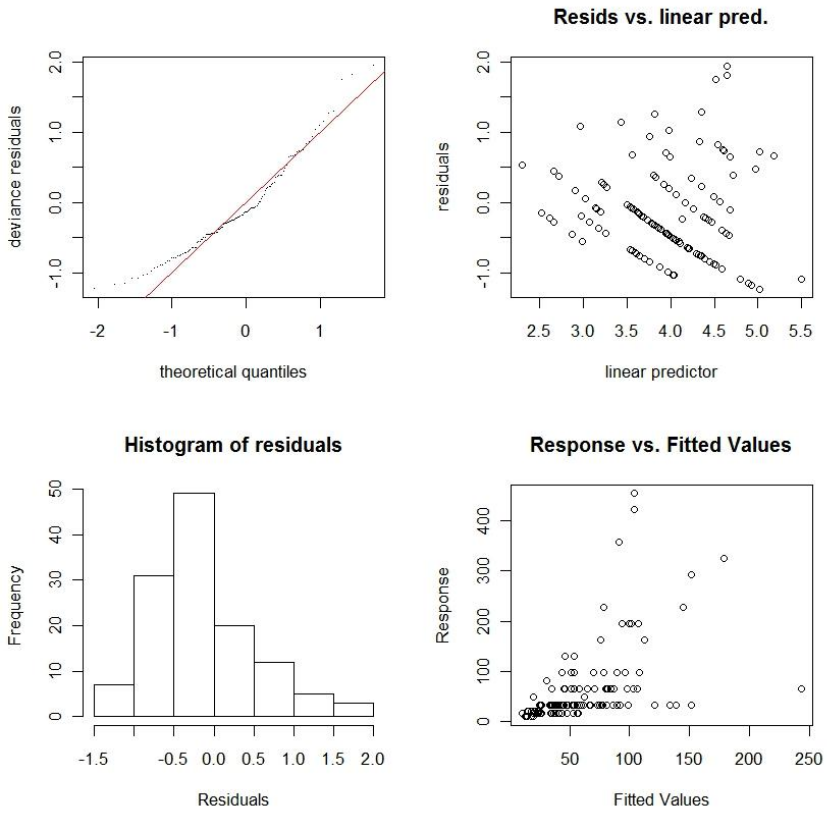

Diagnostic plots for the positive part of the two-part GAM based on digital data for the comparison between visual and digital survey data. Normality of the residuals is displayed in a Q-Q plot (upper left) and in a histogram (lower left). The spread of the residuals is displayed in the upper right plot whereas the predicted against the observed values are plotted in the lower right plot.

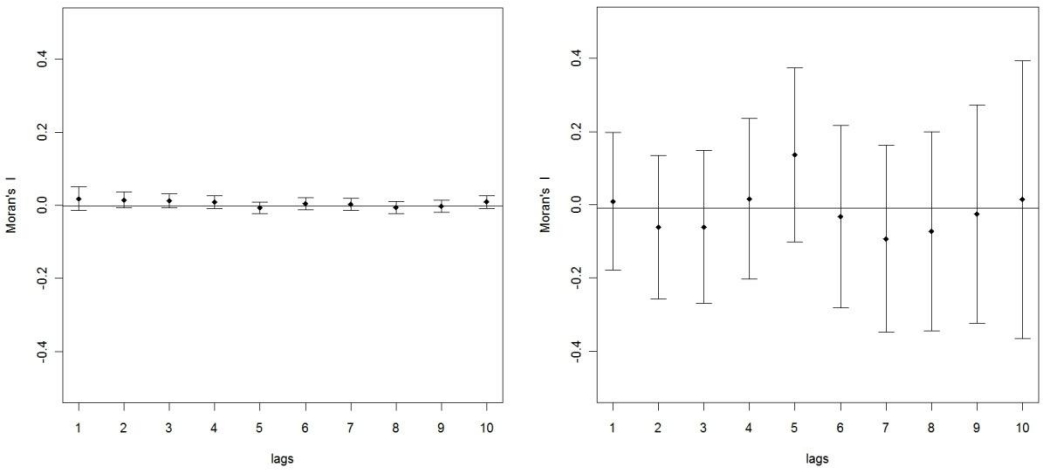

Spatial correlograms displaying the spatial autocorrelation over 10 lags in the residuals for the two-part GAM based on digital data for the comparison between visual and digital survey data. The correlogram for the presence/absence part is shown to the left and the positive part to the right The dots indicate the estimated Moran's I value and the bars show twice the square root of the variance from the estimated Moran's I value. 1 lag equals the defined nearest neighborhood of 1500 meters.

APPENDIX 2: MAPPED PREDICTOR VARIABLES

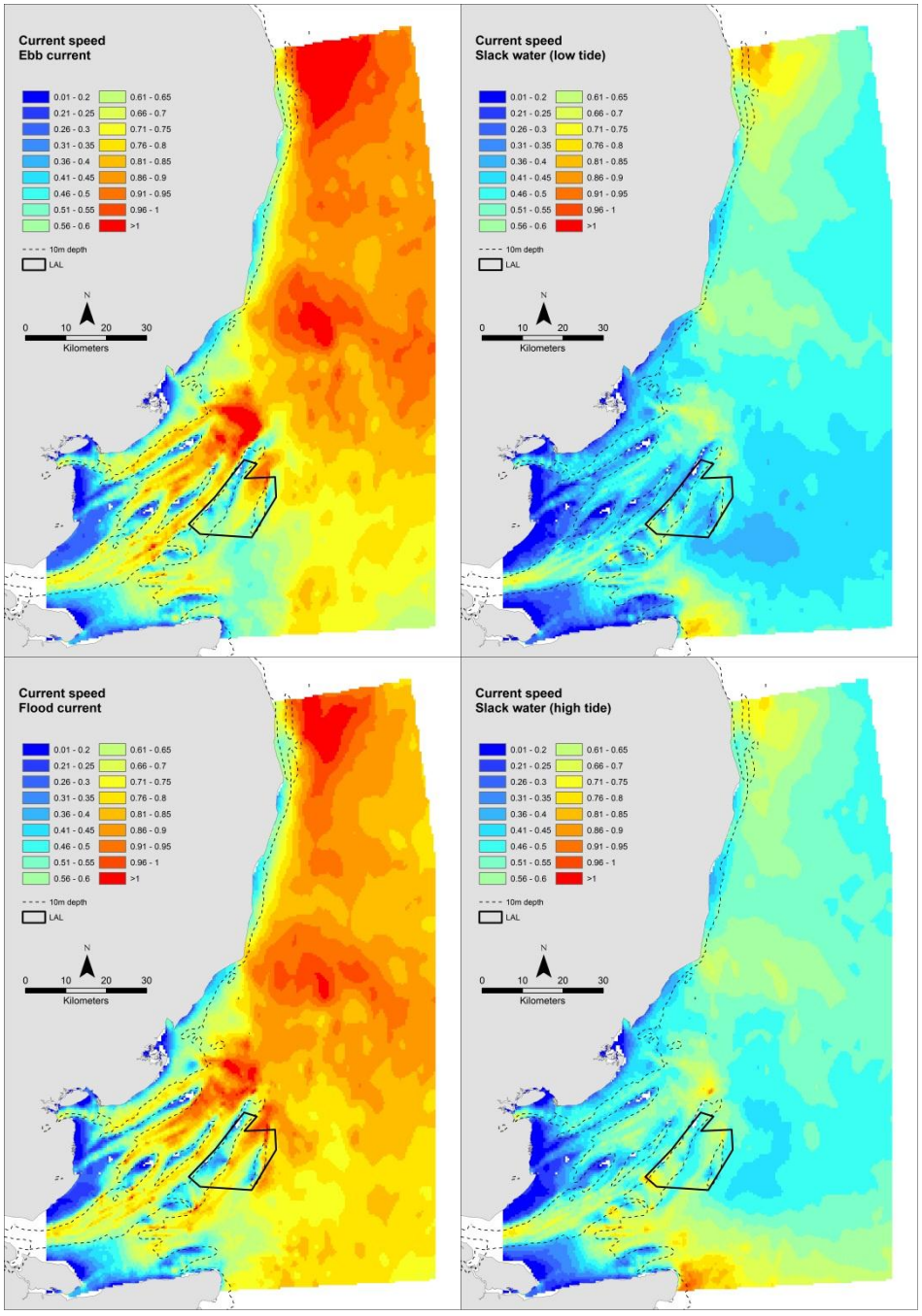

Averaged current speed (in the winters 2003/2004, 2004/2005, 2005/2006 and 2010/2011) during the four current phase. The same classification is used in all maps to facilitate comparison between the phases.

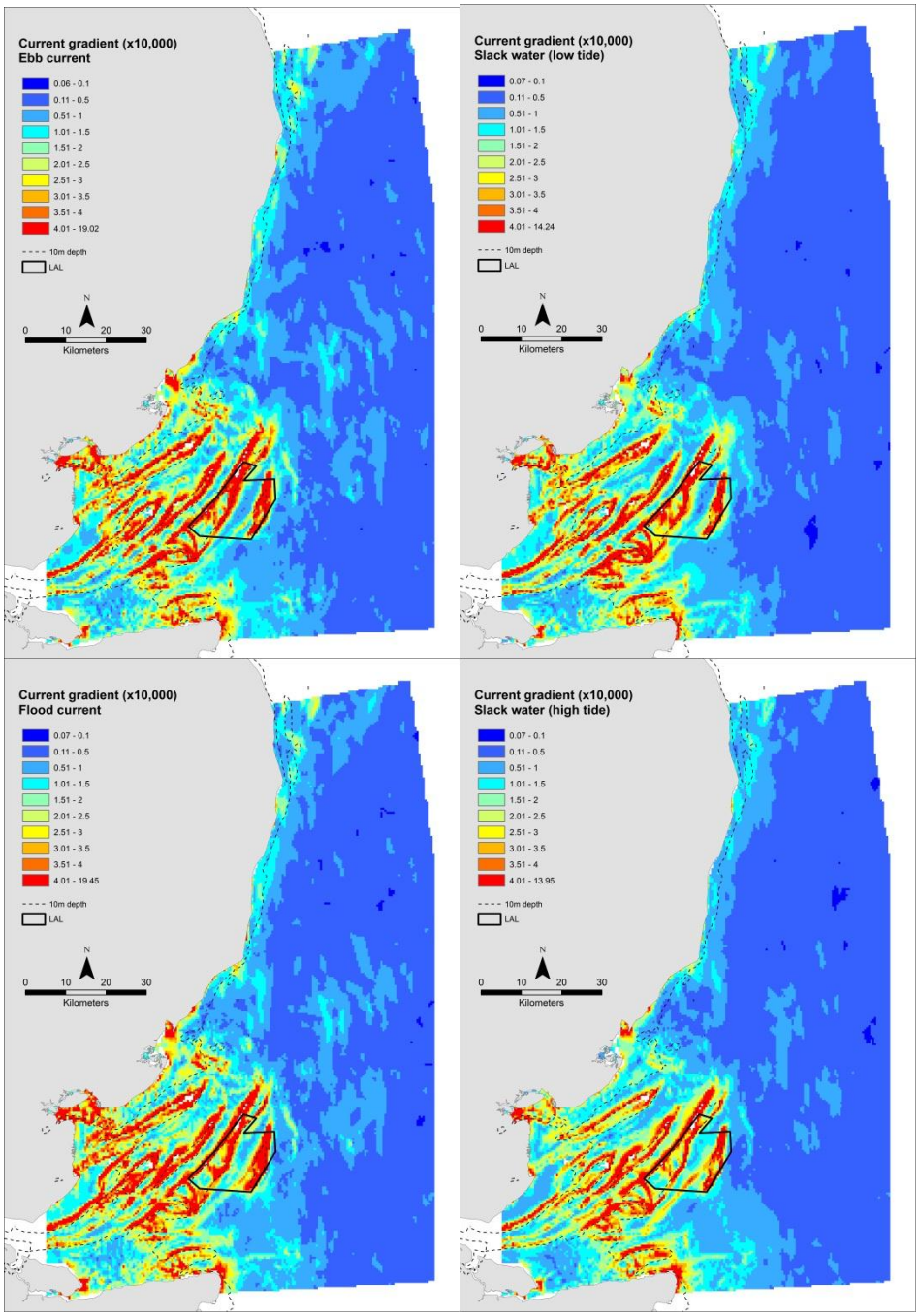

Averaged current gradient (in the winters 2003/2004, 2004/2005, 2005/2006 and 2010/2011) during the four current phase. The same classification is used in all maps to facilitate comparison between the phases.

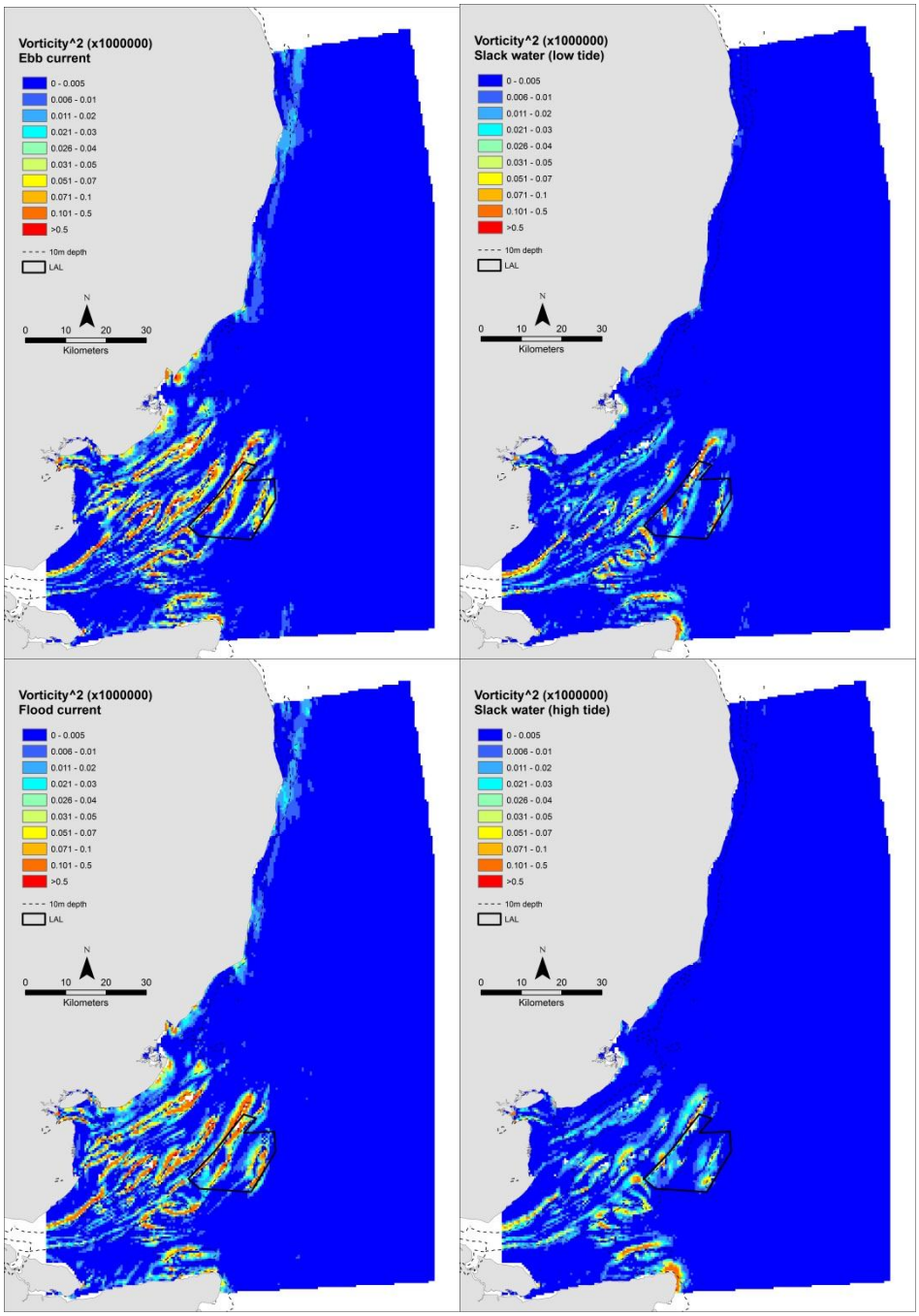

Averaged squared vorticity (in the winters 2003/2004, 2004/2005, 2005/2006 and 2010/2011) during the four current phase. The same classification is used in all maps to facilitate comparison between the phases.

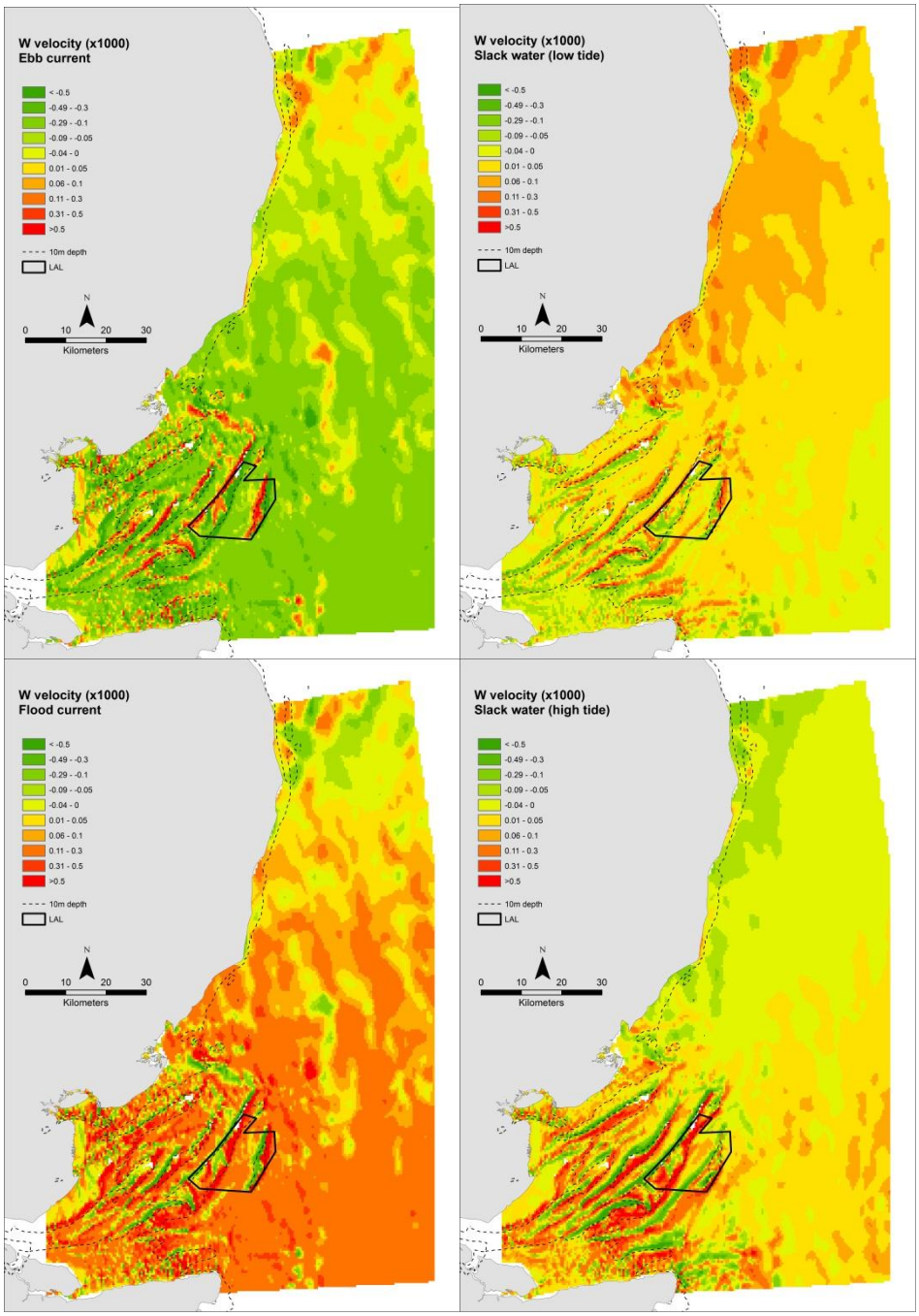

Averaged W (vertical) velocity (in the winters 2003/2004, 2004/2005, 2005/2006 and 2010/2011) during the four current phase. The same classification is used in all maps to facilitate comparison between the phases.

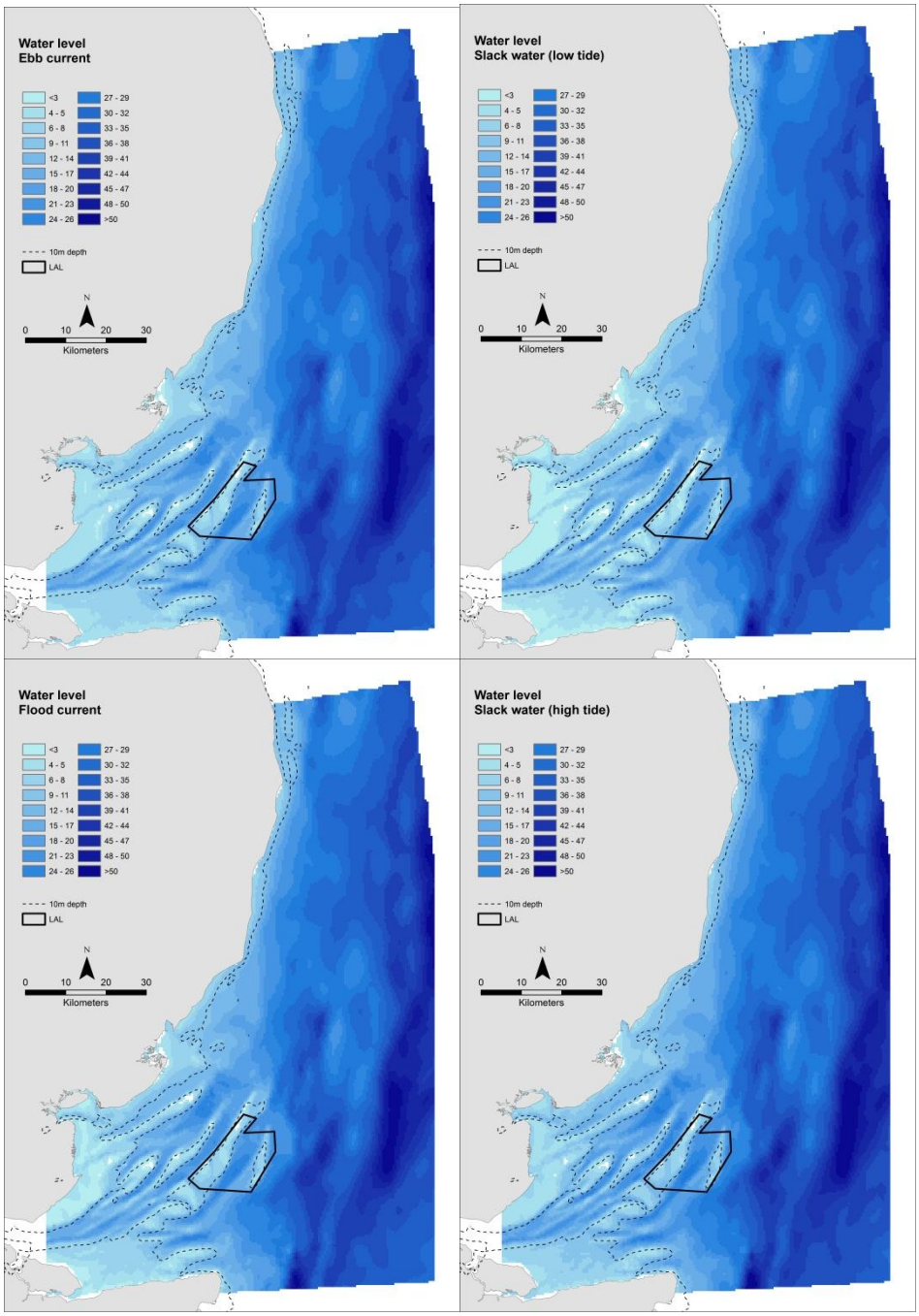

Averaged water level (in the winters 2003/2004, 2004/2005, 2005/2006 and 2010/2011) during the four current phase. The same classification is used in all maps to facilitate comparison between the phases.

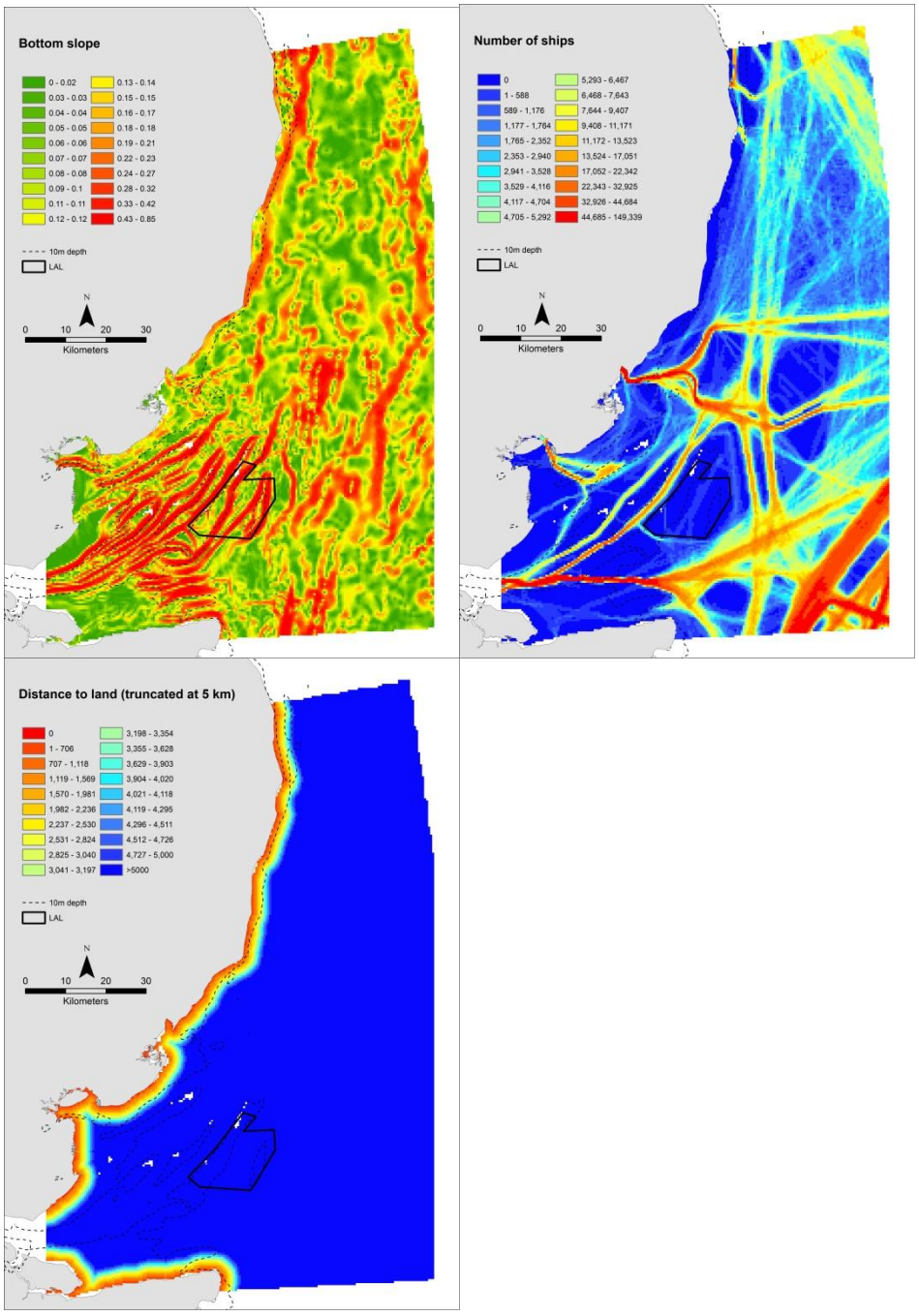

The static predictor variables used in the species distribution models; bottom slope (upper left), number of ships (upper right) and distance to land truncated at 5 km (lower left).